

Special  
Issue

# VYTÁPĚNÍ VĚTRÁNÍ INSTALACE

6 2018  
VOL. 27

Journal of Heating, Ventilation, Sanitation

ISSN 1210-1389 / MK ČR E 6050

## Special Issue of Journal of Heating, Ventilation, Sanitation

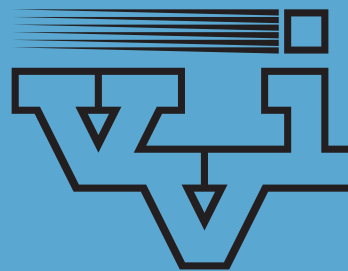
### VVI Journal brings information:

- ❑ about the latest trends in heating, ventilation, air conditioning, cooling, humidification, dehumidification, hygiene, sanitation installation, measurement and control, lighting, noise, air quality, energy conservation, traditional and alternative energy sources at home and abroad;
- ❑ about new products, techniques and domestic or foreign technology for accurate and efficient operation of buildings with examples of practical use;
- ❑ about testing and measures improving quality of domestic production and enhancing sales of domestic products at foreign markets;
- ❑ about theoretical works dealing with new knowledge characteristics of new products, new computational methods and application of computer technology in the field of environmental engineering;

More information: [www.stpcr.cz/en](http://www.stpcr.cz/en)

Since 2014 the VVI journal is included  
into the SCOPUS database

Scopus



OBSAH	Strana	CONTENTS	Page
<b>VNITŘNÍ PROSTŘEDÍ</b>		<b>INDOOR ENVIRONMENT</b>	
DOBIÁŠOVÁ, ADAMOVSÝ: CFD simulace stojícího člověka ve vnitřním prostředí	338	DOBIÁŠOVÁ, ADAMOVSÝ: The CFD Simulation of a Standing Person in an Indoor Environment	338
WEYR, ŠIKULA, HIRŠ: Dynamická simulace vnitřního prostředí v průmyslové hale s nadměrnou tepelnou zátěží	344	WEYR, ŠIKULA, HIRŠ: Building Performance Simulation of Industrial Hall with Excessive Heat Loads	344
<b>SIMULACE BUDOV</b>		<b>BUILDING SIMULATION</b>	
KOPECKÝ, STANĚK: Přezkoumání tří dynamických tepelných modelů budov se sdruženými parametry	348	KOPECKÝ, STANĚK: Review of Three White-Box Lumped Parameter Building Thermal Models	348
<b>VĚTRÁNÍ A KLIMATIZACE</b>		<b>VENTILATION AND AIR-CONDITIONING</b>	
LYSCZAS, KABEL: Adaptivní větrání jako nástroj ke zlepšení kvality vnitřního prostředí: případová studie poutní kaple Svatých schodů	356	LYSCZAS, KABEL: Adaptive Ventilation Towards Better IEQ: A Case Study of the Pilgrimage Chapel of Holy Stairs	356
MAZANEC, KABEL: Osobní větrání s úpravou teploty vzduchu: Dopad na návrh zařízení a tepelnou pohodu uživatele.	362	MAZANEC, KABEL: Personalised Ventilation with Air Temperature Customisation: Impact on the Design and Thermal Comfort of the User	362
NEHASIL, ADAMOVSÝ: Strategie řízení chlazení větracím vzduchem pro systémy s proměnným průtokem vzduchu	366	NEHASIL, ADAMOVSÝ: Ventilative Cooling Control Strategy for Variable Air Volume Ventilation Systems	366
RACHMAN, ZAVŘEL, TORRENS, HENSEN: Simulační posouzení úpravy vlhkosti v systémech chlazení data center s ekonomizérem na straně vzduchu	374	RACHMAN, ZAVŘEL, TORRENS, HENSEN: A Simulation-Based Assessment of Humidity Treatment in Data Centre Cooling Systems with Air-Side Economisers	374
<b>ALTERNATIVNÍ ZDROJE ENERGIE</b>		<b>ALTERNATIVE ENERGY SOURCES</b>	
SKANDALOS, TYWONIAK, STANEK, MAIEROVA: Fotovoltaický potenciál v Praze – Metodika a hodnocení pro obytné budovy	382	SKANDALOS, TYWONIAK, STANEK, MAIEROVA: The PV Potential in the City of Prague: Methodology and Assessment for Residential Buildings	382

## Odborný recenzovaný časopis Společnosti pro techniku prostředí

Člen Českého svazu VTS, člen REHVA, asociovaný člen ASHRAE

### REDAKCE

Vladimir.Zmrhal@fs.cvut.cz, tel.: 224 352 433, homolova.vvi@gmail.com, tel.: 778 444 677.

### PŘEDPLATNÉ

Česká republika: **SEND Předplatné**, s. r. o., Ve Žlíbku 77/1800, hala 3, 193 00 Praha 9, tel.: 225 985 225, fax: 225 341 425, send@send.cz, www.send.cz. Administrace: Marek Rybenský, marek@send.cz.

Roční předplatné **250 Kč**, studenti **125 Kč** včetně poštovného.

Slovenská republika: **MAGNET PRESS, SLOVAKIA s. r. o.**, P. O. Box 169, 830 00 Bratislava. Předplatné: predplatne@press.sk, tel./fax: +421 267 201 930-1. Sídlo firmy Šustekova 8, 851 04 Bratislava. Roční předplatné **10,80 €**.

Volný prodej a zaslání na dobírku: Univerzitní knihkupectví ČVUT, budova NTK, Technická 6, 160 80 Praha 6, vera.mikulkova@ctn.cvut.cz, tel.: 224 355 003 nebo osobně v redakci.

Inzeráty přijímá a informace o podmínkách inzerce podává Věra Jírová, tel.: 241 401 229, 603 180 596, vera.jirova.vvi@gmail.com nebo Vladimír Zmrhal, vladimir.zmrhal@fs.cvut.cz, tel.: 224 352 433.

### Za obsah inzerce ručí objednatel.

Podávání novinových zásilek v ČR povoleno Ředitelstvím pošt, Praha čj. NP 1727/1993 ze dne 23. 3. 1993.

**Jazyková korektura:** Harvey Cook

**Sazba:** Josef Zima, js.zima@email.cz

STP je plátcem DPH. Expedice online. ISSN 1210-1389. Registrace MK ČR E 6050. © Společnost pro techniku prostředí

Časopis je zařazen do mezinárodní databáze SCOPUS.

**Scopus**

Ing. Lucie DOBIÁŠOVÁ  
Ing. Daniel ADAMOVSÝ, Ph.D.

CTU in Prague, Faculty of Civil  
Engineering, Department of  
Indoor Environmental and  
Building Services Engineering

Reviewer  
Ing. Petr ZELENSKÝ

# The CFD Simulation of a Standing Person in an Indoor Environment

## CFD simulace stojícího člověka ve vnitřním prostředí

*The article presents a virtual model of a standing person in an indoor environment. A virtual manikin is placed in the room with displacement ventilation where the cold air supplied to the room at low velocity is heated by heating sources and rises up due to buoyancy forces. The calculation is carried out for three different turbulence models:  $k-\omega$  SST,  $k-\epsilon$  Realizable and  $k-\epsilon$  RNG. The simulation results are compared with experimental data using velocity and temperature profiles in four transverse planes. As a result, the verified model of a person is obtained that can further be applied to the particular conditions.*

**Keywords:** CFD, indoor environment, heat sources, occupants, convective flow, numerical model, turbulence model

*Článek představuje virtuální model stojící člověka ve vnitřním prostředí. Virtuální manekýn je umístěn do prostoru se zaplavovacím větráním, kdy je do místnosti přiváděn chladný vzduch nízkou rychlostí, který je ohříván od tepelných zdrojů a díky vztlačovým silám stoupá vzhůru. Výpočet je proveden pro tři různé modely turbulence –  $k-\omega$  SST,  $k-\epsilon$  Realizable a  $k-\epsilon$  RNG. Výsledky simulace s experimentálními daty jsou porovnány pomocí rychlostních a teplotních profilů ve čtyřech příčných rovinách. Výsledkem je ověřený model člověka, který lze dále aplikovat do konkrétních podmínek.*

**Čláňová slova:** CFD, vnitřní prostředí, zdroje tepla, konvektivní proud, numerický model, model turbulence.

## INTRODUCTION

According to ASHRAE Guidelines [1], people spend 80–90 % of their time in buildings. It is proven that problems with indoor environment quality (IEQ) directly influence the comfort, health and productivity of the people [2, 3]. The indoor environment and its quality can be assessed by a couple of factors such as the thermal comfort, the air quality, the mental comfort, the acoustic comfort, etc. All the aforementioned parts create a set that may have both a short-term and long-term impact on the individuals [4, 5].

There are pollutants of various compositions and in various quantities in the indoor environment. A part of these pollutants enters the building from the outdoor environment due to the ventilation air, while others can be produced directly in the building. Typical sources include building materials and internal equipment such as computers, printers, etc. However, man himself and his activities represent the greatest sources of pollutants in the indoor environment. A person in the indoor environment functions as an obstacle for air flow in the room, is a significant heat source inducing convective flow and, last but not least, a source of carbon dioxide, odours, and microbes.

In recent years, the issue of the possible transfer of pollutants among individuals has come to the forefront. This topic was subject to several experimental studies [6, 7] that have examined the influence of both the distance and position between two people. Such experiments require two or more thermal manikins and the necessary laboratory apparatus, whose purchase price is rather high. As an alternative, a Computation Fluid Dynamics (CFD) simulation with a model comprising one or more people can be used. Thanks to numerical modelling, it is possible to obtain a general picture of the room's airflow and of the temperature field distribution, particularly in the vicinity of the human body. To examine the quality of the inhaled air and the risk of pollutants spreading, advanced models with a breathing function added can be used, for more info, refer to works of Bjorn and Nielsen [8] or Gao and Niu [9].

A disadvantage of the computer model (in addition to the required computational resources and time) is the necessity of having the results verified, preferably using measured data obtained by experimentation. Since it is neither possible nor effective to solve each task experimentally, the model can be validated on the basis of a similar task or using benchmark tests. The latter represent a set of boundary conditions and the resulting data of the required quantities that can be used for the verification of the task. For the purposes of this study, the benchmark test made by Nielsen in 2003 [10] has been used; the test will be described in detail in the following sections.

## THE CFD MODEL

### Model geometry

Models of a virtual person started appearing in the nineties of the last century and prevaillingly featured simplified shapes, i.e., cuboids or cylinders [11, 12, 13]. The advancing development of computer technology allowed for the creation of more precise models and even detailed shapes of a real man. The most complex geometries were then created by laser scanning of thermal manikins. Both groups (simplified as well as detailed models) have both advantages and disadvantages. The main advantage of the simple geometry consists in smaller demands for computational resources; it is more appropriate when providing a general picture of the airflow in the space being examined. If, however, the vicinity of person is a matter of interest, for example, when solving the quality of inhaled air and the spread of the pollutants, real complex geometry needs to be considered.

The model geometry of a person used in this study has been provided by Prof. P. V. Nielsen and his colleague Mr L. Liu. This virtual manikin (see Figure 1) represents a standing woman approx. 1.65 m high. It was created by laser scanning of a virtual manikin to have been used for the aforementioned benchmark test. The virtual manikin is divided into several segments, is naked and without hair. Both hands and feet are

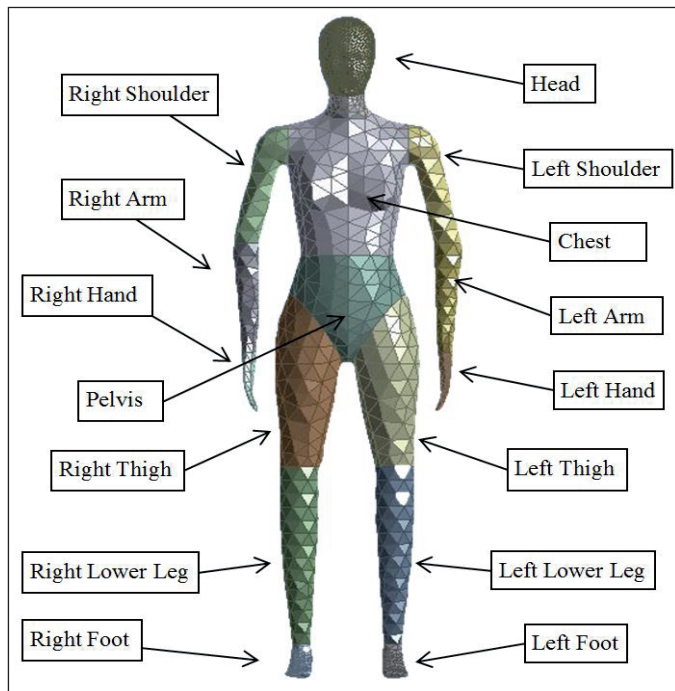


Fig. 1 Geometry of the virtual manikin

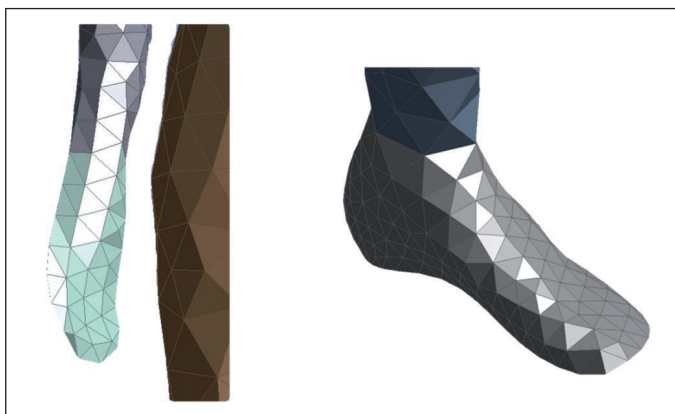


Fig. 2 Simplification of the hands and feet

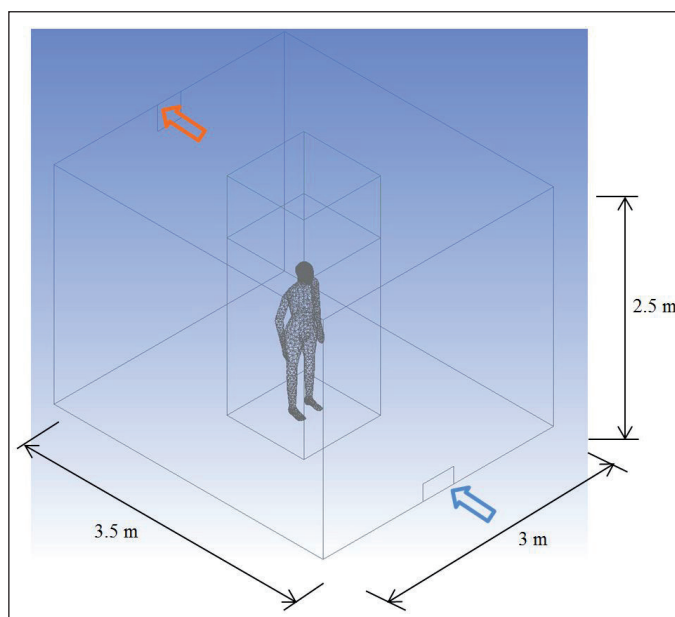


Fig. 3 Diagram of the chamber

simplified (see Figure 2) because they are not critical for the picture of the airflow in the surroundings of the body. The total area of the body is 1.48 sq. meters.

Figure 3 shows the geometry of the solved area corresponding to the experimental chamber in which the benchmark test was made. It is a space that has the dimensions of  $3.5 \times 3 \times 2.5$  m and is equipped with a displacement ventilation system. In general, this system can be described as a system supplying cold air to the lower part of the room where indoor heat sources cause the air being heated to rise so that it carries away the pollutants. In this case the clean air enters the room via the inlet element near the floor that has the dimensions of  $0.2 \times 0.4$  m and is located in the front wall in front of the manikin. An outlet with the dimension of  $0.3 \times 0.3$  m is located in the rear wall under the ceiling. The manikin is placed in the middle of the room, 5 cm above the floor to avoid any heat conduction from the manikin to the floor.

### Boundary conditions

The basic interaction between the human body and the environment is the transfer of heat produced due to the body's metabolism depending on the physical level. A part of this heat is accumulated inside the body, but the prevailing part is released into the surroundings and represents heat losses of man. These losses can be divided into sensible (due to convection, radiation and conduction) and latent (due to sweating, breathing and diffusion of water vapour through the skin). Most numerical calculations only consider the sensible losses, since the modelling of latent losses is a rather difficult process and requires that a thermoregulation model of a human body to be deployed. For the purposes of this study, only the sensible heat losses due to convection and radiation have been taken into account.

For the solution of the heat transfer between the man and his surroundings, the numerical methods can apply to two types of boundary conditions, the body surface temperature or the surface heat flux. The values of the body surface temperature may range from  $31^\circ\text{C}$  to  $34^\circ\text{C}$  [14 – 17]. When the heat flux is used as a boundary condition, its value will differ depending on whether or not the radiation is considered in the calculation. If only the convection is included the heat flux, it is between  $20\text{ W/m}^2$  [18] and  $25\text{ W/m}^2$  [7]. When the radiation is considered in the calculation, the value of the heat flux is usually over  $50\text{ W/m}^2$ , e.g., Ito et al. considered  $51.6\text{ W/m}^2$  [19] or Villi and De Carli used  $53.5\text{ W/m}^2$  [20].

The benchmark test prescribes a total heat load of 38 W for the convection only and 76 W for the model with the radiation. The radiation has been considered in all the simulations, as it may have a considerable influence on the final results [13]. The thermal boundary condition for the manikin was set up as a constant heat flux of  $51.4\text{ W/m}^2$  (i.e., considering the surface body area  $1.48\text{ m}^2$ , the total heat flux was equal to 76 W). The emissivity of the manikin's surface was 0.95 and 0.9 for the walls. In addition, 10 W has been added for the chamber surfaces as the heat flux according to the heat balance calculation by Srebric et al. [21]. The parameters of the inlet air are defined by the temperature of  $21.8^\circ\text{C}$  and the constant velocity of  $0.182\text{ m/s}$  (i.e., the room air exchange rate was approx.  $1.9\text{ h}^{-1}$ ).

### Calculation and model validation

The accuracy of the simulation results depends on the quality of the computational grid, the creation of which takes the prevailing time of the whole simulation process. To ensure the effective creation of the grid, the solved domain was divided into three parts: a cuboid around the virtual manikin, a cuboid in the area above the head where significant convective flow is expected, and a third area in the remaining space. The unstructured mesh was used for the entire domain, but with

different cell sizes for each part. The grid element size was 0.025 m in the cuboid around the manikin (with a surface element size of 0.007 m); 0.03 m above his head and 0.035 in the rest of the domain. In order to solve the boundary layer, ten layers of prismatic cells with a growth rate of 1.2 were created near the manikin's surface and seven layers with the same growth rate near the chamber walls. The value of  $y^+$  over the manikin's surface was less than one. The computational grid has approx. 5 million cells altogether.

The selection of a turbulence model represents an important part of the computation. In the field of indoor environment modelling, two-equation models  $k-\epsilon$  and  $k-\omega$  are the most frequently used. In addition to the selection of a suitable turbulence model, it is important to properly solve the convective boundary layer for solid surfaces. It can be ensured by the application of a wall function or by the integration of the governing equations through the whole boundary layer.

The calculation was carried out for two turbulence models from the group  $k-\epsilon$ , i.e.,  $k-\epsilon$  Realizable and  $k-\epsilon$  RNG (Re-Normalisation Group). In both cases, no wall function was used, which means that the calculation was made across the entire boundary layer. As the third model, which is also frequently used for the indoor environment simulations, the  $k-\omega$  SST (Shear Stress Transport) model was applied. The steady-state simulations have been carried out with the SIMPLE algorithm for the pressure-velocity coupling. For the solver control, the residual target was set to  $10^{-4}$  ( $10^{-6}$  for the energy). The radiation flux was calculated using the Discrete ordinates model.

The used benchmark test provides the measured values of the airflow velocity and air temperature in four poles (L1, L2, L4, L5), at several levels, as well as some results of the Particle Image Velocimetry (PIV) measurements made near the body (L3, L6). The places of the measurements are shown in Figure 4. Using the measured and simulated values, it is possible to assess the vertical profiles of the air velocities and temperatures in the individual locations and compare one turbulence model to another.

DISCUSSION OF THE RESULTS

Temperature field

Figures 5 through 8 show the comparisons of the calculated vertical temperature profiles in the L1, L2, L4 and L5 poles to the experimental

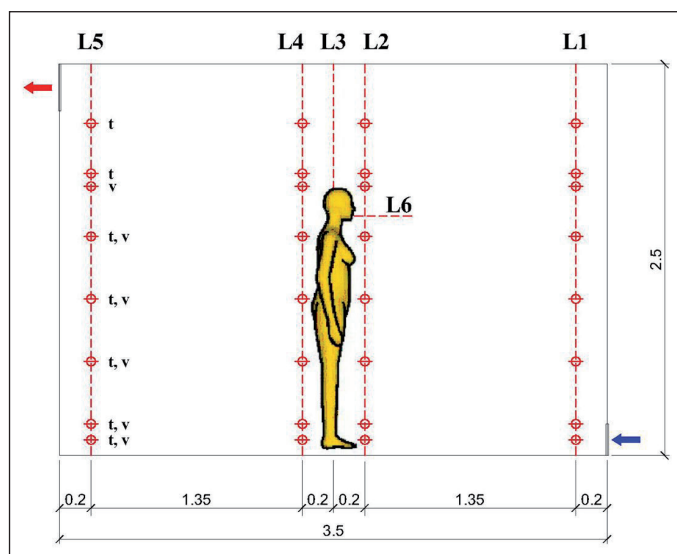


Fig. 4 Measurement locations (t – location for the air temperature measurement, v – location for the air velocity measurement)

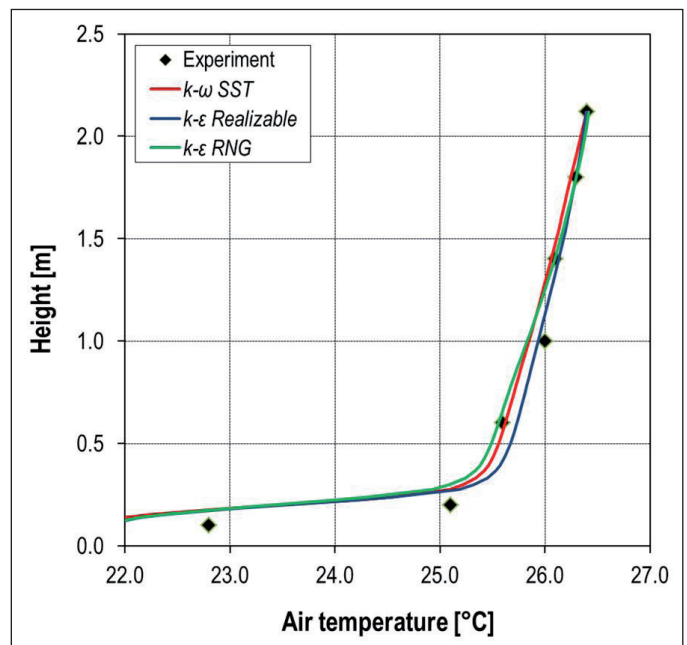


Fig. 5 Temperature magnitude profile (L1)

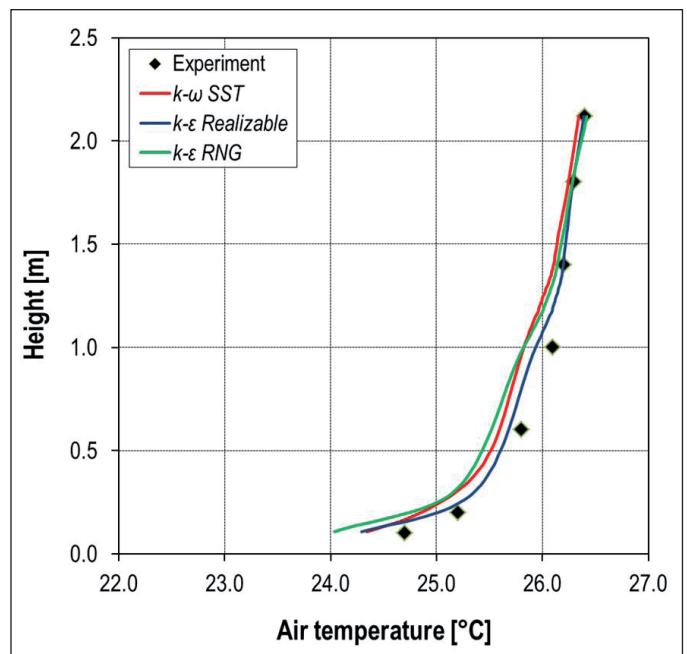


Fig. 6 Temperature magnitude profile (L2)

data. From the first comparison of the individual profiles, it is obvious that the turbulence models  $k-\epsilon$  feature an almost identical course, while  $k-\omega$  SST slightly differs, especially in L4. The models  $k-\omega$  SST and  $k-\epsilon$  Realizable at a level of 1 m show the greatest difference, nearly 0.5 °C. An interesting trend can be observed in the vertical profile, in position L5, where the differences in the individual cases at a level of 0.1 m are approx. 0.2 °C; with the increasing height, this difference gets smaller. In the highest point of the profile, the temperatures are practically identical.

In general, the trend of the results corresponds to the principle of the displacement ventilation when the air temperature shows the lowest value near the floor and starts increasing with the increasing height. Based on the diagrams, it is possible to read the total vertical temperature gradient in the room that shows the greatest value in L1, more than 4 °C. As

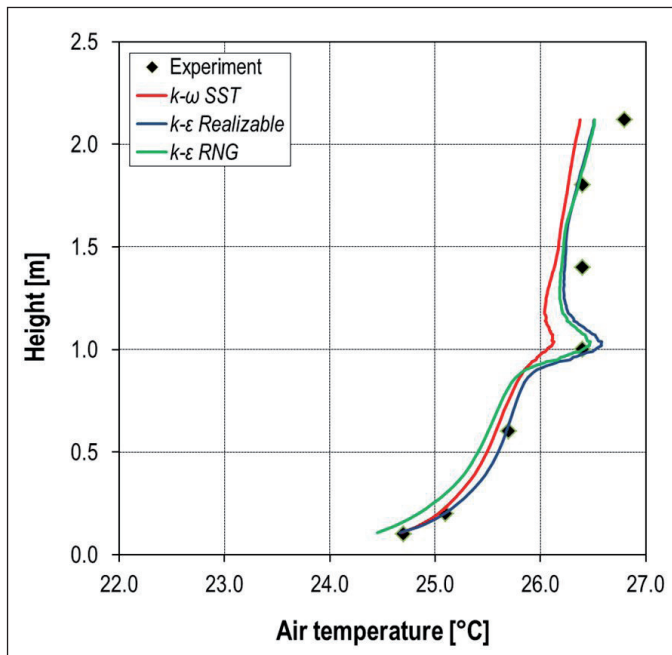


Fig. 7 Temperature magnitude profile (L4)

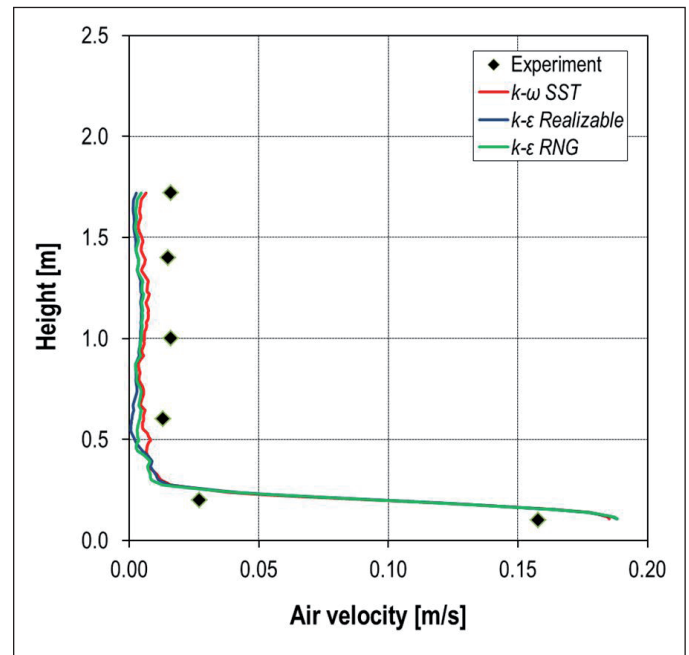


Fig. 9 Velocity magnitude profile (L1)

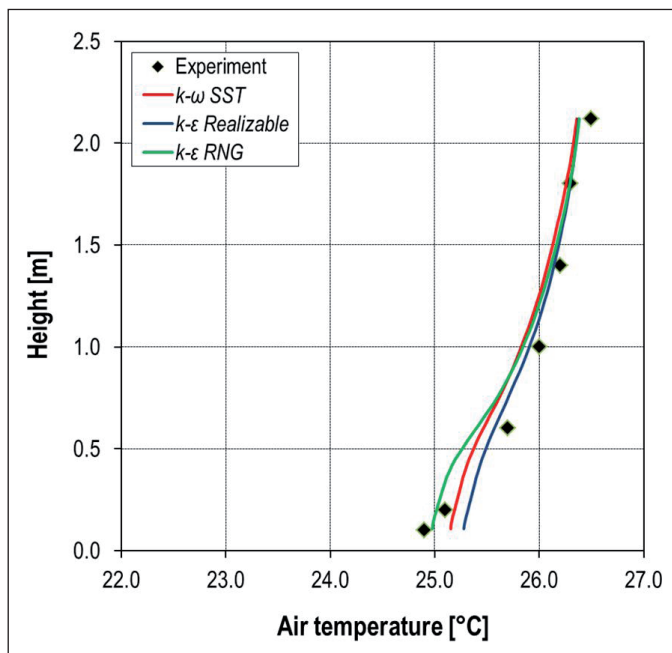


Fig. 8 Temperature magnitude profile (L5)

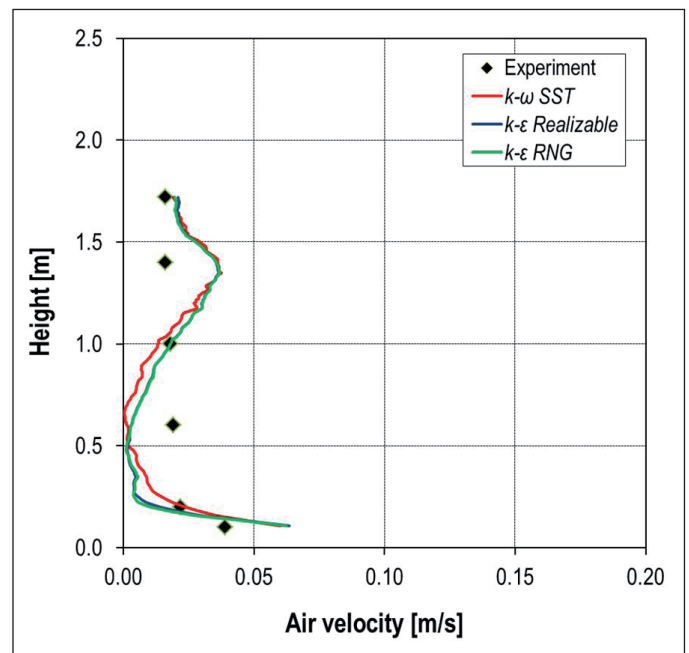


Fig. 10 Velocity magnitude profile (L2)

the air passes through the room, it slowly mixes with the heated air, and the temperature gradient gets lower in the other poles. In the location of the L2 profile and the L4 profile, it equals 2.5 °C and 2 °C, respectively; its lowest value, i.e., only 1.1 °C, was found in the last pole, L5.

### Velocity fields

The following Figures (9 through 12) show the profiles of the airflow velocities. The velocity profiles in the simulations with the models  $k-\epsilon$  are very similar to each other, while the  $k-\omega$  SST slightly differs. The profiles in L1 and L5 show the smallest differences between the turbulence models; at the same time, these profiles show the same trend like the experimental data. Nevertheless, the calculated values in both profiles were lower when compared to the measured values. The reasons are not yet clear for this. One explanation can be the influence of the used turbulence model. Srebric et al. [21] reached

the same results with the  $k-\epsilon$  models in both poles, as well as Deevy et al. [22] with  $k-\omega$  SST, while the Large Eddy Simulation (LES) models slightly overestimated the air velocity in the study of Tagninia et al. [23]. The greatest differences between the individual models were found in L4 again, at the level of 1 m, where the  $k-\epsilon$  models have significantly exceeded the  $k-\omega$  SST model which corresponds to the experimental data very well. When the simulation results are compared to the experimental data, the greatest differences have been found in L4 as well as in L2, i.e., close to the manikin. In both profiles, the calculated velocities in the lower half of the chamber are lower when compared to the measured data, but from the level of 1 m upwards, they exceed the experimental data.

### Summary of the results, and other model possibilities

To obtain a general view of the airflow in the space and the temperature

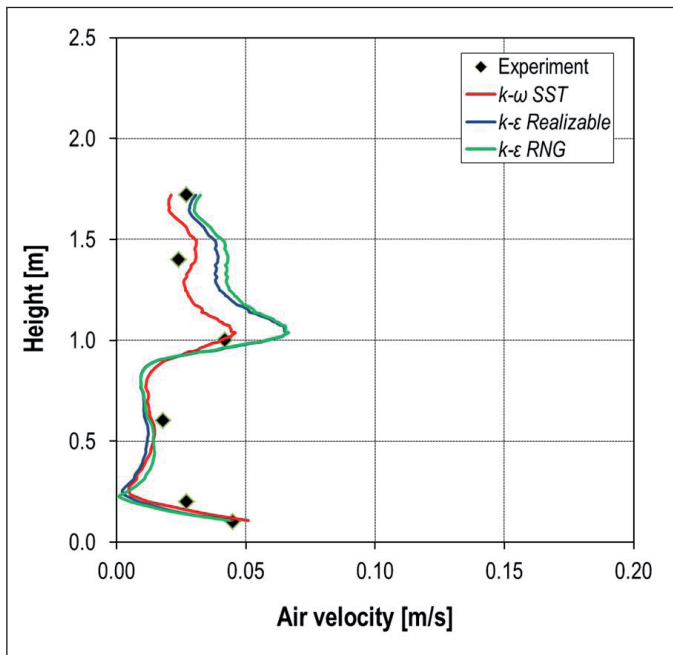


Fig. 11 Velocity magnitude profile (L4)

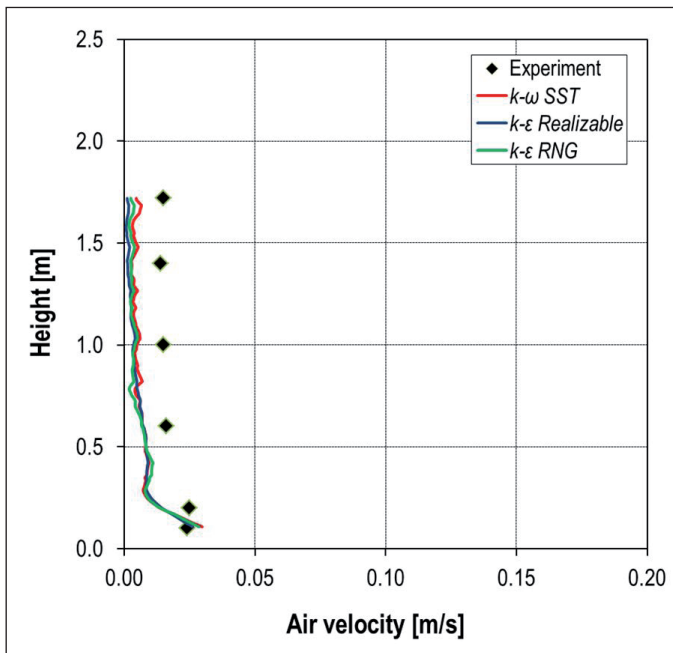


Fig. 12 Velocity magnitude profile (L5)

field distribution, Figures 13 and 14 show the longitudinal cross-sections through the middle of the room being solved. Both cross-sections illustrate the airflow from the inlet element in the front wall, the velocity of which becomes less with the increasing distance. Another significant flow that can be observed in the area around the virtual manikin is caused by the difference in the temperatures of the body surface and of the ambient air; it turns into a convective flow rising above the manikin's head. It is just this resulting buoyancy force that affects the exposure of man to air pollutants, especially when a displacement ventilation system is used [24, 25]. The rising heated air not only brings pollutants from the ambient air to the breathing zone, but also particles released from the human skin and clothing. Hence, it is obvious that the convective boundary layer around the human body imminently affects the occupants and has a high importance when solving the inhaled air quality, thermal comfort, etc.

CONCLUSION

The given article has presented a virtual model of an individual in the indoor environment. It is a woman approx. 1.65 m in height standing in the room equipped with a displacement ventilation system. The model geometry was created based on the benchmark test [10], to which the results have been compared. The calculation was made for three different turbulence models, *k-omega SST*, *k-epsilon Realizable* and *k-epsilon RNG* (in all the cases, no wall function was used). The simulation results were compared to the experimental data using the velocity and temperature profiles in four poles. The results of all the simulations corresponded to the trend of the experiments quite well; greater differences were found in the profile of the airflow velocities, particularly in the surroundings of the manikin. However, it should be noted that airflow velocities were very low in the entire space and did not exceed a value of 0.05 m/s except for the L4 profiles. At such low values, it is disputable as to what extent the measured data is relevant, because common anemometers are operated at an error up to  $\pm 0.03$  m/s. The individual turbulence models can also be compared in the area close to the manikin where the PIV measurements were made. Nevertheless, such an assessment is rather extensive and goes beyond the capacity of this article.

In conclusion, it is possible to say that the best compliance with the experiment was achieved in the turbulence model *k-epsilon Realizable*, namely in all temperature profiles. The *k-epsilon RNG* model showed the same trend like *k-epsilon Realizable*; nevertheless, its resulting temperatures were lower.

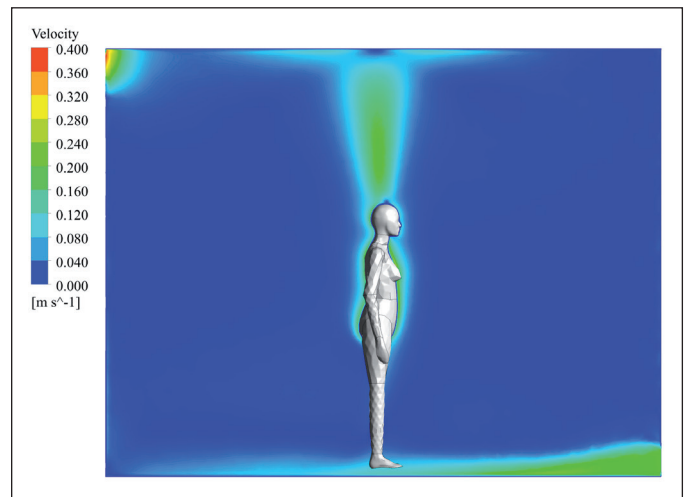


Fig. 13 Velocity contours along the symmetry plane

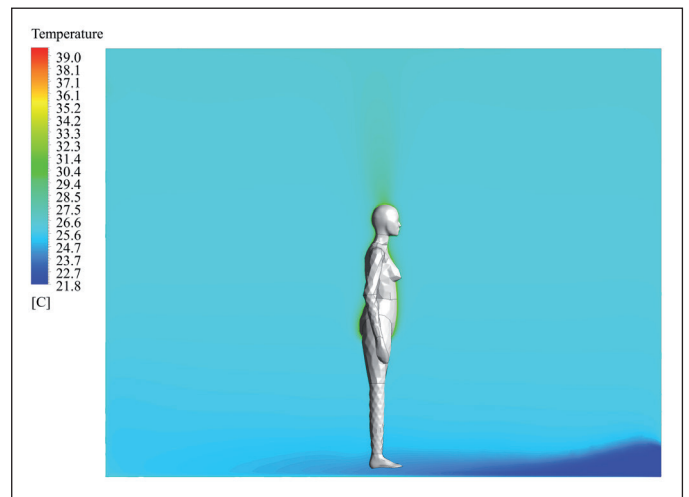


Fig. 14 Temperature contours along the symmetry plane

The lowest air temperatures were found in the case with the  $k-\omega$  SST turbulence model. Yet, this model copied the trend of the velocity profile in L4 very well, where, in contrary, the  $k-\varepsilon$  turbulence models overestimated the results. Both models ( $k-\varepsilon$  Realizable and  $k-\omega$  SST) are widespread in the field of indoor environment modelling.

This study is part of the ongoing research focused on the complex numerical modelling of a human body in an indoor environment. Another part of the research is the evaluation of the methods of heat transfer modelling between the human body and its surroundings (fixed surface temperature vs. fixed heat flux), the influence of radiation modelling, the ways of solving the heat transfer coefficients, etc. The result will be a verified virtual manikin that can be used for assessing the indoor environment whenever in-situ measurements are not feasible. Furthermore, it will be possible to extend the model by other functions such as a breathing model and to focus on the study of the issue of air pollutants spreading and the inhaled air quality. Currently, this can only be carried out using a thermal manikin together with, for example, PIV measurements, which is rather expensive and inflexible. In addition, the virtual environment allows one to change the boundary conditions practically without any limitations and to model very specific spaces.

Contact: [lucie.dobiasova@fsv.cvut.cz](mailto:lucie.dobiasova@fsv.cvut.cz)

This paper was supported by SGS17/120/OHK1/2T/11.

## Literature

- [1] *Guideline 10P: Interactions Affecting the Achievement of Acceptable Indoor Environments*, Second Public Review. Atlanta, USA: ASHRAE, 2010.
- [2] DE GIULI V., DA POS O., DE CARLI M. Indoor environmental quality and pupil perception in Italian primary schools. In: *Building Environment*, 2012, Vol. 56, pp. 335-345.
- [3] BLUYSSSEN P., FERNANDES E., FANGER P. O., GROES L., et al. *European Audit Project to Optimize Indoor Air Quality and Energy Consumption in Office Buildings* (No. LESO-PB-REPORT-2008-006), 1995.
- [4] FISK W. J., LEI-GOMEZ Q., MENDELL M. J. Meta-analyses of the associations of respiratory health effects with dampness and mold in homes. In: *Indoor Air*, 2007, Vol. 17, Issue 4, pp. 284-296.
- [5] WARGOCKI P., SUNDELL J., BISCHOF W., BRUNDRETT G., et al. Ventilation and health in nonindustrial indoor environments: report from a European multidisciplinary scientific consensus meeting (EUROVEN). In: *Indoor Air*, 2002, Vol. 12, Issue 2, pp. 113-128.
- [6] BJORN E., NIELSEN P. V. Dispersal of Exhaled Air and Personal Exposure in Displacement Ventilated Rooms. In: *Indoor Air*, 2002, Vol. 12, No. 3, pp. 147-164.
- [7] Brohus H., Nielsen P. V. Personal exposure in ventilated rooms with concentration gradients. In: *Proceedings of Healthy Buildings 1994*, Vol. 2, pp. 559-564.
- [8] BJORN E., NIELSEN P. V. CFD simulation of contaminant transport between two breathing persons. In: *Proceedings of Roomvent 1998, The 6th International Conference on Air Distribution in Rooms*, Stockholm, Sweden, Vol. 1, pp. 133-140.
- [9] GAO N., NIU J. Transient CFD simulation of the respiration process and inter-person exposure assessment. In: *Building and Environment*, 2006, Vol. 41, pp. 1214-1222.
- [10] NIELSEN P. V., MURAKAMI S., KATO S., TOPP C., YANG J. H. *Benchmark Tests for a Computer Simulated Person*. Department of Building Technology and Structural Engineering Aalborg University, Denmark, ISSN 1395-7953 R0307, 2003.
- [11] Topp C., Hesselholt P., Trier M. R., Nielsen P. V. Influence of geometry of thermal manikins on contaminant distribution and personal exposure. In: *Proceedings of Healthy Buildings 2003*, Vol. 2, pp. 357-362.
- [12] BROHUS H. *Personal exposure to contaminant sources in ventilated rooms* [PhD thesis]. Denmark: Aalborg University, 1997.
- [13] DEEVY M., GOBEAU N. *CFD modelling of benchmark test cases for a flow around a computer simulated person*. HSL/2006/51. Buxton, UK: Health and Safety Laboratory, 2006.
- [14] SORENSEN D. N., VOIGT L. K. Modelling Flow and Heat Transfer around a Seated Human Body by Computational Fluid Dynamics. In: *Building and Environment*, 2003, Vol. 38, pp. 753-762.
- [15] RUSSO J., KHALIFA H. E. Computational study of breathing methods for inhalation exposure. In: *HVAC&R Research*, 2011, Vol. 17, Issue 4, pp. 419-431.
- [16] MURAKAMI S., ZENG J., HAYASHI T. CFD analysis of wind environment around a human body. In: *Journal of Wind Engineering and Industrial Aerodynamics*, 1999, Vol. 83, pp. 393-408.
- [17] NILSSON H. O., BROHUS H., NIELSEN P. V. CFD Modeling of Thermal Manikin Heat Loss in a Comfort Evaluation Benchmark Test. In: *Proceedings of Roomvent 2007, The 10th International Conference on Air Distribution in Buildings*, Helsinki, Finland, 2007.
- [18] HAYASHI T., ISHIZU Y., Kato S., MURAKAMI S. CFD analysis on characteristics of contaminated indoor air ventilation and its application in the evaluation of the effects of contaminant inhalation by a human occupant. In: *Building and Environment*, 2002, Vol. 37, pp. 219-230.
- [19] ITO K., INTHAVONG K., KURABUCHI T., UEDA T., et al. CFD Benchmark Tests for Indoor Environmental Problems: Part 3 – Numerical Thermal Manikins. In: *International Journal of Architectural Engineering Technology*, 2015, Vol. 2, pp. 50-75.
- [20] VILLI G., DE CARLI M. Detailing the effects of geometry approximation and grid simplification on the capability of a CFD model to address the benchmark test case for flow around a computer simulated person. In: *Building simulation*, 2014, Vol. 7, pp. 33-35.
- [21] SREBRIC J., VUKOVIC V., HE G., XANG X. CFD boundary conditions for contaminant dispersion, heat transfer and airflow simulations around human occupants in indoor environments. In: *Building and Environment*, 2008, Vol. 43, pp. 294-303.
- [22] DEEVY M., SINAI Y., EVERITT P., VOIGT L., GOBEAU N. Modelling the Effect of an Occupant on Displacement Ventilation with Computational Fluid Dynamics. In: *Energy and Buildings*, 2008, Vol. 40, pp. 255-264. ISSN 0378-7788.
- [23] TAGHINIA J. H., RAHMAN M. M., LU X. Effects of different CFD modeling approaches and simplification of shape on prediction of flow field around manikin. In: *Energy and Buildings*, 2018, Vol. 170, pp. 47-60.
- [23] HOMMA H., YAKIYAMA M. Examination of free convection around occupant's body caused by its metabolic heat. In: *ASHRAE Transaction*, 1988, Vol. 94, pp. 104-124.
- [24] VOELKER C., MAEMPEL S., KORNADT O. Measuring the human body's microclimate using a thermal manikin. In: *Indoor Air*, 2014, Vol. 24, pp. 567-579.

Ing. Jan WEYR  
 doc. Ing. Ondřej ŠIKULA, Ph.D.  
 prof. Ing. Jiří HIRŠ, CSc.

Institute of Building Services,  
 Brno University of Technology

Reviewer  
 Ing. Miloš Lain, Ph.D.

# Building Performance Simulation of Industrial Hall with Excessive Heat Loads

## Dynamická simulace vnitřního prostředí v průmyslové hale s nadměrnou tepelnou zátěží

Numerical simulations are becoming an integral part of the design procedure of buildings, building systems and technologies allowing for not only evaluating the building energy demands and indoor quality but also for studying the influence of various design parameters and aspects of a building's internal microclimate. In this case study, a numerical simulation of an internal microclimate in an industrial building in the simulation software BSim 2002 was performed in order to assess the internal microclimate, examine the effect of pre-cooling and determine the required cooling capacity. Furthermore, this article deals with the analysis of the influence of excessive internal gains caused by bogie-hearth chamber furnaces and their implementation into the simulation software. The results illustrate the minor effect of precooling for this case study and the insufficiency of the cooling capacity in the investigated industrial object.

**Keywords:** transient simulation; BSim; Industrial building; Internal microclimate; Chamber furnaces

Dynamické numerické simulace se postupně stávají nedílnou součástí procesu návrhu budov a jejich technických zařízení. Tyto simulace nejen umožňují vyhodnocení energetické náročnosti návrhu budovy, ale také studium rozličných návrhových parametrů a aspektů vnitřního prostředí. V této případové studii průmyslového objektu sloužícího k tiskařským účelům bylo provedeno zhodnocení vnitřního prostředí, zjištění možného pozitivního vlivu předchlazování budovy upravovaným vnějším vzduchem a určení potřebného chladicího výkonu pomocí simulace v softwaru BSim 2002. Dále se tento článek zabývá analýzou vlivu nadměrných vnitřních zisků z velkokapacitních vozokomorových pecí na keramiku a implementací provozu těchto pecí do dynamického simulačního procesu. Výsledky této práce ilustrují malý vliv předchlazování pro daný typ objektu a množství nadměrných vnitřních zisků z technologií, a také nedostatek navrženého chladicího výkonu vzhledem k úpravám výrobních postupů ve zkoumané budově.

**Klíčová slova:** dynamická simulace; BSim; průmyslová budova; vnitřní prostředí; komorová pec

## INTRODUCTION

With computer advancements, numerical simulations are quickly becoming an integral part of the design procedure of buildings, building systems and technologies. The numerical simulations allow us not only to evaluate the building energy demands and the internal microclimate but also to study the influences of various design parameters [1]. In this paper, a procedure of the creation and simplification of a building model in BSim 2002 software environment is described with a strong emphasis on the balance between the final accuracy and complexity of the given model. BSim is a software tool to simulate the dynamic behaviour of transient systems, an integrated PC tool is used to analyse buildings and their installations [2]. Furthermore, this paper describes the models' validation using *in situ* measured data in the given building object during a summer period.

The task of this case study was also to examine the possibility of night cooling during the summer period and to investigate its effect on the internal microclimate. The application of building precooling leads to reducing the peak cooling requirements, described in [3]. The major part of the internal gains in the test object is produced by bogie-hearth chamber furnaces. The analysis of these furnaces is also assessed and described in the following study.

## BUILDING DESCRIPTION

The examined building is located in Brno in the Czech Republic and serves for purposes of a company engaged in the manufacture, sale and printing of promotional items and gifts together with the relat-

ed services. There are several printing operations and procedures in the new printing hall and adjacent rooms generating excessive internal gains and odour. The simple situational plan is displayed in Fig. 1 in a satellite view with the highlighted position of the new printing hall and its adjacent buildings. The surrounding of the investigated object is formed by commercial and industrial buildings and by mid-rise apartment buildings.

The old part of the investigated object was built in the 1970s; the big printing hall was constructed in 2008. The external walls of the older part of the printing complex are made of burnt bricks; these walls are not thermally insulated. The internal walls in the older part of the object are made of drywall, panels made of calcium sulphate dihydrate and

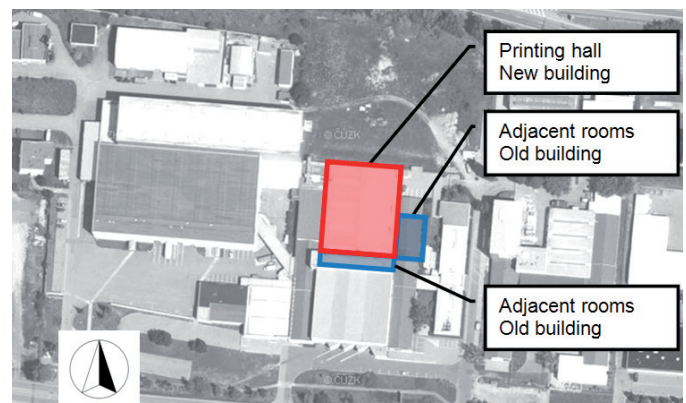


Fig. 1 The examined industrial complex with the location of assessed building objects highlighted

insulated with mineral wool between the panels. The new building is a bigger printing hall with no internal walls between the workplaces with different printing procedures. The external walls in this new part are made of wall sandwich PUR panels (a rigid polyurethane core coated with galvanised sheet metal). Floors in contact with the ground in both the older and the newer part consist of load-bearing concrete, mineral wool insulation and a finishing layer made of PVC. The detailed building compositions used for the BSim computational model are described in Table 1 and 2.

The ventilation and heating of the inspected spaces is provided by one air handling unit placed on the roof of the older object. The heating capacity of this unit is 177 kW according to the technical lists. The only cooling system in the hall is a multi-split air conditioner whose total nominal cooling capacity is 62.0 kW. The operation of all the units is controlled by a BMS (Building Management System). Historical data obtained from the building's BMS were used for the calibration of the heating, ventilation and cooling system in the BSim model.

Tab. 1 The compositions of the building elements in the old building used for the BSim simulation

Structure	Material	Thickness [mm]	Thermal conductivity $\lambda$ [W/m.K]	Specific heat capacity [J/kg.K]	Bulk density [kg/m <sup>3</sup> ]
Adjacent rooms (old building)					
Floor structure in contact with the ground	PVC floor	1	0.900	1200	1200
	Concrete	100	1.340	1020	2400
	Mineral wool	0.060	0.039	1310	120
	Concrete	250	1.340	1020	2400
External wall	Brick	300	0.250	900	1900
Internal wall 1	Brick	300	0.800	900	1700
Internal wall 2	Plasterboard	125	0.220	1060	1150
	Mineral wool	175	0.036	800	25
	Plasterboard	125	0.220	1060	1150
Floor structure between the two floors	Concrete	250	1.340	1020	2400
Roof	Thermal insulation + metal sheeting	160	0.042	1370	160

Tab. 2 The compositions of the building elements in the new building used for the BSim simulation

Structure	Material	Thickness [mm]	Thermal conductivity $\lambda$ [W/m.K]	Specific heat capacity [J/kg.K]	Bulk density [kg/m <sup>3</sup> ]
Printing hall (new building)					
Floor structure in contact with the ground	PVC floor	1	0.900	1200	1200
	Concrete	100	1.340	1020	2400
	Thermal insulation	160	0.039	1310	120
	Concrete	250	1.340	1020	2400
External wall	PUR panel	120	0.045	1310	112
Roof	Panel roof	160	0.042	1370	160

## INDOOR ENVIRONMENT AND HEAT GAINS

The major problems concerning the internal microclimate occurred during the hot summer periods in 2013 and 2014. The indoor temperatures in the hall were reaching values around 30 °C for longer periods of time and occasionally even above 35 °C with a low relative humidity around 25%. Such high temperatures during the work shifts are in conflict with both European [4] and Czech [5] legislation. Moreover, due to the printing machinery, techniques and technologies, the desired relative humidity for the hall is 45%. There was also a problem with the excessive inconvenient odour from the used technologies in the investigated building object.

A significant part of the heat gains in the buildings serving the printing industry purposes are heat gains from technologies [6]. Overheating of the building was observed during the full working load in the summer period, especially in the part of the printing hall where the bogie-hearth chamber furnaces were located. The values of the heat gains from the installed technologies were determined; the bogie-hearth chamber furnaces were measured *in situ* and further analysed in order to more exactly specify their work cycles and thermal loads.

### THERMAL LOADS OF CHAMBER FURNACES

There are 3 more powerful bogie-hearth chamber furnaces with forced circulation of the internal atmosphere installed in the printing hall together with two smaller furnaces. These furnaces are used for various types of heat treatment of large batches at temperatures up to 850 °C. The electrical input of each of the more powerful chamber furnaces is 45 kW.

A decisive criterion for determining the maximum furnace heat production into the hall space is the ceramic firing process. The work cycle of each of the pumps is divided into 4 phases: warming up of the furnace and ceramics until the temperature reaches 450 °C, the maintaining phase, the burning phase with a temperature up to 850 °C and a cooling phase of both kiln and ceramics. At the end of the warming up phase and the burning phase, a major part of the thermal load is ventilated into the exterior by an independent air handling unit.

Long-term measurements and observations of the electrical consumption, the temperatures in the furnace during the individual phases and airflows in the ventilation ducts were conducted over the years 2014 and 2015. Furthermore, we carried out the short-term *in situ* measurements of the temperatures above the ceramic products during the last phase when the furnace is open and the ceramic products are cooled down in the open space of the printing hall. The simplified diagram of the work cycle with the rates of heat flow from the furnace is displayed in Fig. 2.

The average thermal production of each of the two most powerful bogie-hearth chamber furnaces is 9.8 kW and the smaller chamber furnace is 7.7 kW. In the case of calculating the heat load discharge by the forced ventilation, the calculation heat load of the more powerful furnaces was determined by a time average to 6.5 kW and the smaller furnace to 5.1 kW. These average heat loads must be included with 100% simultaneity into the total heat load of the hall.

The obtained values of heat flows acquired from the long-term and short-term measurements and the subsequent analysis of the work cycle of the chamber furnaces were used for configuring the internal loads in the BSim simulation. The average calculated thermal load per cycle was used as the equipment load in the BSim simulation. The time schedule of this load was configured according to the real historical utilisation data of these furnaces in the hall.

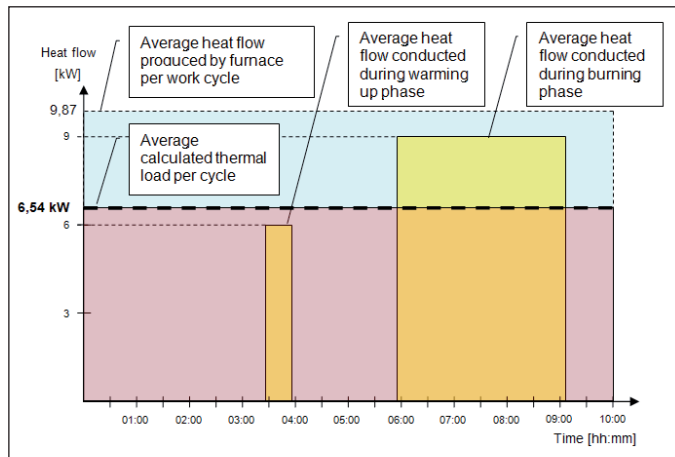


Fig. 2 Diagram of the heat flows from the furnace during the work cycle

**CALCULATION METHODS**

Simulations were carried out in the software BSim 2002. BSim is based on the law of conservation of energy and the law of conservation of mass with calculations solved non-stationary. Heat is described by the equations of heat balance, using the heat balance formula balanced for the zone:

$$\Phi_{constr} + \Phi_{wind} + \Phi_{sol} + \Phi_{sys} + \Phi_{vent} + \Phi_{inf} + \Phi_{mix} = 0$$

where  $\Phi_{constr}$  represents the heat flows from the adjoining constructions,  $\Phi_{wind}$  symbolises the heat flows through the windows,  $\Phi_{sol}$  is the solar radiation through the windows,  $\Phi_{sys}$  is the heat flows from the air penetration from the outdoor air (infiltration, venting),  $\Phi_{vent}$  is the heat flows from the air supplied from the ventilation systems,  $\Phi_{inf}$  stands for the the heat flows from air transferred from other zones [7].

**GEOMETRICAL AND CALCULATION MODEL**

The model created in BSim 2002 was created following the main building characteristics and the boundary conditions using the SimView graphic user interface. The geometrical model of the industrial hall and adjacent room is shown below in Fig. 3. The detailed geometrical model of the roof skylights in the printing hall was implemented due to their large area in size and the large amount of solar gains through these opening anticipated prior to the simulation (see Fig. 4).

Fifty time-steps per hour and a Petersen solar radiation model were se-

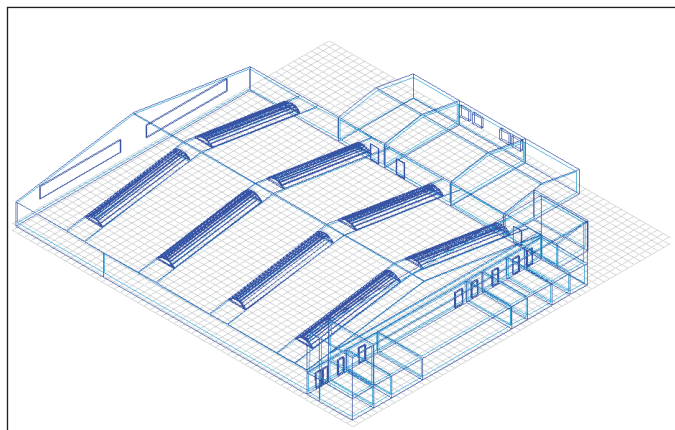


Fig. 3 The geometrical model of the flat and adjacent rooms in BSim

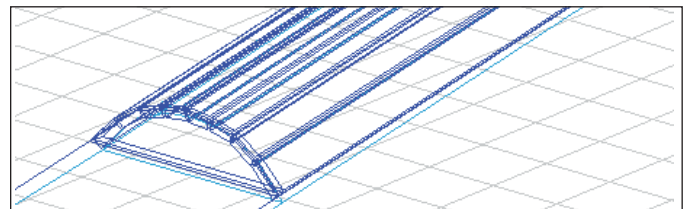


Fig. 4 The geometrical model of the roof skylights

lected for the simulation due to the complexity of the model and the building construction properties.

Real weather data continuously collected by a weather station located at the Brno airport were used; therefore, the model can be validated by this data to create the calculation model as exact as possible.

**CALIBRATION**

First, BSim was calibrated to comply with the room air temperatures measured *in situ* in the printing hall during November and December 2014. The calibration was carried out by changing the amount of ex-filtration/infiltration into the exterior. The value of the infiltration is configured in BSim by setting the value of the basic air change [1/h]. For the BSim simulation, we have tested the infiltration for the following values of basic air change: 0.1, 0.2, 0.3 and 0.4. The data presented in Fig. 5 represents the room temperature difference (the real measured temperature minus the simulated temperature values) for the values of the basic air change in hour time steps during the inspected period. According to Shapiro-Wilk normality test, the KS normality test and the D'Agostino and the Pearson omnibus normality test, the data of the temperature difference does not evince Gaussian distribution; therefore, the median was used as a decisive statistical factor.

The model with the basic air change 0.2 was used as a reference model for the summer simulation (from the 1<sup>st</sup> of June 2014 to the 31<sup>st</sup> of August 2014). The effect of precooling of the building was examined and the cooling capacity of the current cooling system was assessed.

We made simulations of two different methods of operating the building. The first method is the current state: the building heating and also a cooling system which is in operation only during the work shifts and one hour prior the first morning work shift (the first morning shift begins at 6:00) every day during the working days to ensure the internal microclimate conditions meeting the requirements of the Czech and European legislation. The other method of operating the building in-

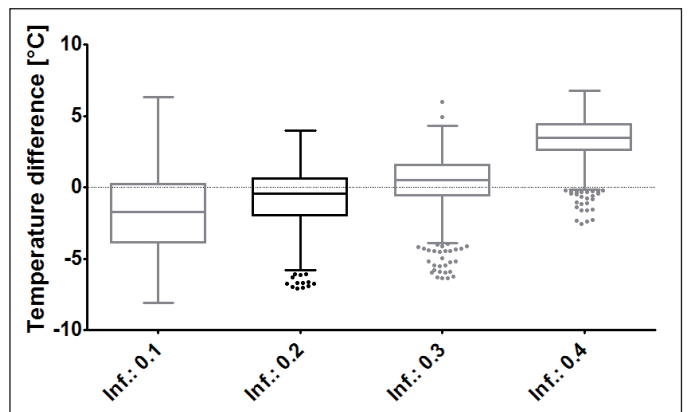


Fig. 5 Configuration of the BSim models using different values of basic air change [1/h] – Tukey box plots with a band inside the box representing the second quartile (median)

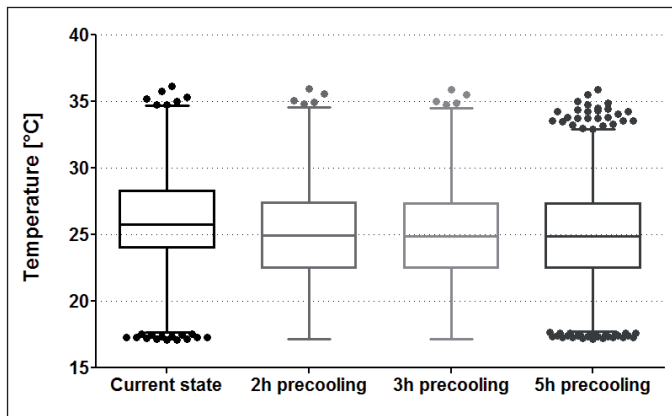


Fig. 6 Box plot displaying the variation in average room temperature samples with different precooling time periods

cludes the night precooling of the printing hall with the multi-split air conditioners and night ventilation prior to the beginning of the morning work shift to 18 °C. The heating and cooling set points were configured to 18 °C and 26 °C, respectively, according to the work classes IIa and IIb given by the Czech legislation [4]. The effect of the precooling of the printing hall was simulated with a different time period before the beginning of the morning work shifts.

## RESULTS

The Tukey box plot in Fig. 6 graphically depicts the sample of the hourly average room air temperatures over the inspected summer period during work hours (workdays from 6:00 to 22:00) with different settings of the precooling of the printing hall.

The results from our simulations show a minor difference for each cooling schedule model. In case of the current state, the room's air temperature above 28 °C occurs for 310 hours in the printing hall during the simulated summer time period, requiring 227 hours for cooling turned on 2 hours before the start of the morning shifts, 223 hours cooling turned on 3 hours prior the start of the morning shifts and 223 hours for a 5 hour-long precooling. The simulated hourly room air temperature averages during the working days in July and August 2014 are displayed in Fig. 7.

The second part of this study deals with the simulation of the printing hall with unlimited cooling power to determine the required power of the building's cooling system. The resulting minimal required cooling power gained from the BSim simulation is 326 kW for the summer period 2014, therefore, the required capacity is about 5 times higher than the installed capacity of the current multi-split air conditioners.

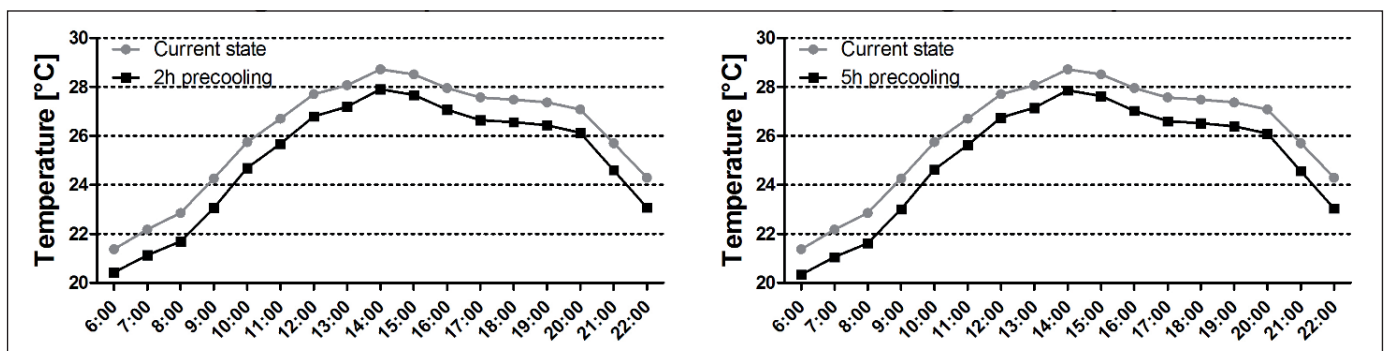


Fig. 7 The hourly room air temperature averages in the printing hall in July and August 2014 for a precooling start 2 hours and 5 hours prior to the morning shift

## DISCUSSION AND SUMMARY

This paper is aimed at the creation of a geometrical and calculation model in BSim in order to investigate the precooling possibilities in the industrial hall and to determine the required cooling power. The industrial hall – printing hall – is constantly overheated during the summer periods with temperatures reaching values around 30 °C for longer periods of time and occasionally even above 35 °C. The large part of the thermal load is generated by 3 bigger and 2 smaller bogie-hearth chamber furnaces. The simulation results of the precooling demonstrate the low improvement of the internal microclimate in the printing hall. It is caused primarily by the excessive instant internal thermal loads during the working shifts in combination with extensive solar gains through the roof skylights and the impossibility of the current cooling system to react to these heat gains due to the insufficient cooling capacity.

Contact: weyr.j@fce.vutbr.cz

Acknowledgment: This paper has been worked out under the project No. L01408 "AdMaS UP - Advanced Materials, Structures and Technologies", supported by the Ministry of Education, Youth and Sports under the "National Sustainability Programme I".

## References

- [1] DIPASQUALE, C., D'ANTONI, M., FEDRIZZI, R., KUMMERT, M., MARLETTA, L. Procedure for buildings' energy modeling suited for integrated control simulation. Berlin: BS13. 2012.
- [2] GRAU, K., WITTCHEN, K.B., SØRENSEN, C.G. Visualisation of Building Models. In: *Eighth International IBPSA Conference*. Eindhoven: Netherlands, August 2003, 11-14.
- [3] KEENEY, K., BRAUN, J.E. Application of Building Precooling to Reduce Peak Cooling Requirements. *ASHRAE Transactions*. Volume 103, pp.463 – 480, 1997.
- [4] Council Directive 89/654/EEC of 30 November 1989 concerning the minimum safety and health requirements for the workplace.
- [5] Nařízení vlády č. 361/2007 Sb. kterým se stanoví podmínky ochrany zdraví při práci (in Czech).
- [6] American Society of Heating, Refrigerating and Air-Conditioning Engineers. *ASHRAE handbook: Fundamentals*. Atlanta, GA: American Society of Heating, Refrigeration and Air-Conditioning Engineers, 2009.
- [7] WITTCHEN, K.B., JOHNSEN, K., GRAU, K. *BSim 2002-User's Guide*. 2002.

Ing. Pavel KOPECKÝ, Ph.D.  
Ing. Kamil STANĚK, Ph.D.

CTU in Prague, University Centre  
for Energy Efficient Buildings

# Review of Three White-Box Lumped Parameter Building Thermal Models

## Přezkoumání tří dynamických tepelných modelů budov se sdruženými parametry

Reviewer  
Ing. Jiří Cigler, Ph.D.

*This paper deals with simplified lumped parameter thermal models of a building. Lumped parameter building thermal models break down building components into a small number of temperature-uniform parts and can be graphically depicted in resistance-capacitance (RC) thermal circuits. The number of unknown variables is extensively reduced which, as a result, considerably increases the speed of the calculation. First, three principal lumped parameter building thermal models are described. Simplifying assumptions on the lumped parameter models are commented on. Then, a simple method for estimating the input parameters from the available information about the buildings is proposed. Finally, comparison with the measured data is reported.*

**Keywords:** building simulation, heat transfer, lumped parameter models, electrical analogy, RC model

*Tento článek se zabývá zjednodušenými dynamickými tepelnými modely budovy se sdruženými parametry. Tyto modely rozdělují stavební prvky do velmi malého počtu teplotních uzlů a mohou být graficky zobrazeny tepelnými obvody (elektrická analogie). Nejprve jsou popsány tři základní modely včetně komentáře zjednodušujících předpokladů. Poté je popsána jednoduchá metoda odhadu vstupních parametrů využívající běžně dostupné informace o budově. Nakonec je uvedeno porovnání výsledků jednotlivých modelů s naměřenými daty z experimentu se dvěma identickými neobývanými rodinnými domy.*

**Klíčová slova:** simulace budov, přenos tepla, modely se sdruženými parametry, elektrická analogie, RC model

## INTRODUCTION

Lumped parameter building thermal models break down building components into a small number of temperature-uniform parts. Lumped parameter thermal models can be understood as simplified resistance-capacitance (RC) thermal circuits reduced from complex thermal building models. RC thermal circuits have been used for various purposes already. Some examples are listed hereafter.

Nielsen (2005) used a simple lumped parameter model to develop a building design tool. Kämpf et al. (2007) developed a model which was used for the calculations of a building's heat demand on the district level. Huijbregts et al. (2012) used a lumped parameter hygro-thermal building model to study the impact of global warming scenarios on museum buildings. Reynders et al. (2013) used a lumped parameter building model to investigate an intelligent control strategy used to activate structural thermal mass in a single-family house equipped with a heat pump and photovoltaics. Prívarva et al. (2011) used a simple lumped parameter room model to implement an advanced predictive controller of a heating system in a real building.

Only a few literature references report the validation of lumped parameter models. Mathews et al. (1994) reported the validation study of a first order model based on the measured data from 32 buildings. Kramer (2012) compared predictions from several lumped parameter models with measured data. Kopecký (2016) used a methodology of BESTEST, see Judkoff and Neymark (1995), to verify three simplified lumped parameter thermal models described in this paper hereafter.

The model predictive control of heating or cooling systems is one of the important practical applications of lumped parameter thermal models. The major challenge of model predictive control is to formulate an accurate and fast model of a building's thermal balance. System identification methods are often utilised for the identification of a suitable model. The measured data, however, does not exist in newly built buildings and buildings in the design stage. The ability to propose model equations

prior to identification experiments is, therefore, essential. The ability to estimate input parameters in model equations (i.e., a reasonable interval of physically acceptable values) in a forward manner from the available information about the building (i.e., drawings, material properties, composition of the building components) is important as well.

The main objective of the paper is to review three existing principal lumped parameter building thermal models. The simplifying assumptions incorporated in the lumped models will be elaborated upon in detail and commented on. A simple white-box method for estimating the input parameters will be proposed. Finally, comparison with the measured data will be reported.

## LUMPED PARAMETER BUILDING THERMAL MODELS

### RC thermal circuits

#### Building components

RC thermal circuits of three selected lumped parameter building thermal models are depicted in Figure 1, Figure 2 and Figure 3. They could represent a room, a thermal zone, and even an entire building. Lumped parameter

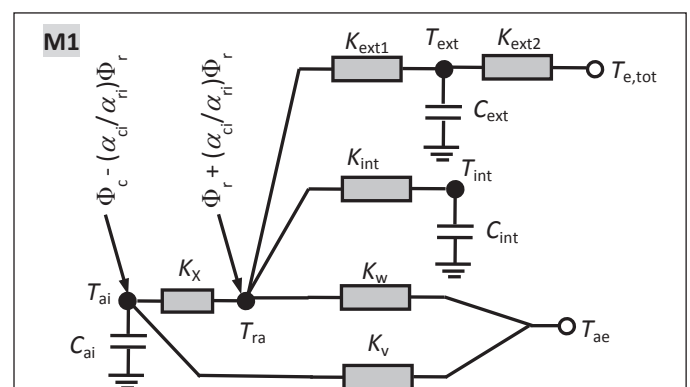


Fig. 1 The RC thermal circuit of model M1

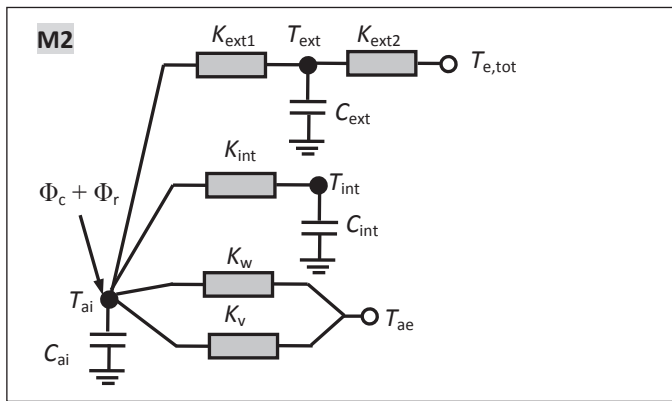


Fig. 2 The RC thermal circuit of model M2

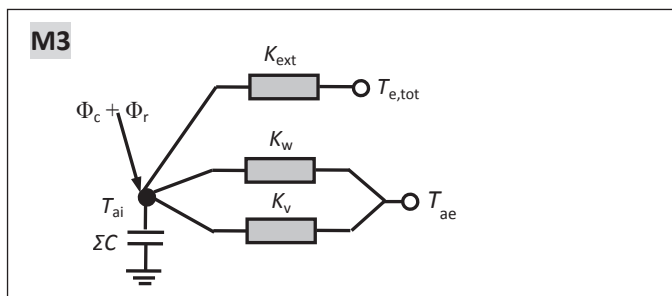


Fig. 3 The RC thermal circuit of model M3

thermal models can be understood as simplified resistance-capacitance (RC) thermal circuits reduced from complex thermal building models.

The identical model structure in model M2 was presented in Masy (2007). Kramer (2012) successfully used the almost identical model structure as model M2 to simulate historical buildings with significant thermal mass. Model M1 was probably first introduced in Tindale (1993). A one-node lumped parameter model similar to model M3 can be found in Burmeister and Keller (1998).

**Thermal bridges**

No lumped parameter models of thermal bridges have been found in literature. In principle, the following RC thermal circuits could be used to model different types of thermal bridges, see Figure 4.

**Comments on model simplifications**

**Description of the internal environment**

Model M1 decouples the radiative and convective heat transfer in the internal environment. There are two temperature nodes for the internal environment (the internal air temperature and the rad-air temperature). The coupling conductance  $K_x$  between the rad-air temperature node and the internal air temperature node is calculated as:

$$K_x = (\alpha_{ci} + \alpha_{ri}) \frac{\alpha_{ai}}{\alpha_{ri}} A \tag{1}$$

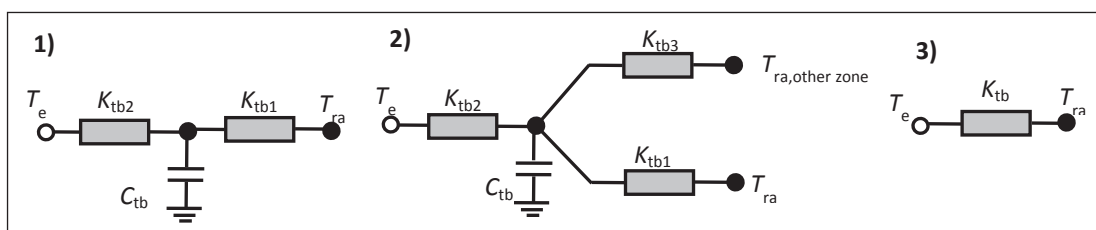


Fig. 4 Various RC thermal circuits for thermal bridges

where  $\alpha_{ci}$  is the internal convective heat transfer coefficient,  $\alpha_{ri}$  is the internal radiative heat transfer coefficient, and  $A_i$  is the area of the building components in contact with the internal air.

The way the concept of the two-node description of the internal environment has been derived and discussions on its validity are described in Davies (2004). Two temperature nodes for the internal environment are a mathematical product of series-parallel transformation where separate radiative and convective links with the surfaces are merged together. The internal surfaces of the building components are, thus, connected to the rad-air temperature by the combined surface thermal resistances. The coupling conductance  $K_x$  between the rad-air node and the internal air node and augmentation of the radiant heat gain do not have any physical interpretation.

Contrary to model M1, model M2 does not decouple the radiative and convective heat transfer (i.e., the internal environment is represented by one node). This corresponds to the very high value of the coupling conductance  $K_x$  in model M1. If the heat capacity of the thin mass layer in touch with internal surfaces is added to the value of  $C_{ai}$ , the central temperature  $T_{ai}$  in model M2 could be understood as the mean temperature composed of the internal air temperature, and the mean temperature of the thin mass layer close to the internal surface. Some error is, therefore, introduced into the ventilation heat flow. Moreover, some error is introduced into the thermostatic control, if the set-point is based on the internal air temperature.

**Single-node representation of building components**

The building components with significant thermal mass are represented by the one-node thermal networks in model M1 and M2. The one-node thermal network is used irrespective of the amount of material layers. Representation of a building component by a one-node thermal network can only be reasonable if the building component does not contain more than one layer with a significant thermal capacity. If an additional capacitive layer is located at the external surface (e.g., a veneer wall), a two-node model would be more appropriate.

**Aggregation of parallel heat transfer paths**

The thermal model of the external and internal building components in models M1 and M2 adopted two fundamental simplifying assumptions:

- ❑ The parallel heat transfer paths of the external building components were aggregated together.
- ❑ The parallel heat transfer paths of the internal building components were aggregated together.

Fraisse et al. (2002) analysed the aggregation of several heat transfer paths. He states that the aggregation of building components can only be reasonable if the thermal response of the building components in parallel to the boundary excitation is similar. This can be approximately true in many real-world cases (i.e., when a similar wall type or an internal partition is used within one building).

In some cases, either the internal or external building components may not contain significant amount of thermal mass, e.g., external

curtain walls or thin internal plasterboard partition walls. In this case, the structure of models M1 or M2 may be further reduced to second order models by omitting the corresponding thermal capacitance from the RC thermal networks.

The special case of model M2 (designated as M3) is introduced if the infinite value of the thermal conductance between the internal node and the capacity nodes is assumed (i.e., the temperature of thermal mass is in thermal equilibrium with the internal temperature), see Figure 3. The thermal mass in the building components is modelled using only one thermal capacitance which is immediately accessible for the purpose of storing heat gains.

**Thermal excitation functions**

Lumped parameter models are thermally excited both from the internal side of the building enclosure and from the exterior. For both sides, solar radiation plays an important role.

Solar heat gains through the windows are calculated by a separate model. The complexity of the solar heat gain model may differ. The calculated solar heat gains are then distributed between the internal air temperature node and the rad-air temperature node. Analogously, the internal heat gains (the metabolic heat of the occupants, the heat from electric appliances) and the heating or cooling power are split between both internal temperature nodes. The values of the convective/radiative split factors depend on, e.g., the amount of furniture in the case of solar heat gains, on the type of heating or cooling system, etc.

The heat exchange at the external surface of a building's components consists of the long-wave radiation exchange, particularly to the sky, the convective exchange, and the absorbed short-wave solar radiation. The net long-wave radiant surface-to-sky heat exchange cools the external surface, which is especially notable during clear windless nights. The short-wave radiation heats the external surface during the daytime. These three influences are mathematically expressed by the external equivalent temperature of a building component which can be calculated as:

$$T_e = \frac{\alpha_s G_{gt} + \alpha_{ce} T_{ae} + \alpha_{re} T_{re}}{\alpha_{ce} + \alpha_{re}} \quad (2)$$

where  $\alpha_s$  is the short-wave absorptivity,  $\alpha_{ce}$  is the convective heat transfer coefficient,  $\alpha_{re}$  is the radiative heat transfer coefficient, and  $T_{re}$  is the mean radiant temperature of the surrounding surfaces. The long-wave radiation transfers heat between the external surface of a building component, the sky and the ground (the latter two surfaces are represented by the mean radiant temperature  $T_{re}$ ).

The total external equivalent temperature  $T_{e,tot}$  (i.e., the aggregated external temperature for the whole building) is calculated as the weighted mean from the thermal conductance of the individual external building components according to:

$$T_{e,tot} = \frac{1}{K_{ext}} \sum_{i=1}^m K_{ext,i} T_{e,i} \quad (3)$$

where  $K_{ext}$  is the total thermal conductance of the external building components and  $K_{ext,i}$  is the thermal conductance of the  $i$ -th external building component. Equation (3) results from the equivalent thermal circuit where several parts of the parallel thermal conductance  $K_{ext,i}$  were aggregated together. It is often reasonable to assume that total external equivalent temperature is equal to the temperature of the external air.

**A simple white-box approach for estimating input parameters**

The values of the input parameters in the lumped parameter models can be estimated in a forward manner from the available information about the buildings using standard and simple calculation procedures.

**Building components**

The thermal conductance  $K_{ext}$  and  $K_w$  are standard steady-state heat

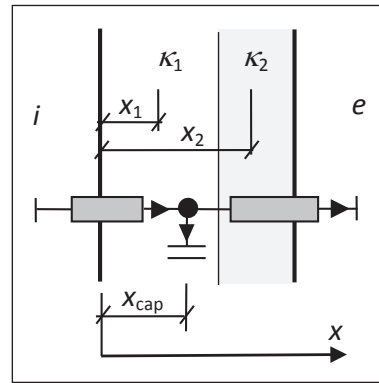


Fig. 5 The centre of the capacitance for a two-layer wall with a corresponding thermal circuit

transfer coefficients calculated from the thermal transmittance and corresponding heat exchange areas of the external building components ( $K_{ext} = \sum U_i A_i$ ) and the windows, doors and any other fast heat transfer paths ( $K_w = \sum U_{w,i} A_{w,i}$ ). The system of internal dimensions is used. The ventilation thermal conductance  $K_v$  is equal to the air flow rate multiplied by the volumetric heat capacity of air.

The thermal conductance  $K_{ext1}$  is calculated using the following procedure: At first, the total value of the thermal capacitance of the  $i$ -th external building component  $C_{ext,i}$  is assumed to be located in the centre of the capacitance (see Figure 5).

The centre of the capacitance of the building components can be calculated as:

$$X_{cap} = \frac{\kappa_1 X_1 + \kappa_2 X_2}{\kappa_1 + \kappa_2} \quad (4)$$

where  $\kappa_1$  (J/(m²K)) denotes the areal thermal capacity of layer 1, and  $\kappa_2$  (J/(m²K)) denotes the areal thermal capacity of layer 2.

Based on the position of the centre of the capacitance, the values of the conductance  $K_{ext1,i}$  for each external  $i$ -th building component are calculated. Finally, the thermal conductance  $K_{ext1,i}$  are summed up to get the total lumped value of  $K_{ext1}$ . The same procedure is used for the calculation of the thermal conductance related to the internal building components  $K_{int}$ .

The thermal conductance  $K_{ext2}$  is then calculated from the relation:

$$\frac{1}{K_{ext}} = \frac{1}{K_{ext1}} + \frac{1}{K_{ext2}} \quad (5)$$

The total thermal capacitance of all the building component are summed up as well to get the total lumped values ( $C_{ext} = \sum C_{ext,i}$ ,  $C_{int} = \sum C_{int,i}$ ). The values of the thermal capacitance are not reduced in this study.

**Thermal bridges**

The thermal capacitance of the central node of a thermal bridge  $C_{tb}$  represents the thermal mass associated with intersections between the building components. Since the system of internal dimensions is used for calculations, the thermal mass in the intersections of the building components would be missing in the simulation models if not otherwise incorporated. The thermal conductance  $K_{tb}$  can be calculated from the estimated value of the linear thermal transmittance and the length of the corresponding thermal bridge ( $K_{tb} = \Psi \times L$ ), respectively, from the point thermal transmittance and the number of point thermal bridges ( $K_{tb} = X \times N_{tb}$ ).

**COMPARISON WITH MEASURED DATA**

**Description of the experiment**

Two side-by-side experiments were set up in the framework of the

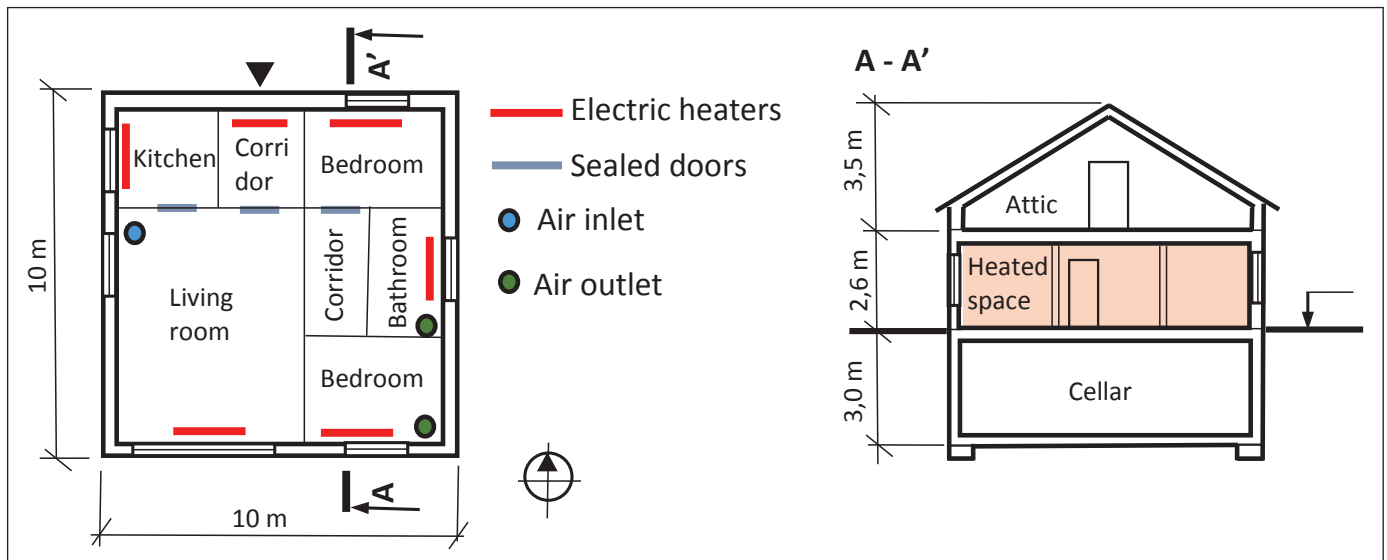


Fig. 6 Basic drawings of test family house

IEA Annex 58 “Reliable Building Energy Performance Characterisation Based on Full Scale Dynamic Measurements” with two identical family houses (designated as N2 and O5), see Figure 6.

The detailed specification of the experiments and measured data are accessible, see Strachan (2015). Kopecký and Staněk (2014) used the measured data in experiment 1 for comparison against the lumped parameter building models.

Experiment 1 consisted of consecutive periods of free-floating operation, random sequence for heat input (ROLBS) and a temperature-controlled operation (see Table 1 for the basic overview). There were no inhabitants in either house. Heating was ensured by conventional electrical heaters placed in front of the windows. The thermostatic control of the heaters was based on the measured air temperature at the mid-height of the room. The temperature in the attic, cellar and external environmental boundary conditions were monitored during the experiment.

Tab. 1 Time schedule of experiment 1

Period	Date	Description	Blinds on southern windows	
			House O5	House N2
P1	21.8.2013 – 29.8.2013	Initialisation, set-point 30 °C	Blinds up	Blinds down
P2	30.8.2013 – 13.9.2013	ROLBS in living room, no heat input in other rooms	Blinds up	
P3	14.9.2013 – 19.9.2013	Re-initialisation, set-point 25 °C	Blinds down	
P4	20.9.2013 – 30.9.2013	Free-floating	Blinds up	

For the purpose of modelling with the lumped parameter models, the house was divided in two zones. The south zone (zone 1, Z1) consisted of the living room, the internal corridor, the bedroom and the bathroom. The north zone (zone 2, Z2) consisted of the kitchen, corridor and bedroom. The north zone was not ventilated. The south zone was ventilated (a constant air flow rate of 120 m<sup>3</sup>/h). It was assumed that there was no air exchange between both zones (the doors were closed and sealed between both zones during the experiment, and had airtight building components between both zones).

The thermal zone was characterised by a measured mean internal air temperature and total heat input (see Figure 7). The mean internal air temperature of the zone was calculated from the measured data as a volume weighted average from the corresponding internal air temperatures.

#### Model details

The basic RC thermal circuits of the lumped parameter models (see Figure 1 to 3) were expanded in order to model the heat transfer through the floor (a thermal connection with the cellar), the heat transfer through the ceiling (a thermal connection with the attic) and the heat transfer through the dividing walls between both zones. These thermal paths in model M1 and model M2 were modelled by one-node RC thermal networks. The simplified model M3 used a single-conductance model for the above-mentioned building components. The doors between both zones were modelled by a single-conductance thermal network in all models.

Tab. 2 List of thermal bridges

No.	Description	Connected environments	Type of RC thermal circuit**	$\Psi$ [W/(m·K)]	$\chi$ [W/K]
1	Ext. wall/Ext. wall	Int/Ext	1	0.09	-
2	Floor/Ext. wall	Int/Ext/Cellar	2	0.11	-
3	Ceiling/Ext. Wall	Int/Ext/Attic	2	0.085	-
4	Int. wall/Floor	Int/Cellar	1	0.38	-
5	Int. wall/Ceiling	Int/Attic	1	0.20	-
6	Partition/Floor	Int/Cellar	1	0.24	-
7	Partition/Ceiling	Int/Attic	1	0.13	-
8	Column/Floor	Int/Cellar	1	-	0.58
9	Column/Ceiling	Int/Attic	1	-	0.44
10	Window sill*	Int/Ext	3	0.03	-
11	Window lining*	Int/Ext	3	0.03	-
12	Window overhead*	Int/Ext	3	0.03	-

\*Included in thermal conductance  $K_w$

\*\*See Figure 4 for thermal circuits.

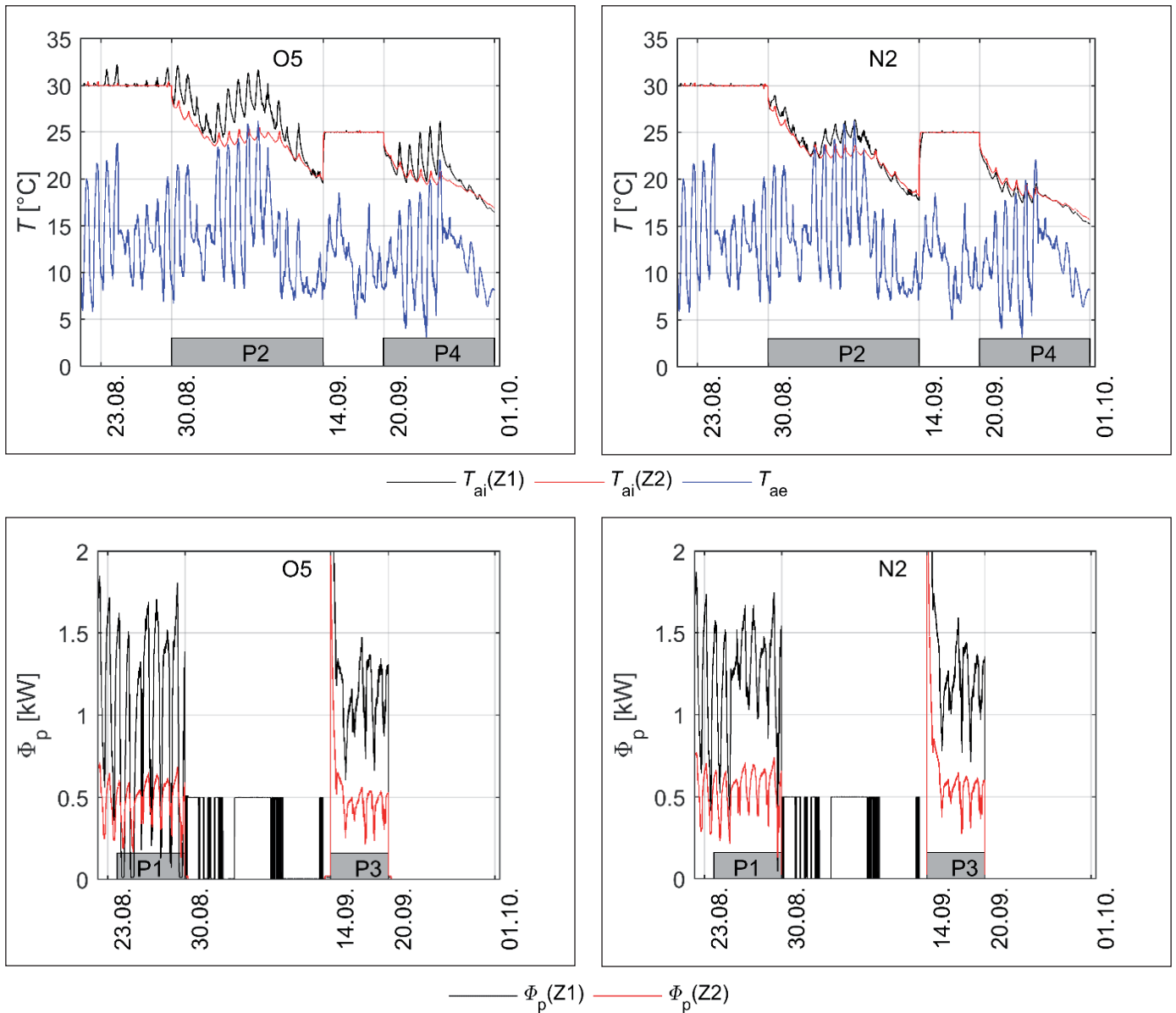


Fig. 7 The measured internal air temperature and the total heating power during experiment 1

The electric heaters were modelled as ideal heat sources with a negligible thermal capacity. The heat input from the convector heaters was distributed from 50 % to the air node, and from 50 % to the rad-air node.

The isotropic sky model was used to calculate the solar irradiance on a tilted oriented plane from the available solar irradiance on a horizontal plane. The solar energy transmittance of the glazing was treated as angular dependent. The solar heat gains were distributed from 90 % to the rad-air node, and from 10 % to the air node.

The list of thermal bridges is provided in Table 2. The values of the linear and point thermal transmittance were taken from the specification document.

**Estimation of input parameters**

The identical procedure as described in the previous text was used for the estimation of the input parameters. All material properties, component dimensions, and glazing properties, were consistently taken from the specification documents. The estimated input parameters in simplified parameter models are specified in Table 3.

The thermal conductance in the RC circuits of the thermal bridges were estimated from the total values of the thermal conductance  $K_{tb}$ . The thermal capacitance  $C_{tb}$  appearing in the RC circuits of the thermal bridges was estimated from the cross-sectional area of the thermal mass associated with the corresponding thermal bridge.

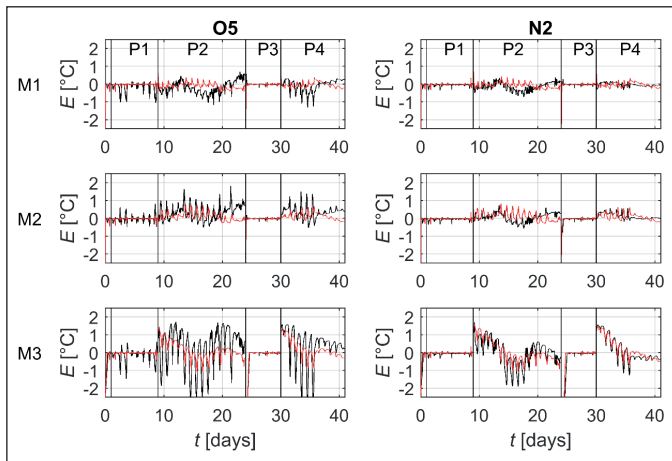
Tab. 3 The estimated values of the thermal parameters

Case	$K_{ext}$ [W/K]	$K_w$ [W/K]	$K_v$ [W/K]	$K_{ext1}$ [W/K]	$K_{int}$ [W/K]	$K_x^*$ [W/K]	$C_{ext}$ [MJ/K]	$C_{int}$ [MJ/K]	$C_{ai}^{**}$ [MJ/K]	$\Sigma C^{***}$ [MJ/K]
Z1	9.41	18.6	40.4	52.7	194.2	1079	12.6	5.63	1.79	28.4
Z2	7.68	8.77	0	39.2	96.5	552	9.74	2.84	1.70	18.1

\*The coupling conductance  $K_x$  between the internal air temperature node and the rad-air temperature node was calculated with the assumption of:  $\alpha_{ai} = 3 \text{ W}/(\text{m}^2\text{K})$ ,  $\alpha_{ri} = 5 \text{ W}/(\text{m}^2\text{K})$ , the total internal surface area  $A_i = 224.8 \text{ m}^2$  (zone 1), resp.  $A = 115.0 \text{ m}^2$  (zone 2).

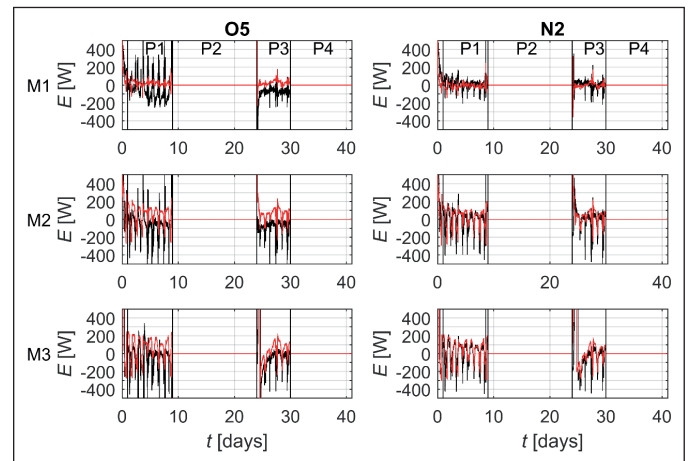
\*\*The value of  $C_{ai}$  contains the thermal capacity of concrete columns and the thermal capacity of the internal window pane.

\*\*\*The thermal capacity of the floor screed and half of the dividing walls was included.



— Z1 — Z2

Fig. 8 The simulation error of the internal air temperature (time profiles and histograms)



— Z1 — Z2

Fig. 9 The simulation error of the heating power (time profiles and histograms)

RESULTS AND DISCUSSION

The simulation was performed in an open loop mode with no feedback from the measured temperatures. The simulation error is defined as  $E = \text{the calculated value} - \text{the measured value}$ . The simulation errors (10-min averages) and the distribution of the simulation errors are depicted in Figure 8 and Figure 9. The mean errors (ME) of the heating power and internal air temperature are listed in Table 4. The relative errors (RE) of the delivered heat are listed in Table 5.

Generally, the simulation errors in house N2 are lower than the simulation errors in house O5. The simulation errors in both houses fluctuated with the daily period as they were correlated to the solar radiation. The daily oscillation of the simulation error was stronger in the unshaded house O5. Therefore, the inaccuracy is, to some extent, attributed with the quality of the solar heat gain calculation model. Moreover, the time profile of the simulation error of the internal air temperature contains the periodic component with a time period longer than one day. The long-term component of the simulation error is expected to be related to the number of temperature nodes in the models (coarse spatial resolution) and the inaccuracy of the solar heat gain calculation model.

Model M1 predicted the comparable shapes of the internal air temperatures and the heat inputs with the measured data. Model M1 exhibited the smallest error in the delivered heat (< 7 %), a small mean error in

Tab. 4 The mean error in the internal air temperature and heating power

House	Zone	Period	$ME - T_{ai} [^{\circ}C]$			House	Zone	Period	$ME - \Phi_p [W]$		
			M1	M2	M3				M1	M2	M3
O5	Z1	P2	-0.18	0.34	0.31	O5	Z1	P1	-36.4	-61.9	-86.4
		P4	-0.06	0.35	0.36			P3	-83.6	-87.4	22.2
	Z2	P2	-0.10	0.10	0.12		Z2	P1	18.6	54.4	65.6
		P4	-0.04	0.11	0.22			P3	30.7	71.2	130.7
Mean (abs(ME))			0.10	0.22	0.25	Mean (abs(ME))			42.3	68.7	76.2
N2	Z1	P2	-0.13	0.07	-0.02	N2	Z1	P1	6.4	-3.0	6.5
		P4	-0.03	0.13	0.15			P3	-4.5	-0.8	77.8
	Z2	P2	-0.07	0.10	0.09		Z2	P1	-7.2	27.1	35.8
		P4	-0.04	0.08	0.24			P3	2.7	51.6	114.5
Mean (abs(ME))			0.07	0.10	0.12	Mean (abs(ME))			5.2	20.6	58.7

the heating power (< 84 Watts) and a small mean error in the internal air temperature (0.18 °C). The error of model M1 has been mostly located within a bandwidth of  $\pm 1$  °C, i.e., the error was comparable with the uncertainty of the measured internal air temperature.

Tab. 5 The relative error of the delivered heat over the heating periods P1 and P3

House	Zone	Period	RE [-]		
			M1	M2	M3
05	Z1	P1	0.96	0.93	0.91
		P3	0.93	0.93	1.02
	Z2	P1	1.04	1.11	1.13
		P3	1.06	1.13	1.24
Mean(RE)			1.00	1.03	1.08
N2	Z1	P1	1.01	1.00	1.01
		P3	1.00	1.00	1.06
	Z2	P1	0.99	1.05	1.07
		P3	1.00	1.08	1.17
Mean(RE)			1.00	1.03	1.07

Model M3 achieved the worst match with the measured data. The time profile of the heating power was not accurately predicted. The shape of the internal air temperature was not accurate as well. The daily swing of the internal air temperature was attenuated too much and the daily peak culminated too late. However, the mean error in the heating power, the mean error in the internal air temperature and the delivered heat were close to the measured values of the experiment.

Model M2 achieved better agreement with the measured data than model M3. The time profile of the internal air temperature was very similar to the measured profile. The mean error in the heating power was higher than in the case of model M1. The shape of the heating power was not predicted as good as in the case of model M1. The simulation errors of model M2 were distributed in a wider interval than in model M1.

Model M1 distributed the heat between the internal air temperature node and the rad-air temperature node. This feature probably better represents the physical reality. However, it also imposes uncertainty of the real values of the convective/radiative split for the solar heat gains and the heat emitted by the heating system. In fact, the time profile of the heating power in the experiment was rather sensitive to the setting of the heat distribution from the electric heating bodies.

The compensation of the errors is the principal problem of the validation. The similar internal air temperature profiles may be generated by different input parameter setups. For instance, heat gains and heat losses could be simultaneously overestimated or underestimated. Both combinations would lead to similar model outputs. Moreover, if a modeller gets an impression that heat losses have been probably underestimated it is difficult to distinguish whether the heat transfer path is inaccurately modelled (i.e., the model is too coarse) or is there is an inadequate setting of the input parameters.

CONCLUSIONS

This paper assessed three selected lumped parameter building thermal models. The simplifying assumptions and a simple method for the estimation of the input data have been discussed and described. We identified the third order lumped parameter thermal model as being capable of predicting the dynamic thermal performance of a real scale test buildings. The third order model could, therefore, be used as an initial

choice if the objective is to implement a model predictive controller in a building. In reality, some additional temperature nodes might be needed to be added in the basic thermal circuit, e.g., if the heating and cooling system are integrated in the thermal mass.

Contact: pavel.kopecky@fsv.cvut.cz

Acknowledgement. This work has been supported by the Ministry of Education, Youth and Sports within the National Sustainability Programme I (NPU I), project No. LO1605 – University Centre for Energy Efficient Buildings – Sustainability Phase.

Symbols:

- $A_i$  Area of the building components in contact with the internal air [m<sup>2</sup>]
- $C_{ai}$  Thermal capacitance of the internal air [J/K]
- $C_{ext}$  Total thermal capacitance of the external building components [J/K]
- $C_{int}$  Total thermal capacitance of the internal building components [J/K]
- $C_{tb}$  Thermal capacitance of a thermal bridge [J/K]
- $G_{gt}$  Global solar irradiance on a tilted oriented plane [W/m<sup>2</sup>]
- $K_{ext}$  Total thermal conductance of the external building components [W/K]
- $K_{ext1}$  Total thermal conductance between the internal environment and the aggregated external building components [W/K]
- $K_{int}$  Total thermal conductance between the internal environment and the aggregated internal building components [W/K]
- $K_w$  Total thermal conductance of the windows [W/K]
- $K_v$  Thermal conductance due to ventilation [W/K]
- $K_x$  Coupling conductance between the internal air node and rad-air node [W/K]
- $T_{ai}$  Internal air temperature [°C]
- $T_{ae}$  External air temperature [°C]
- $T_{ra}$  Rad-air temperature [°C]
- $T_{ext}$  Mean temperature of the external building components [°C]
- $T_{int}$  Mean temperature of the internal building components [°C]
- $T_{tb}$  Mean temperature of a thermal bridge [°C]
- $T_e$  External equivalent temperature (sol-air temperature) [°C]
- $\Phi_r$  Radiant part of the heat gains [W]
- $\Phi_c$  Convective part of the heat gains [W]
- $\Phi_p$  Heating or cooling power [W]
- $\alpha_c$  Convective heat transfer coefficient [W/(m<sup>2</sup>K)]
- $\alpha_r$  Radiative heat transfer coefficient [W/(m<sup>2</sup>K)]
- $\alpha_s$  Absorptivity of the short-wave radiation (solar absorptivity) [-]

Lower indexes

- ext External building components (thermal connection to the exterior)
- int Internal building components (no thermal connection to the exterior)
- V Ventilation
- inf Infiltration
- w Windows
- i Internal
- e External
- a Air
- c Convection or cooling
- r Radiation
- ae Air, external
- ai Air, internal
- tb Thermal bridges

References

[1] TOKE, RAMMER, NIELSEN. Simple tool to evaluate energy demand and indoor environment in the early stages of building design. *Solar Energy*. 2005, vol. 78, issue 1, pp. 73-83. ISSN 0038-092X. <https://doi.org/10.1016/j.solener.2004.06.016>.

[2] REYNDERS, G., NUYTEN, T., SAELENS, D. Potential of structural thermal mass for demand-side management in dwellings. *Building and Environment*. 2013, vol. 64, pp 187-199. ISSN 0360-1323. <https://doi.org/10.1016/j.buildenv.2013.03.010>.

- [3] KÄMPF, J., H., ROBINSON, D. A simplified thermal model to support analysis of urban resource flows. *Energy and Buildings*. 2007, vol. 39, issue 4, pp. 445-453. ISSN 0378-7788. <https://doi.org/10.1016/j.enbuild.2006.09.002>.
- [4] HUIJBREGTS, Z., KRAMER, R.P., MARTENS, M.H.J. van SCHIJNDEL, A.W.M., SCHELLEN, H.L. A proposed method to assess the damage risk of future climate change to museum objects in historic buildings. *Building and Environment*. 2012, vol. 55, pp. 43-56. ISSN 0360-1323. <https://doi.org/10.1016/j.buildenv.2012.01.008>.
- [5] KRAMER, R., van SCHIJNDEL, J., SCHELLEN, H. Simplified thermal and hygric building models: A literature review. *Frontiers of Architectural Research*. 2012, vol. 1, issue 4, pp. 318-325. ISSN 2095-2635. <https://doi.org/10.1016/j.foar.2012.09.001>.
- [6] BURMEISTER, H., KELLER, B. Climate surfaces: a quantitative building-specific representation of climate. *Energy and Buildings*. 1998, vol. 28, issue 2, pp. 167-177. ISSN 0378-7788. [https://doi.org/10.1016/S0378-7788\(98\)00012-7](https://doi.org/10.1016/S0378-7788(98)00012-7).
- [7] TINDALE, A. Third-order lumped-parameter simulation method. *Building Service Engineering Research Technology*. 1993, vol. 14, issue 3, pp. 87-97. <https://doi.org/10.1177/014362449301400302>.
- [8] MASY, G. *Definition and Validation of a Simplified Multizone Dynamic Building Model Connected to Heating System and HVAC Unit*. PhD Thesis. Université de Liège, 2007. Available at: <http://bictel.ulg.ac.be/ETD-db/collection/available/ULgetd-11052008-145605/>
- [9] DAVIES, M., G. *Building Heat Transfer*. Wiley, 2004.
- [10] PRÍVARA, S., ŠIROKÝ, J., FERKL, L., CIGLER, J. Model predictive control of a building heating system: The first experience. *Energy and Buildings*. 2011, vol. 43, issues 2-3, pp. 564-572. ISSN 0378-7788. <https://doi.org/10.1016/j.enbuild.2010.10.022>.
- [11] JUDKOFF, R., NEYMARK, J., *International Energy Agency Building Energy Simulation Test (BESTEST) and Diagnostic Method*. NREL, 1995.
- [12] MATHEWS, E.H., RICHARDS, P.G., LOMBARD, C. A first-order thermal model for building design. *Energy and Buildings*. 1994, vol. 21, issue 2, pp. 133-145. ISSN 0378-7788. [https://doi.org/10.1016/0378-7788\(94\)90006-X](https://doi.org/10.1016/0378-7788(94)90006-X).
- [13] FRAISSE, G., VIARDOT, CH., LAFABRIE, O., ACHARD, G. Development of a simplified and accurate building model based on electrical analogy. *Energy and Buildings*. 2002, vol. 34, issue 10, pp. 1017-1031. ISSN 0378-7788. [https://doi.org/10.1016/S0378-7788\(02\)00019-1](https://doi.org/10.1016/S0378-7788(02)00019-1).
- [14] STRACHAN, P. *Twin Houses Empirical Dataset: Experiment 1*. University of Strathclyde. *Empirical\_Modelling\_Specification\_200514*(.pdf), *Supplementary\_files*(.zip), *Supplementary\_file\_structure*(.txt). 10.15129/8a86bbb-7be8-4a87-be76-0372985ea228

Ing. arch. Michala LYSCZAS  
prof. Ing. Karel KABELA, CSc.

CTU in Prague, Faculty of Civil  
Engineering, Department of  
Indoor Environmental and  
Building Services Engineering

# Adaptive Ventilation Towards Better IEQ: A Case Study of the Pilgrimage Chapel of Holy Stairs

## Adaptivní větrání jako nástroj ke zlepšení kvality vnitřního prostředí: případová studie poutní kaple Svatých schodů

Reviewer  
Ing. Vojtěch Zavřel, Ph.D.

*The paper presents the problem of unsatisfactory indoor environmental quality in the Chapel of Holy Stairs in the north of the Czech Republic, which is represented by a high value of air moisture leading to the degradation of the historic interior and frescoes. In order to understand the overall hygro-thermal properties of the airflow in the chapel, monitoring of the air temperature and relative humidity in the chapel and the cloister was carried out. The monitoring data, which provides a basis for examining the initial condition of the Chapel, is used for the calibration of the numerical model developed within the current research. The model is created in a simplified form based on physical principles and the heat balance method. The numerical model enables one to find a suitable control algorithm for the adaptive ventilation system*

*The main aim of this work is to present the benefits and limitations of adaptive ventilation. The analysis highlights the influence of the controlled air supply on the indoor environmental quality and the overall reduction in the amount of air moisture.*

**Keywords:** adaptive ventilation, indoor environmental quality, heat balance method, regression-based numerical model, historic interior

*V příspěvku je prezentována studie Poutní kaple Svatých schodů v Rumburku, která se potýká s problémem nevyhovující kvality vnitřního prostředí z hlediska vysokých hodnot vzdušné vlhkosti. Vysoká míra vlhkosti vede k degradaci historického interiéru a fresky na stropě kaple. Za účelem stanovení počátečních podmínek a pochopení tepelně vlhkostních procesů byl proveden monitoring teploty vzduchu a relativní vlhkosti v kapli a přilehlých chodbách. Naměřená data posloužila jako základ pro kalibraci zjednodušeného numerického modelu, který funguje na fyzikálních principech zachování energie. Cílem modelu je najít a ověřit vhodný algoritmus pro přívod venkovního vzduchu do interiéru, který by vedl ke zlepšení podmínek v kapli. Tato práce si dává za cíl poukázat na přínosy a limity aplikace adaptivního větrání. Prezentovaná analýza ukazuje vliv kontroly přísunu venkovního vzduchu na kvalitu vnitřního prostředí a celkové snížení množství vzdušné vlhkosti v interiéru.*

**Klíčová slova:** adaptivní větrání, kvalita vnitřního prostředí, metoda tepelné rovnováhy, regresní metoda, historický interiér

## INTRODUCTION

Historically valuable interiors require special attention in terms of the indoor environmental quality, where hygro-thermal properties of the indoor air play a significant role. The level of the air temperature and relative humidity, and, in particular, their sudden fluctuation over the time, have wide implications on the preservation of the interior. Unfortunately, in many cases, the indoor air properties are far beyond the tolerance zone given by the relevant standards.

Most of the historic interiors contend with problems related to high moisture level, which can lead to cultural heritage deterioration [1]. Leaving aside the structural faults, one of the most common problems is condensation on the internal surfaces, which occurs due to the high accumulation capability of the heavy historical construction. Especially in spring, the surface temperature of the walls is still under the dew point of the inlet outdoor air and the condensation of water vapours in the air can appear. As a result, the historic frescoes can be irreversibly damaged.

The ideal solution for maintaining appropriate internal conditions in order to preserve the artefacts is the installation of an air conditioning system. Nevertheless, this solution may be unacceptable for two main reasons: the high investment and maintenance cost and the high impact on the historical interior related with the new addition of the air condi-

tioning system, which is in contradiction with the preservation attempts. [2]. Therefore, this solution is not a preferable option for most historical buildings. Adaptive ventilation is potentially a low-energy and low impact alternative. By using sensor technology, a ventilation system only runs when the outdoor air has the potential to improve hygro-thermal properties in the interior [8].

An adaptive ventilation strategy is provided via controlled openings, air dampers or fans. This strategy takes the change of the air temperature and the level of the air moisture in the exterior and the interior into account. Based on the evaluation of the current conditions, the control algorithm recommends an action to achieve the desired airflow of the outdoor air. The actuation can be executed manually by an operator, who manually opens the window or automatically opens the window via a servomechanism [5]. If the wind and buoyancy effects are not sufficient enough for providing the right amount of outdoor air, fans are utilised. [6, 7].

The goals of the adaptive ventilation strategy are to:

- adjust the indoor conditions (air temperature and relative humidity) as close as possible to the required (tolerated) zone, which is defined in the ASHRAE standard [10];
- minimise the risk of condensation associated with natural ventilation;

- minimise the intensive fluctuation of the relative humidity associated with natural ventilation [8].

The paper represents a feasibility study which evaluates the potential of the adaptive ventilation strategy and its influence to the hygro-thermal properties of the air in the pavilion with an historic fresco. The simplified numerical model was developed for the assessment of the ventilation strategy. The aim of the paper is to evaluate the influence of the timing ventilation to the conservation risk reduction for the historic frescoes.

**THE CASE STUDY**

**Object description**

The Pilgrimage Chapel of the Holy Stairs is part of the important cultural monument called the Loreto in Rumburk in the north of the Czech Republic. Since 2014, it has been included as one of the significant places on the “Via Sacra” Pilgrims’ Way [3]. The Chapel was built between 1767 and 1770 and its staircase is surrounded by unique sculptural decorations and historical ceiling frescoes, which underwent a complete renovation between 2007 and 2012 [3, 4]. However, shortly after the renovation, the fresco painting and artefacts began to show signs of damage. The presumed reason for this damage is the unsatisfactory in-

door environmental quality. The damage is likely caused by the recurring conditions of the higher air humidity combined with the lower air and surface temperatures, resulting in the condensation of water vapour on the ceilings with the frescoes. Moreover, during the winter period, the air temperature often falls below zero, causing the condensed water vapour to freeze and ice to develop on the surfaces. (Fig. 1)

The previous analysis described in [12] evaluated the hygro-thermal conditions in the chapel based on the monitoring data. The analysis confirmed the assumption of a moisture ingress from the adjacent corridor. On the basis of a comparison of the results from the previous analysis and the available literature describing an adaptive ventilation application [6, 7, 8], it is possible to assume the positive effects of the adaptive ventilation for the reduction of air moisture in the chapel. These publications suggest adaptive ventilation as a possible solution for similar interiors like the Chapel of Holy Stairs.

**Monitoring data**

In order to understand the hygro-thermal conditions in the interior, the monitoring of the air temperature and the relative humidity of the interior and the exterior was carried out during the period of November 2012 to June 2013 with 15-minute time steps. 14 dataloggers were used in the chapel and the adjacent cloister (Fig. 2).



Fig. 1 The Pilgrimage Chapel of Holy Stairs [3], frost on the frescoes.

The comparison between the results of the air temperature and relative humidity in the north-facing corridor, south-facing corridor of the ambit and the area of Holy Stairs indicates an interesting finding. Although the values of the air temperature do not indicate significant differences (except a slight fluctuation due to solar radiation), the values of the relative humidity show considerable dissimilarities. The extremely high value of the relative humidity in the north-facing corridor has a direct impact on the relative humidity values in the area of the Holy Stairs with the historic fresco. Based on

these results, an additional source of moisture is expected in some parts of the cloister. This fact is supported by a visual inspection.

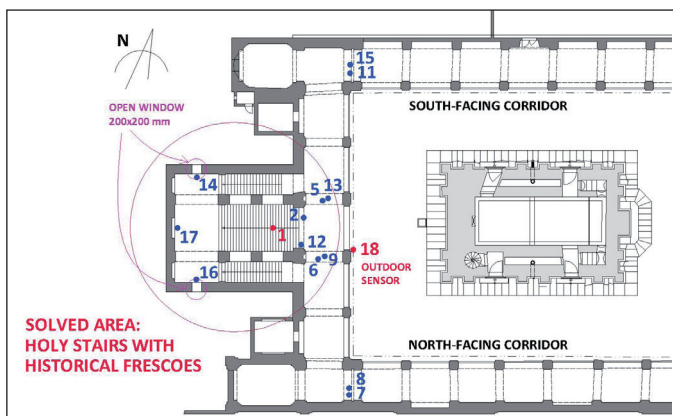


Fig. 2 Position of the sensors in the Chapel and Cloister during the measurements. Sensor No. 1 is located under the ceiling in space of the Holy staircase. Outdoor sensor No. 18 is placed out of direct sunlight.

**NUMERICAL MODEL**

**Modelling method**

In order to assess the ventilation strategy, a simplified model was created in Microsoft Excel. For the determination of the hydro-thermal microclimate properties, the variables of the indoor temperature, the indoor humidity ratio and the surface temperature,  $T_p$ ,  $x_i$  and  $T_m$ , respectively, must be calculated. To indicate the dependency with the other variables and parameters in the numerical model, the key variables are represented as functions (1), (2) and (3). The model is governed by these systems of equations.

The calculation of the indoor air temperature and the temperature of mass (representing the temperature of the walls) is influenced by several

properties. These properties, where it is possible to determine more or less exactly, represent  $c_a$  (the specific heat capacity of the air),  $c_m$  (the specific heat capacity of the mass),  $A$  (the area of the mass),  $U_i$  (the individual heat transfer coefficient),  $T_e$  (the exterior air temperature),  $\rho_a$  (the density of the air),  $\rho_m$  (the density of the mass),  $V_e$  (the volume of the exterior air),  $V_i$  (the volume of the interior air). Other properties  $h$  (the convection heat transfer coefficient) and  $d$  (the effective thickness) are the subject of calibration.

The calculation of the air moisture is represented by  $T$  (the air temperature),  $\rho_a$  (the density of the air),  $x_e$  (the exterior humidity ratio),  $p_v''$  (the saturation vapour pressure),  $V_e$  (the volume of the exterior air),  $V_i$  (the volume of the interior air). It is possible to determine these properties more or less exactly and they are the subject of the explicit calculation.  $G$  (the accumulation moisture uptake) represents the amount of moisture, which is possible to be absorbed by the mass. The calculation of the accumulation moisture uptake is a complex process; thus it is the subject of the regression method.

$$T_{i,\tau(x)} = T_{i,\tau(x-1)} + f(c, A, U, T_e, T_m, h, \rho, d, V_e, V_i) \quad (1)$$

$$x_{i,\tau(x)} = x_{i,\tau(x-1)} + f(\rho, G, x_e, T_i, p_v'', V_i, V_e) \quad (2)$$

$$T_{m,i,\tau(x)} = T_{m,\tau(x-1)} + f(c, A, h, U, T_e, T_i, \rho, d, V_i, V_e) \quad (3)$$

The variables  $T_i$  and  $T_m$  were determined by the explicit method based on the principle of the heat balance method, which forms the basis of all load estimation methods [14]. The most important assumption is that the temperature of the air in the thermal zone is homogeneous. The other important assumptions are that the surfaces (walls, windows, floors, ceilings, etc.) have a uniform temperature. Based on these assumptions, the heat balance can be set up. The convective heat balance is calculated for the room air by (4) [9].

$$m_i c_i \frac{dT_i}{d\tau} = Q_{conv} + Q_{iv} + Q_{ce} \quad (4)$$

where:

$m_i c_i \frac{dT_i}{d\tau}$  the rate of the increase of the heat stored in the room [W]

$Q_{conv}$  the convective heat transfer from the surfaces [W]

$Q_{iv}$  the load caused by the infiltration and ventilation air [W]

$Q_{ce}$  the convective parts of the internal loads [W][14]

Contrary to the temperature calculation, the variable  $x_i$  is calculated by using the regression method. The regression formula is used to describe the complex process related to the accumulation of the moisture in the structures. The calculation takes the outdoor air humidity entering the space with the ventilation and the infiltration, as well as the ability of the material to absorb the moisture, into account.

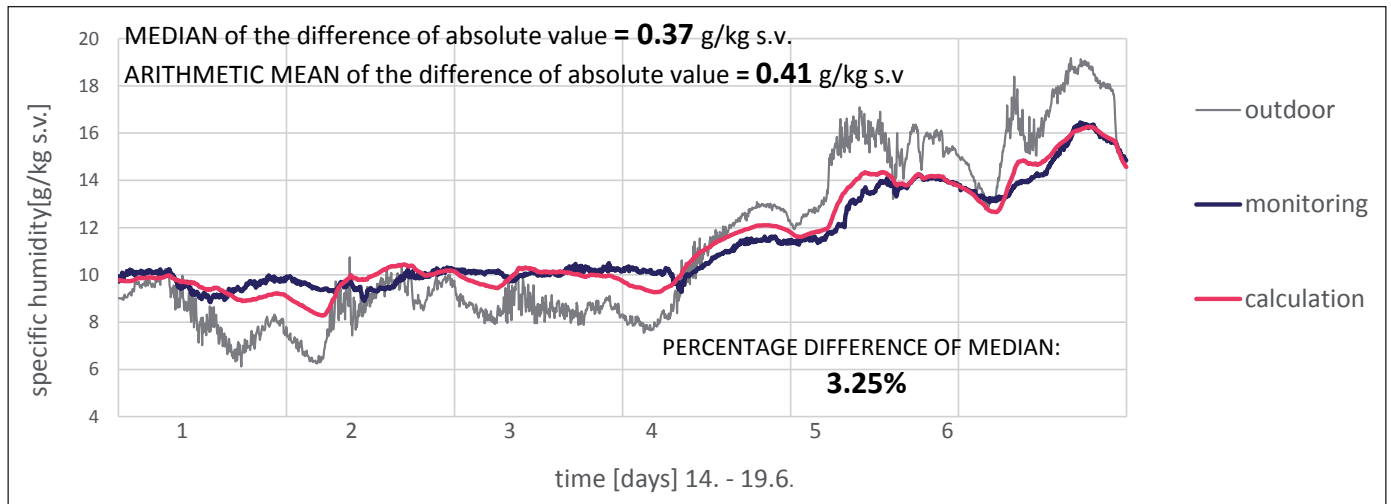


Fig. 3 Comparison of the measured and calculated air temperature values in the chapel.

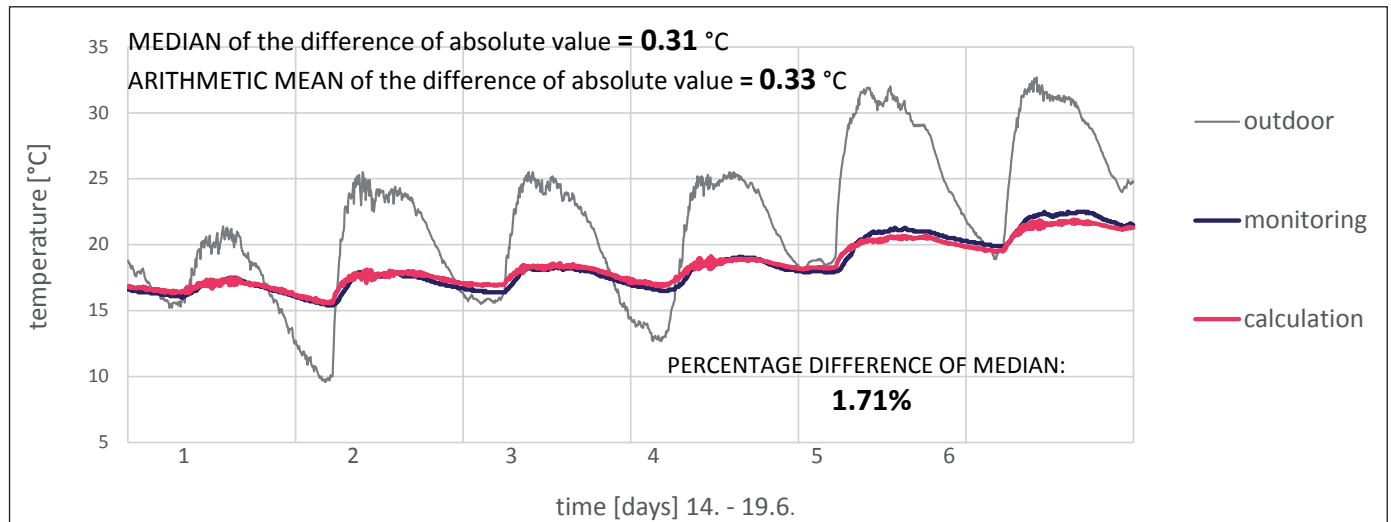


Fig. 4 Comparison of the measured and calculated specific humidity values in the chapel.

The principle of the numerical model is based on the calculation dependent variables  $T_p$ ,  $T_m$  and  $x_i$  in specific time steps. The transient simulation is an iterative process, where the calculated values at the end of the time step enter the calculation of the next time step as the initial values. Therefore, the selection of the appropriate time step is essential. The numerical model works with a 5-minute time step. This interval is short enough for the elimination of computational errors. These errors are caused as a result of the calculation of several equations within one time-step, where they are interdependent.

The model is not able to take the possibilities and limits of natural ventilation in terms of buoyancy driven and wind driven ventilation into account. The task of the model is to verify the influence of the timing for the outdoor air supplied to the interior. The way of supplying outdoor air to the interior (fan or natural ventilation) is not the subject of the study.

**Model calibration**

The model was calibrated based on the measured data for a period of 6 days and subsequently validated for other periods using the measured data for the calibration as reference.

The graphs (Fig. 3 and 4), show the results of the model verification for the randomly selected period of 6 days. The air temperature results are almost identical to the measured values in all periods that have been verified after calibration. The average absolute errors between the monitored and calculated data is 0.31 °C, which represents 1.71% from the average value of the monitored air temperature. The specific humidity values show acceptable deviations, where they are represented by the median of the difference of the absolute value between the monitored and calculated values. The median was calculated to be 0.37 g/kg, which means a 3.25% difference from the average value of the monitored specific humidity. These differences can be attributed to the considerable simplification of the extensive problems of moisture accumulation in the masonry, and the non-linear influence of the measured values by the additional air humidity coming from the adjacent corridor.

**CONTROL ALGORITHM FOR THE ADAPTIVE VENTILATION**

After validation of the model, the control algorithm for the adaptive ventilation were applied to determine the appropriate time for increasing the outdoor air supply. The two conditions mentioned in (5) and (6) were applied in order to move the parameters of air temperature and relative humidity closer to the tolerance zone. The control algorithm (7) avoids

undesirable fluctuations in the relative humidity in the interior during the day. The last one (8) prevents the increase in the risk of condensation on the interior surfaces.

$$T_i < T_e \wedge T_i < 25 \Leftrightarrow \text{"OPEN"} \tag{5}$$

$$x_i > x_e \wedge RH_i > 60 \Leftrightarrow \text{"OPEN"} \tag{6}$$

$$\left| \max(RH_{\tau,0} - RH_{\tau,30min}) - \min(RH_{\tau,0} - RH_{\tau,30min}) \right| > 1.5 \Leftrightarrow \text{"CLOSE"} \tag{7}$$

$$T_{dp,ex} > T_m \Leftrightarrow \text{"CLOSE"} \tag{8}$$

In case the model evaluated at least one of the conditions as a “CLOSE” mode, it only considers infiltration.

The results of the impact of the adaptive ventilation on the interior, were evaluated in terms of three criteria: the fluctuation of the relative humidity, the risk of condensation and the reduction of air moisture.

The three ventilated modes are presented for assessment (in ach – air changes per hour):

- only infiltration: constant 0.2 ach;
- permanent ventilation: constant 1.5 ach;
- adaptive ventilation: 0.2 or 1.5 ach (depending on the boundary conditions).

In reality, of course, the air change in the interior will not be constant. On the other hand, the exact value of air change in the interior is not essential to assess the effect of adaptive ventilation. It is only necessary to determine what happens if the outdoor air supply will suddenly increase or decrease.

**RESULTS**

**Prevention of high fluctuation during the day**

Figure 5 represents the comparison of the relative humidity results. Even though more than half a year was measured, the graph only shows a short period (10 days) for visualisation purposes. The results with the infiltration mode only (blue line) indicate minimal fluctuation, however, these values, in just a few cases, fall over the critical value of 75 % RH. On the other hand, the permanent ventilation results (green line) show extreme daily fluctuations reaching almost 30 % RH. Moreover, in some

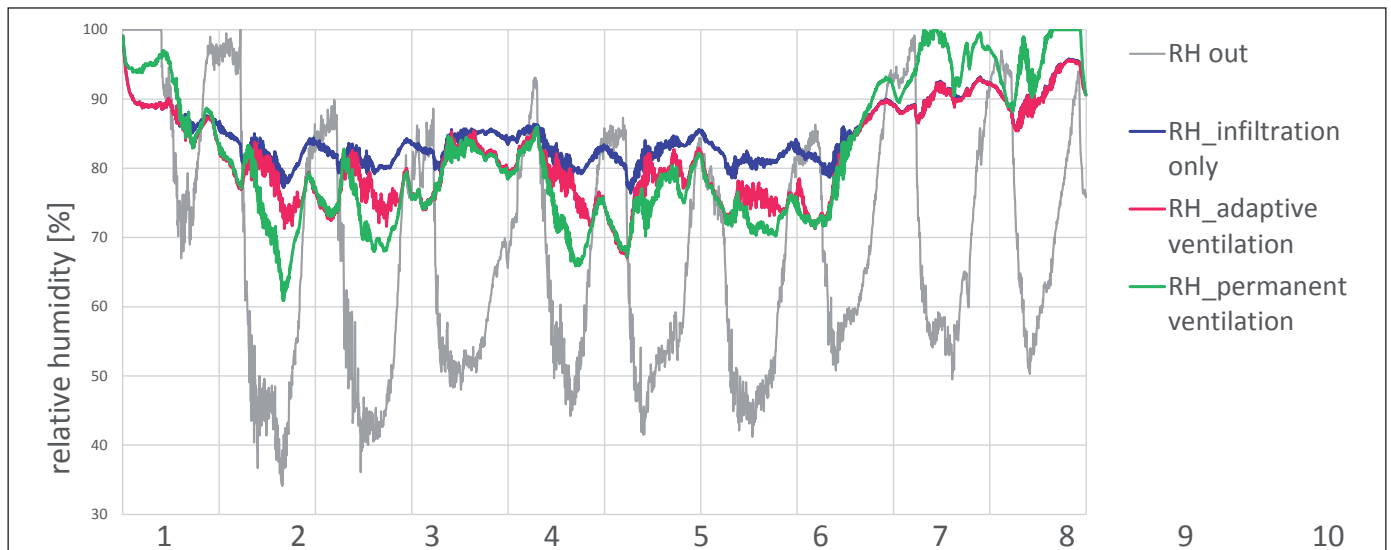


Fig. 5 Comparison of the relative humidity values for the different ventilation modes during the selected period of 10 days.

cases it could also lead to increased values. The adaptive ventilation (red line) represents an acceptable rate in the relative humidity decrease, and leads to an overall decrease in the relative humidity values.

**Reduction of the risk of the condensation on surfaces**

The graphs in Fig. 6 assess the degree of condensation risk during the year for the individual modes of ventilation. The percentage of time in which the indoor dew point temperature drops below the surface temperature of the walls is indicated in the red region.

The spring season represents the critical periods for all the variants. In spring, the surface temperature is still low, caused by the high heat capacity of the massive walls, and the warm wet outdoor air together with the moisture from the corridor, caused the condition for condensation. Due to the lower relative humidity in the interior, the adaptive ventilation

reaches the conditions with the lower condensation risk in the infiltration mode only. As was expected, the highest potential for condensation risk, is represented by the constant ventilation.

**Reduction of the relative humidity fluctuation**

The assessment of the adaptive ventilation mode was based on the Performance Index (PI) defined as the percentage of time in which the indoor air conditions (air temperature and relative humidity) lie within the required range [13]. The parameters of the indoor environment for the historical interior are defined in the ASHRAE standard [10], which divides the indoor environment into several categories according to the degree of preservation risk. An acceptable risk is defined by the values with  $\pm 10\%$  RH and  $\pm 5\text{ K}$  deflection from the ideal values of 50 % RH and 20 °C. An extremely high risk is defined for the relative humidity values higher than 75 % [10].

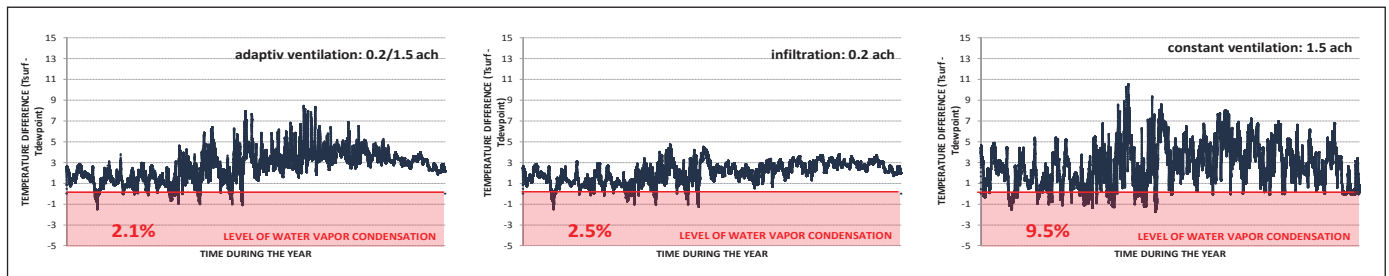


Fig. 6 Comparison of the condensation risk for the different ventilation modes during the year.

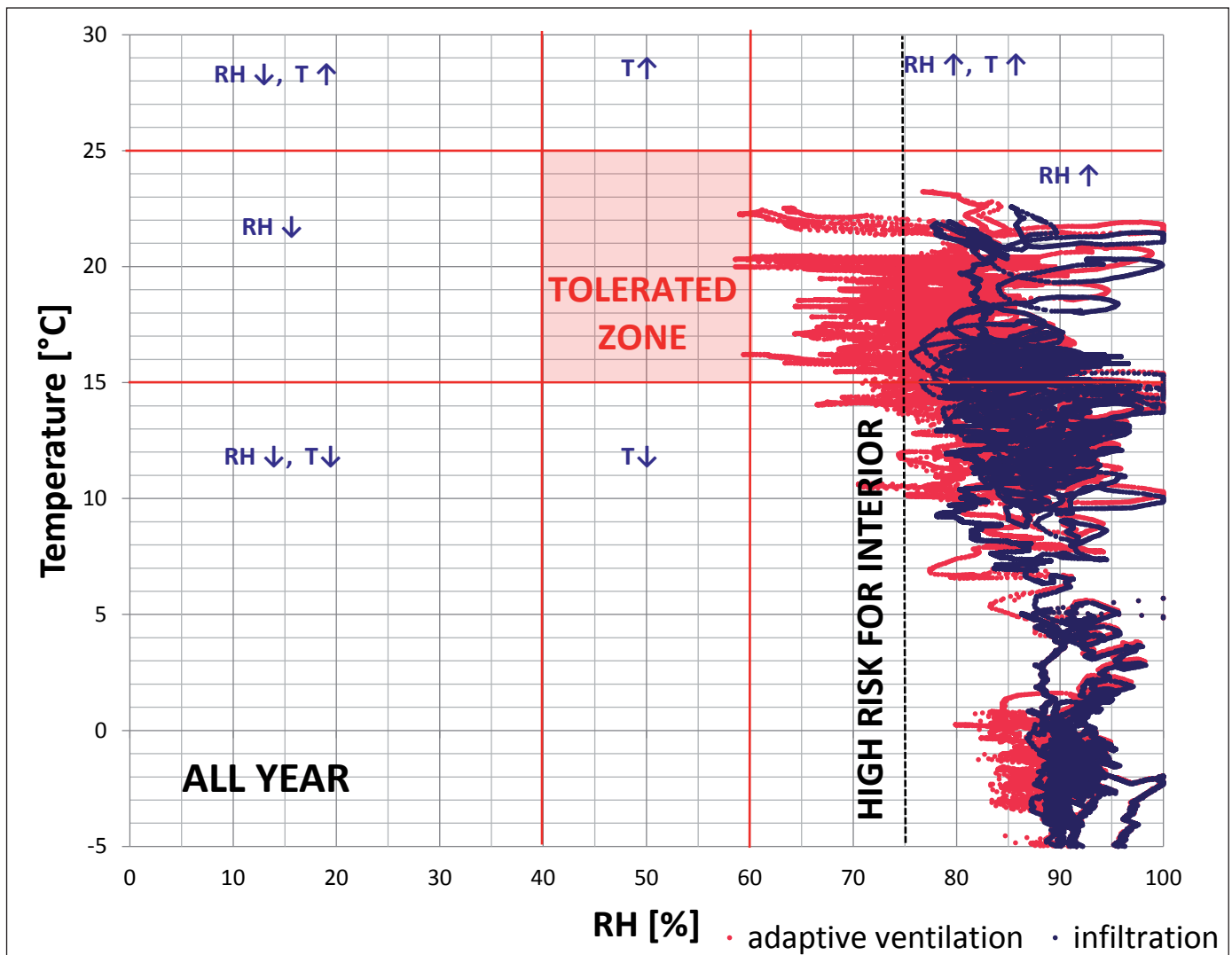


Fig. 7 Comparison of the calculated air temperature and the relative humidity values (blue dots: with infiltration only, red dots: with adaptive ventilation).

The red dots in Fig. 7 representing the performance of the adaptive ventilation indicate the improvements, where the values of the relative humidity are shifted towards the tolerated zone. On the other hand, no improvements can be observed in some periods. For example, the values in the winter period only show a slight improvement due to the low outdoor temperature, which prevents the use ventilation most of the time.

## DISCUSSION

In order to maintain the indoor environmental parameters in the historic interior, especially with the air moisture reduction, these interiors are often manually ventilated. However, there is the possibility that the outdoor air supply could have a negative impact on the interior. It depends on the climatic conditions. For this reason, in depth knowledge regarding ventilation of the interiors is necessary.

As expected, adaptive ventilation can only partially satisfy the quality requirements of the indoor environment. However, the results of the adaptive ventilation have shown the improvement in the indoor air quality. Minimal energy use of this system can be expected when compared to the energy use of the mechanical air-conditioning systems. It can be assumed that the influence of the adaptive ventilation on the quality of the indoor environment will not be similar for buildings with different operations. A positive effect is especially expected in buildings with some added source of moisture, which can be caused by the occupants or a structural defect. In this case, adaptive ventilation is able to provide a cheap solution to achieve acceptable conditions that preserve the historical interior.

However, the results for one-year study presented in this paper reveal that the adaptive ventilation strategy can have a positive effect over a longer period of time. The results show that the adaptive ventilation strategy reduces the specific humidity by 12% on average over the one-year period. Thus, further reduction of the moisture in the indoor air can be expected in the following years.

## CONCLUSION

The presented simulation using a simplified numerical model demonstrates that the selection of a suitable control algorithm for adaptive ventilation can have a positive effect on the quality of the indoor environment. The model was created by the regression method using the measured data of the air temperature and relative humidity in the interior and exterior. The paper describes the boundary conditions ensuring that the interior will not be damaged due to the sudden change of internal conditions and a large amount of outside air. The results of the numerical model confirmed the positive effect of adaptive ventilation on buildings with some additional source of moisture (e.g., occupants or structural defects). At the same time, the assumption of a different efficiency in the individual periods was verified, proving that the influence on the parameters in winter is minimal.

**ACKNOWLEDGEMENTS:** This paper was supported by the grant SGS18/013/OHK1/1T/11 and the Competence Centres Programme of the Technology Agency of the Czech Republic, project No. TE02000077 "Smart Regions - Buildings and Settlements Information Modelling, Technology and Infrastructure for Sustainable Development"

Contact: [michala.lysczas@fsv.cvut.cz](mailto:michala.lysczas@fsv.cvut.cz)

## REFERENCES

- [1] PAVLOGEORGATOS, G. Environmental parameters in museum. *Building and Environment*. 2003, 38, pp. 1457 – 1462.
- [2] FILLIPI, M. Remarks on the green retrofitting of historic building in Italy. *Energy and Environment*. 2003, 38, pp. 1457 – 1462.
- [3] Loreto Chapel. *Loreto Chapel* [online]. Available at: [www.loretarumburk.cz](http://www.loretarumburk.cz)
- [4] Biskupství Litoměřické. *Measurement report of Loreto in Rumburk* [online]. Available at: <http://www.dltm.cz/ceske-vysoke-uceni-technicke-provadi-vyzkum-v-lorete-v-rumburku>.
- [5] ERHARDT, D., ANTRETTETTER F., KILIAN R. Measured and Modelled Influence of the Moisture Buffer Effect in a Historic Stone Church and its Influence on Possible HVAC Measures. *Proceeding of CLIMA 2013 - 11th REHVA World Congress and the 8th International Conference on Indoor Air Quality, Ventilation and Energy Conservation in Buildings 2013*.
- [6] SINIVEE, V., KURIK, L., KALAMEES, T. A simple adaptive ventilation controller for mediaeval church. In: *11th Nordic Symposium on Building Physics, NSB2017, Trondheim, Norway. Energy Procedia*. 2017. 132, pp. 957 – 962.
- [7] OMRANI, S. et. al. Effect of natural ventilation mode on thermal comfort and ventilation performance: Full – scale measurement. *Energy and Buildings*. 2017, 156, pp. 1 – 16.
- [8] BROSTRÖM, T., HAGENSTOFL, C. E., WESSBERG, M. Humidity Control in Historic Buildings through Adaptive Ventilation: A Case Study. In: *9th Nordic Symposium on Building Physics, Tampere, June 2011*.
- [9] GHIAUS, CH. Causality issue in the heat balance method for calculating the design heating and cooling load. *Energy*. 2013, vol. 50, pp. 292-301.
- [10] ASHRAE. *Ashrae application book: Museum, libraries, and archives*. 2017, pp. chapter 21.
- [11] KINDLER, E., KRIVÝ, I. *Simulace a modelování*. University of Ostrava guide-book, 2001.
- [12] BALOUNOVÁ, M., KABEL, K., CORGNATI, S. P. Condensation Risk assessment and IEQ in Pilgrimage chapel of Holy stairs. *proceeding of the 12th REHVA World Congress*.
- [13] CORGNATI, S. P., FILIPPI, M., PERINO, M. A new approach for the IEQ (Indoor Environmental Quality) assessment, Research in Building Physics and Building Engineering. *Proceeding of 3rd International Conference on Research in Building Physics IBPC 2006, Montreal*.
- [14] ASHRAE. *Ashrae hand book: Nonresidential Cooling and Heating Load Calculation*. 2005, Chapter 30.

## LIST OF SYMBOLS

$c$	specific heat capacity [J.kg <sup>-1</sup> .K <sup>-1</sup> ]
$T_i$	indoor air temperature [°C]
$T_e$	outdoor air temperature [°C]
$T_m$	temperature of the mass [°C]
$T_{dp}$	dew point temperature [°C]
$RH$	relative humidity [%]
$\rho$	density [kg.m <sup>-3</sup> ]
$A$	area [m <sup>2</sup> ]
$V_i$	volume of indoor air [m <sup>3</sup> ]
$V_e$	volume of outdoor air [m <sup>3</sup> ]
$U$	overall heat transfer coefficient [W.m <sup>-2</sup> .K <sup>-1</sup> ]
$d$	effective thickness [m]
$h$	convection heat transfer coefficient [W.m <sup>-2</sup> .K <sup>-1</sup> ]
$x_i$	indoor humidity ratio [kg.kg <sup>-1</sup> ]
$x_e$	outdoor humidity ratio [kg.kg <sup>-1</sup> ]
$\tau$	time [s]
$G$	accumulation moisture uptake [kg/m <sup>2</sup> ]

Ing. arch. Vojtěch MAZANEC <sup>1)</sup>  
Prof. Ing. Karel KABELE, CSc. <sup>2)</sup>

<sup>1)</sup> CTU in Prague, University  
Centre for Energy Efficient  
Buildings

<sup>2)</sup> CTU in Prague, Faculty of  
Civil Engineering, Department  
of Indoor Environmental and  
Building Services Engineering

Reviewer  
Ing. Petra Šťávořová, Ph.D.

# Personalised Ventilation with Air Temperature Customisation: Impact on the Design and Thermal Comfort of the User

**Osobní větrání s úpravou teploty vzduchu: Dopad na návrh zařízení a tepelnou pohodu uživatele.**

*The paper deals with the customisation of the supply air temperature in a personalised ventilation system and its impact on the air flow, the efficiency of the ventilation, and the thermal comfort of the human body. The system was designed to enable customisation of the surrounding environment conditions mainly for people working in open space types of offices. Our measurement evaluated the system design and efficiency in different temperature states of the air: for the isothermal flow and for the heating and cooling of the supply air. A prototype of the micro air handling unit (a device for personal air customisation) was used for the measurement, a thermal manikin was used to simulate the convective boundary layers around a sitting human body. A Particle Image Velocimetry (PIV) was used to measure and visualise the air conduction and air-flow interaction. The thermal manikin was also measuring the thermal comfort of the user in different modes of operation.*

**Keywords:** personalized ventilation, micro air handling unit, thermal comfort, thermal manikin, PIV anemometry

*Článek se zabývá možností přizpůsobení teploty přiváděného vzduchu v systému personalizovaného větrání a dopadem takové úpravy na efektivitu daného systému a tepelný komfort uživatele. Systém personalizovaného větrání byl navržen pro úpravu prostředí v blízkém okolí uživatele a to převážně pro pracovníky ve sdílených kancelářích typu open-space. Prováděná měření mají za cíl zhodnotit, jaký má navržený systém s úpravou teploty reálný dopad na tepelný komfort, a jestli je pro takovou možnost správně nastaven. Pro měření bylo použito prototypu mikro klimatizační jednotky (zařízení pro osobní úpravu a distribuci vzduchu), termálního manekýna, který zároveň simuloval chování konvektivních proudů vzduchu kolem lidského těla a měřil dopad teploty a množství přiváděného vzduchu na uživatele. Pro měření a vizualizaci proudění bylo využito anemometrie typu PIV (Particle Image Velocimetry).*

**Klíčová slova:** osobní větrání, personalizované větrání, mikro klimatizační jednotka, tepelný komfort, PIV anemometrie, termální manekýn

## INTRODUCTION

We live in an age where the majority of people are continuously separated from the outside world and are enclosed by an impermeable building envelope. We spend almost 90 % of our time inside buildings or in means of transport [1]. Separation between the indoor and outdoor environment is necessary to decrease our energy needs, but, in many cases, it has a negative impact on the environment in which we spend the majority of our time. A lot of people do not have access to a healthy environment today and it is becoming a problem that we should seriously deal with.

A personalised ventilation system is one of the modern alternatives to create a healthy, adaptable and energy efficient indoor environment in places shared by many people, like open space offices, where it is quite difficult to maintain a good quality environment by a central ventilation system. Personalised ventilation provides fresh air directly to the places where it is needed the most, in the personal zone of every user. It creates a customised space for every person in the room, which lowers the risk of disease transmission, increases the wellbeing and productivity of the users [1]. It is also more adaptable to personal differences and needs caused by the uniqueness of every person and their actual condition [9]. The impact of the standard personalised ventilation has been measured in several studies [1, 6], but what if we can personalise not just the amount of air supply, but even its temperature?

## Problem description

In our previous work, we designed a personalised ventilation system, which uses a micro air handling unit as personal device to customise the air temperature and volume. In previous studies we dealt with the efficiency of the fresh air distribution, the shape of the airflow and other conditions of the personalised ventilation system in an isothermal state (which means that the supply air had the same temperature as the room's air) [3]. But the unit was designed to mainly operate in non-isothermal modes. In this study, we focused on the thermal comfort of the user and the efficiency of the ventilation, if the unit is in a heating or cooling mode.

## Experimental setup

For the measurement, we used a prototype of the personalised ventilation system designed in our previous work [7] [10]. It is designed for open space offices with displacement ventilation, where the fresh air is supplied thorough the doubled floor. The system consists of a micro air handling unit placed in the doubled floor space and personalised ventilation diffusers mounted on the workspace. It is connected by insulated piping. The system design and layout is shown in Figure 1. The micro air handling unit sucks the fresh air from the doubled floor. Through its fan and Peltier cells, it is able to adjust the volume and temperature of the air supplied to the personalised ventilation. The range of the air temperature supply is approximately 8 K (from -4 to +4 K) and the air flow supply rate is from 20 to 50 m<sup>3</sup>/h. The personalised diffusers are mounted on the

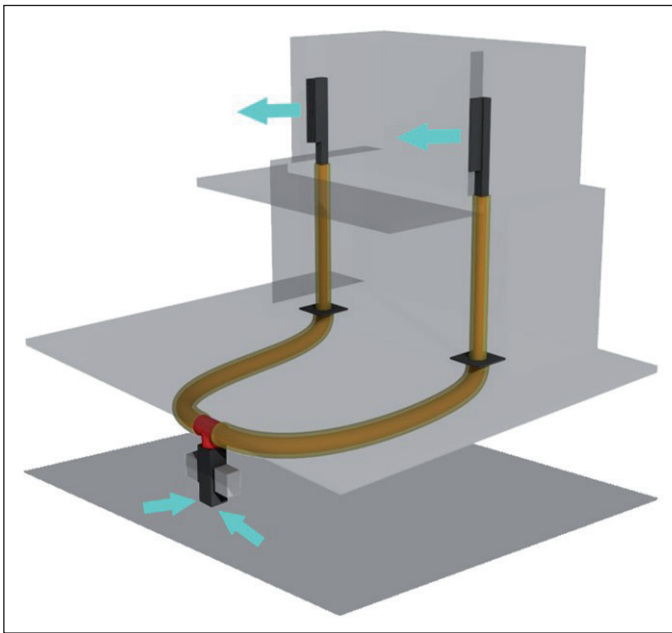


Fig. 1 The system of the personalised ventilation used in the measurement.

back corners of the workspace table (from the users perspective), and are directed to the middle of the opposite side.

To simulate the real velocity field of the air around the human body and to measure the thermal comfort of the user, a thermal manikin was used. It is a physical model of a male human body and produces convective boundary layers similar to a real user. For measurement of the air velocities, a Particle Image Velocimetry (PIV) was used. It creates a thin laser layer illuminating the particles spread into the air. The movement of those particles is captured on fast capturing cameras and the velocity field is then computed from the particle shift.

The measurement was set to simulate a regular workspace in the office. The manikin was sitting in front of the table and the diffusers were placed in the back corners as should be used in the real situation. In Figure 2, we can see the layout of the measurement and a presumed flow from the diffusers based on the previous CFD simulations [8] and measurements [3]. We can see, from Figure 2, that the main airflows will come from the sides and meet in the middle of the table, where it creates one flow parallel to the laser layer and directed to the manikin (the airflow shape used in Figure 2 is based on the CFD simulation and was verified by the measurement, it is noticeable that the flow does not come from the side, but develops in the measured area in the figures in the result part).

The manikin was clothed to a clothing value commonly used in offices. We used a long-sleeved shirt and a pair of trousers to set the thermal insulation value to 0.54 clo. The manikin was set to a surface

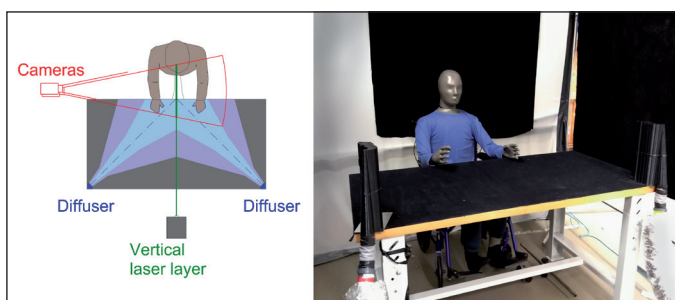


Fig. 2 The measurement setting

temperature of 35 °C, it was neither breathing nor was producing any moisture.

The room temperature was set to 24 °C and measured at three points of different height (the ankles, belly and head of sitting person) as required by the standard. The deviation of the ambient air temperature during the measurement was 0.63 K and the ambient air velocity was in the range of 0.05 to 0.13 m/s at a distance of 1.5 from the manikin. In the personal zone of the manikin, the temperature range was higher due to heating and cooling of the zone, but has a deviation of less than 0.3 K for each separate measurement. The room was equipped with a separate cooling and heating system to keep a steady temperature.

Three different modes of operation were measured – isothermal, heating (+4 K) and cooling (-4 K) and every mode of operation were measured for two airflow volumes – 25 and 50 m<sup>3</sup>/h.

## EXPERIMENT 1 VELOCITY FIELDS

One can see the setting of the PIV anemometry in Figure 2. The laser was set in a vertical position in the middle of the table in front of the manikin to measure the airflows around its chest and the head. Two cameras for the PIV anemometry were placed in a vertical setting (to extend the measured area) and measured the 2-dimensional array.

The average vector field is computed from 50 continually captured images and the time sample (length of capture) is about 2 minutes. Measurements were conducted after a steady state was achieved.

### The velocity field results

In the results, we can see that the main flow was influenced by three main effects. The first is the interaction of the two diffusers, which is mostly visible on the flow with a lower volume and velocities. The main connected flow develops in front of the manikin at the edge of the table and continues towards the manikin. The second effect represents the convective boundary layers around the human body, caused by the difference between the air temperature and the surface of the body. It creates a vertical flow with air speed in a range of 0.1 to 0.2 m/s [6]. This flow mixes with the main flow of the fresh air from the diffusers and changes its direction upwards. It has a major influence on the efficiency of the personalised ventilation and its ability to supply fresh air to the breathing zone [6]. The last effect is the buoyancy force of the air supply of different temperature, which is quite strong, although the difference is only 4 K. It also has a significant impact on the efficiency of the ventilation, because the diffusers were primarily designed for isothermal conditions.

The first measurement was made in the isothermal state as the system was originally designed. One can see from Figure 3 that the results look very good. The airflow is developing as it should and transports the fresh air to the breathing zone. It is deflected by the convective layers upward, but not too early. It creates a personal zone of a microenvironment of moving fresh air as was simulated and measured in previous studies. Even in higher volumes, the air velocity of supply air does not exceed the limits of the draft. It ranges in an optimal range between 0.1 and 0.2 m/s around the manikin.

The air flow of the heating mode of the personalised ventilation shows slightly worse results. The temperature of the air supply was set to 28 °C and we can see that the buoyancy effect deflects the fresh air flow upwards above the head of the user in Figure 4, which means that most of the fresh air does not reach the breathing zone and is ineffectively mixed with the ambient polluted air out of the personal zone. The impact of the fresh air is less efficient and the design of the diffuser has to be changed

in further development to balance the buoyancy force by the direction of a muzzle velocity vector.

Contrary to heating, during the cooling mode, the air slides on the surface of the table and reaches the users breathing zone lower than the isothermal flow. We can see the results in Figure 5. The temperature was set to 22 °C. The airflow slightly cools the surface of the chest and lowers the velocity of the convective layers, which both benefits the personalised ventilation efficiency, but it can cause a temperature discomfort for the hands if the air temperature is too low. The velocity can also cause a problem because it is almost reaching the velocities of the draft (about 0.25 m/s) in the zone of the hands.

### EXPERIMENT 2 THERMAL COMFORT

The thermal manikin is a well-known device, widely used for measuring the temperature balance and feeling of the human body and trans-

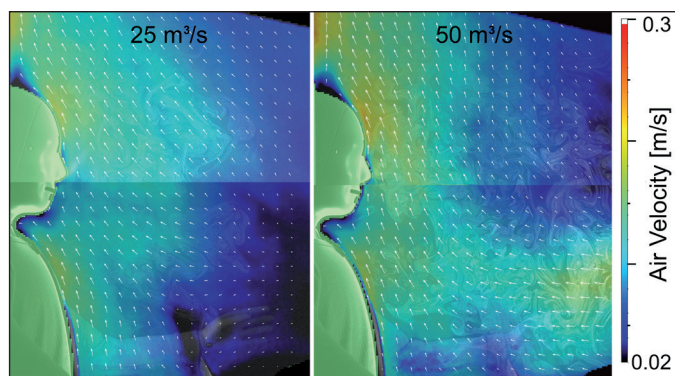


Fig. 3 The isothermal state of the ventilation for a 25 and 50 m<sup>3</sup>/h volume of air supply

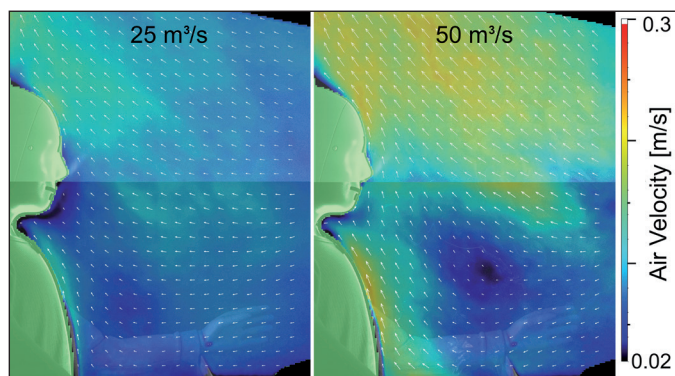


Fig. 4 The heating mode of the personalised ventilation for a 25 and 50 m<sup>3</sup>/h volume of air supply

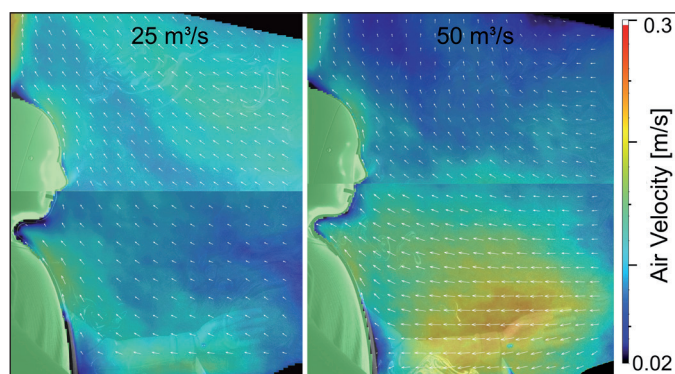


Fig. 5 The cooling mode of the personalised ventilation for a 25 and 50 m<sup>3</sup>/h volume of air supply

lates the senses of human body to some solid data form [2]. It can be used in a wide variety of spaces, from tight vehicle cabins to the open space indoor environment of buildings. It measures many separate zones of the body and can define the places of comfort and discomfort caused by drafts or inappropriate temperatures. It also produces heat as a standard human body does, which is crucial for the interaction of the personalised ventilation diffuser flow with conductive boundary layers of the human body.

For our measurement, we used a Czech standard for the measurement with the thermal manikin ČSN EN ISO 14505-2 [5], which is made to measure the environment in a vehicle, but can be easily used for a building as well. The assessment is based on the measurement of the equivalent temperature, which integrates the independent effects of convection and radiation on the heat exchange of a person [2]. It describes the level of thermal neutrality on the separate zones. The equivalent temperature measurement is based on the measurement of energy consumed by the manikin to heat the zone and keep the temperature on the set value.

The measurement of the thermal comfort by a thermal manikin uses the TMS (thermal manikin sensation) method instead of the equivalent temperature  $t_{eq}$ . There are two values, TMS<sub>o</sub> (thermal manikin overall sensation) and TMS<sub>z</sub> (thermal manikin zone sensation). This new index enables the easier interpretation of the results and comparison with the widely used PMV (Predicted Mean Vote) index also. To compare the results with the PMV index, the standard ASHRAE scale is used. It goes from -3 to +3, where -3 is cold, 0 is temperature neutral and comfortable and +3 is hot [4] [2].

### Results and discussion

The thermal manikin was measuring the thermal comfort in the different zones of the human body. Figure 6 shows the impact of the different mode and air volume on the whole body and the separate zones. The horizontal axis of the figure shows the TMS, respective the PMV index. Because of the quite small differences, we just used part of the scale from -1.5 to +1.5 to make the results clearer. The vertical axis shows the different zones of the body and the top line is for the overall body sensation.

Each zone had its own different sensitivity to the different influences and we can see how the velocity field impacts the results. In our case, the thermal comfort shift is based on both the air temperature and the velocity, but it differs not simply by the mode. For example, we can see that the heating mode feels colder than the cooling mode in the face zone that for 25 m<sup>3</sup>/h. It is caused by the upward direction of the flow in the heating mode and higher velocities around the face. In the cooling mode, the main velocity field is centred by the hands and the belly and the air velocity around the face is lower. Another interesting fact is that the lower air volumes cool the body under the desk more. It is probably caused by the high velocities of the air around the body, decreasing the effect of buoyancy of the cool air.

We also have to mention that the posture of the body changes the impact and is more difficult to say how the effect is on someone working and changing their posture often. We can see the example of the different impacts in different places on the left and right hand. The left hand was placed closer to the centre of the table, which means more in the airflow direction and the impact of cooling on it was significantly higher than on the right hand.

For the overall sensation we can say that the cooling and heating of the air supply has its impact on the thermal comfort. And although it is not significant, it is in the scale we were trying to achieve, because the temperature customisation is not meant to completely change the

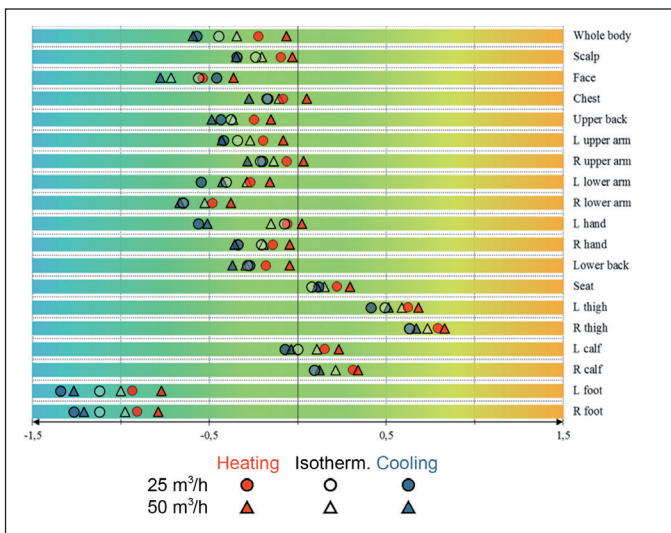


Fig. 6 The impact of the heating and cooling system to the thermal comfort zone

environment, just make it more personalised. However, the environment is not as stable as we wanted to have it.

## CONCLUSION

In our study, we were trying to measure the impact of the heating and cooling of the air supply of the personalised ventilation system. We heated and cooled the air by 4 K to measure the difference and compare it with the isothermal operation. Basically, we can say that the heating and cooling has an impact on the thermal comfort of the user and it can be used to adjust the temperature of the personal space. The possibility of the air customisation could have a positive effect on the wellbeing and the number of people dissatisfied with the environment.

On the other hand, we have to say that the present design of the personalised ventilation system is not as efficient as it could be and in the next research we should focus on creating a diffuser more adapted on the different temperature and A more stabilised environment could have

better results on both the side of the thermal comfort impact and the ventilation efficiency.

Contact: vojtech.mazanec@fsv.cvut.cz

This work has been supported by the Ministry of Education, Youth and Sports in the project NPU I no. LO1605 - University Centre for Energy Efficient Buildings – Sustainability phase and by the Grant Agency of the Czech Technical University in Prague, grant No. SGS18/014/OHK1/1T/11

## References

- [1] MELIKOV, A. K. Advanced air distribution: improving health and comfort while reducing energy use. *Indoor Air*. 2016, 26: 112–124. doi:10.1111/ina.12206
- [2] HORVÁTHOVÁ, J., KABELE, K. Vytápění budov s téměř nulovou spotřebou energie – platí osvědčené principy hodnocení? *Vykurovanie*. 2018. Bratislava: SSTP. ISBN 978-80-89878-20-8.
- [3] MAZANEC, V., KNY, M., KABELE, K. The impact of the Human Body's Convective Boundary Layers on the Design of a Personalized Ventilation Diffuser. *Vytápění, větrání, instalace*. 2017, 6, 355-359. ISSN 1210-1389.
- [4] HORVÁTHOVÁ, J. *Vliv způsobu vytápění na kvalitu vnitřního prostředí*. Praha, 2017. Disertační práce. České vysoké učení technické v Praze, Fakulta stavební.
- [5] ČSN EN ISO 7730. Ergonomie tepelného prostředí – Analytické stanovení a interpretace tepelného komfortu pomocí výpočtu ukazatelů PMV a PPD a kritéria místního tepelného komfortu. Český normalizační institut. 2006.
- [6] MELIKOV A. K. Human body micro-environment: The benefits of controlling airflow interaction. *Building and Environment*. 2015; 91:70-77. Available from, DOI: 10.1016/j.buildenv.2015.04.010
- [7] MAZANEC, V., KABELE, K. Optimalizace prototypu mikroklimatizační jednotky pro systém osobního větrání CFD simulací. *Vytápění, větrání, instalace*. 2017, 4, 212-217. ISSN 1210-1389.
- [8] MAZANEC, V., KABELE, K. Personalizované větrání pro pracoviště dispečera, In: *22. konference Klimatizace a větrání*. Praha: Společnost pro techniku prostředí, 2017, pp. 118-123. ISBN 978-80-02-02739-3.
- [9] ČERMÁK, R., MELIKOV A. K. Osobní větrání. *Vytápění, větrání, instalace*. 2003, 5, pp. 199-202. ISSN 1210-1389.
- [10] MAZANEC, V., KABELE, K. The Personal Ventilation System with Air Temperature Customization Using a Peltier Effect. In: *CLIMA 2016 - proceedings of the 12th REHVA World Congress: volume 5*. Aalborg: Aalborg University, 2016. ISBN 87-91606-30-6.

Ing. Ondřej NEHASIL  
Ing. Daniel ADAMOVSÝ, Ph.D.

CTU in Prague, University Centre  
for Energy Efficient Buildings

# Ventilative Cooling Control Strategy for Variable Air Volume Ventilation Systems

## Strategie řízení chlazení větracím vzduchem pro systémy s proměnným průtokem vzduchu

Reviewer  
Ing. Jan ŠIROKÝ, Ph.D.

*One disadvantage of highly insulated buildings is their overheating, with the subsequent necessity of removing excess heat. This is often done via mechanical cooling. However, increased energy consumption related to mechanical cooling is far from compatible with achieving zero-energy buildings. This paper presents a detailed description of a control mechanism that can be implemented in newly designed or even existing buildings with a VAV (Variable Air Volume) ventilating system, which leads to a significant reduction in the annual energy consumption of mechanical cooling. A control strategy has been developed and validated on the multi-zone model of a school building. The results show energy savings above 40% when using ventilative cooling. The maximum efficiency was found in the range between 0.5 and 0.7 times the nominal volumetric flow rate.*

**Keywords:** air handling units, control, cooling, VAV

*Jednou z nevýhod dobře zaizolovaných budov je jejich sklon k přehřívání s následnou nutností odvádění tepelné zátěže. K tomu se obvykle používá strojní chlazení. Spotřeba energie související se strojním chlazením je však v rozporu se snahou stavět budovy s téměř nulovou spotřebou energie.*

*Tento článek představuje podrobný popis řídicího mechanismu, který lze realizovat v nově navržených nebo dokonce existujících budovách s větracím systémem VAV (Variable Air Volume), což vede k významnému snížení roční spotřeby energie na chlazení. Byla vyvinuta a potvrzena strategie řízení chlazením větracím vzduchem na vícezónovém modelu školní budovy. Výsledky ukazují úsporu energie větší než 40% při použití chlazení větracím vzduchem na případové studii. Maximální účinnost byla zjištěna v rozmezí 0,5 až 0,7 násobku jmenovitého objemového průtoku vzduchu.*

**Klíčová slova:** vzduchotechnická jednotka, regulace, chlazení, VAV

## INTRODUCTION

Cooling is an important issue for contemporary buildings, and its importance is growing with the increasing quality of a building's envelope, the indoor heat gains due to the increasing amount of electronic equipment, and the tightening of the requirements on indoor environments and climatic change [1]. Cooling devices came into the market in the 1930s as rare luxury devices, which first became affordable in 1947 [1]. In 2015, they represented a rapidly developing industry sector, approaching a total annual turnover of close to 100 billion dollars, and it is still growing.

The cooling of buildings represents a considerable percentage of the total energy consumption in the world. The world annual energy consumption for cooling in 2010 was close to 1.25 PWh. More than 45% of that energy was consumed by commercial buildings. The future average cooling energy demand for commercial buildings is calculated to rise 275% by the year 2050 from the consumption in 2016 [2], despite the efforts to achieve energy efficient buildings [3].

However, unlike heating, cooling can often be provided by natural and economic systems of low-energy cooling techniques, with no compressor-based cooling. Most of those techniques are based on the alternation of day/night temperatures, the temperature differences between the outdoor and indoor air, and high temperature sources of natural coolness, such as the ground or a water mass. All these techniques have their own individual limitations, especially regarding the available power or the total amount of available coolness [4].

Ventilative cooling, a frequently discussed method for low-energy cooling techniques, requires the use of outdoor air at a lower temperature than the indoor air to cool the interior. In residential buildings, this is a

convenient way to keep the indoor temperature low enough to be comfortable [5]. The potential for using outdoor air is certainly not negligible, especially in combination with night pre-cooling, at least in European climates [6], in North Africa [7] or in China [8]. Even in southern Europe or central Turkey, there are places where the mean climatic potential is more than 40 Kelvin-hours per night during July [6]. And in a very hot and humid climate, such as in Taiwan, it is still convenient to cool by using outdoor air via hybrid ventilation [9].

But natural night or hybrid ventilation also holds the risk of overcooling, which leads to discomfort for the occupants in the morning. This suggests adding a weather forecast and a building model to the BMS (Building Management System), and it has been proven that this leads to better results [10-12].

Night-time cooling is also very sensitive to the usable thermal capacity. Coolness, which is available during the night-time, is needed during the daytime. The accumulation of the coolness is possible in the building, as well as outside the building in the groundmass [13]. The thermal capacity of a building can be increased by PCM materials, which can be used not only as a plastering material, but can also be implemented directly in air-ducts to store the night-time coolness for daytime utilisation [14].

The idea of utilising the 24-hour continuous one-way operation of a ground-tube with a high accumulation ability has also been found to be particularly successful. Due to the phase shifting of the temperature peaks, this brings the night-time coolness into the interior during the day, but, due to the same phenomenon, hot air during the night as well [14]. To eliminate this disadvantage, it is necessary to add multiple dampers and an additional fan to the pipes, as well as to employ the more sophis-

ticated operation of the ground-tubes or, alternately, to abandon the idea of utilising the groundmass heat capacity.

It has been proven that problems with ventilative cooling, such as too small a cooling capacity during the day or overcooling during the night, can be solved if the ventilative cooling is controlled and if an adaptive model of the thermal comfort is used [15]. Commercial buildings are usually equipped with mechanical ventilation to satisfy the indoor air quality requirements [16]. Under these circumstances, the utilisation of ventilation equipment for cooling would clearly be advantageous [17].

Multiple studies [5, 6, 10, 18] prove that the major issue in ventilative cooling is the fan energy consumption and optimal fan operation. To provide effective ventilative cooling, the supply-air temperature and supply-air flow rate are the primary parameters to be optimised in time in order to reach a high energy efficient VAV system [19].

Most previously published strategies deal with airside economisers in VAV systems, used for fresh air supply and heating/cooling [20-30], with no heat recovery between the fresh and exhaust air. Much less attention has been paid to heat recovery usage in VAV [31-33]. This has led to the necessity of finding a balance between the fresh air rate, the total amount of the supply-air (and its temperature) to simultaneously satisfy the requirements of thermal comfort and Indoor Air Quality (IAQ) [20] [23-26]. Some attention must also be paid to the speed of the response to regulatory intervention and the energy consumption in the transition states of VAV [22, 28, 34].

This paper deals with idea that the most effective VAV ventilation system serves the fresh air supply only, when the thermal comfort of any room is ensured by the additional systems of heating or cooling. The strategy presented develops the idea of synergy between ventilation, heating and cooling, while describing how to operate systems mainly designed for ventilation in order to assist the cooling of the ventilated spaces.

Using heat recovery exchangers and delegating the responsibility for the thermal comfort to the additional heating/cooling systems, VAV sys-

tems no longer need an economiser and operate at all times with 100% fresh air. The supply air temperatures can then be modified by altering the amounts of ventilated air by bypassing the heat recovery exchanger. A continuous control strategy for the bypass valve position and supply air volume is described in the paper.

Unlike most previously presented strategies [24, 28, 30, 33], the physical quantity regulated is not the temperature in the intake air-duct, with little regard for the needs of the space, but directly attributed to the temperature of ventilated spaces. The temperature in the inlet duct is only measured so as not to exceed certain safety and hygienic limits.

**CONTROL STRATEGY**

The method entails a newly developed control strategy, driving both the position of a bypass valve around the heat recovery exchanger and the air flow supply. This strategy was then tested in a case study – a TRNSYS model of an actual building located in the Netherlands.

**Boundary conditions for the Ventilative cooling control**

The operation is intended for an AHU with heat recovery, which also has a bypass channel around the heat recovery installed (or equivalent ability to stop or slow the rotary exchanger) to stop or slow the rotary exchanger in the VAV systems, with a high level of control – its actual critical route must be ascertained continuously. In the commercial buildings sector, VAV systems are the most energy efficient systems in use today [19].

To increase the power and efficiency of ventilative cooling, an adaptive model of thermal comfort [35] must be utilised, setting a range of comfortable indoor temperatures. The adaptive model adopted must include all contexts, such as adjusting the dress-code or allowing the occupants to change seats, as well as an individual setting of the local heating or cooling elements.

This strategy is appropriate for office buildings and public buildings such as schools, where similar temperature requirements pertain to multiple rooms.

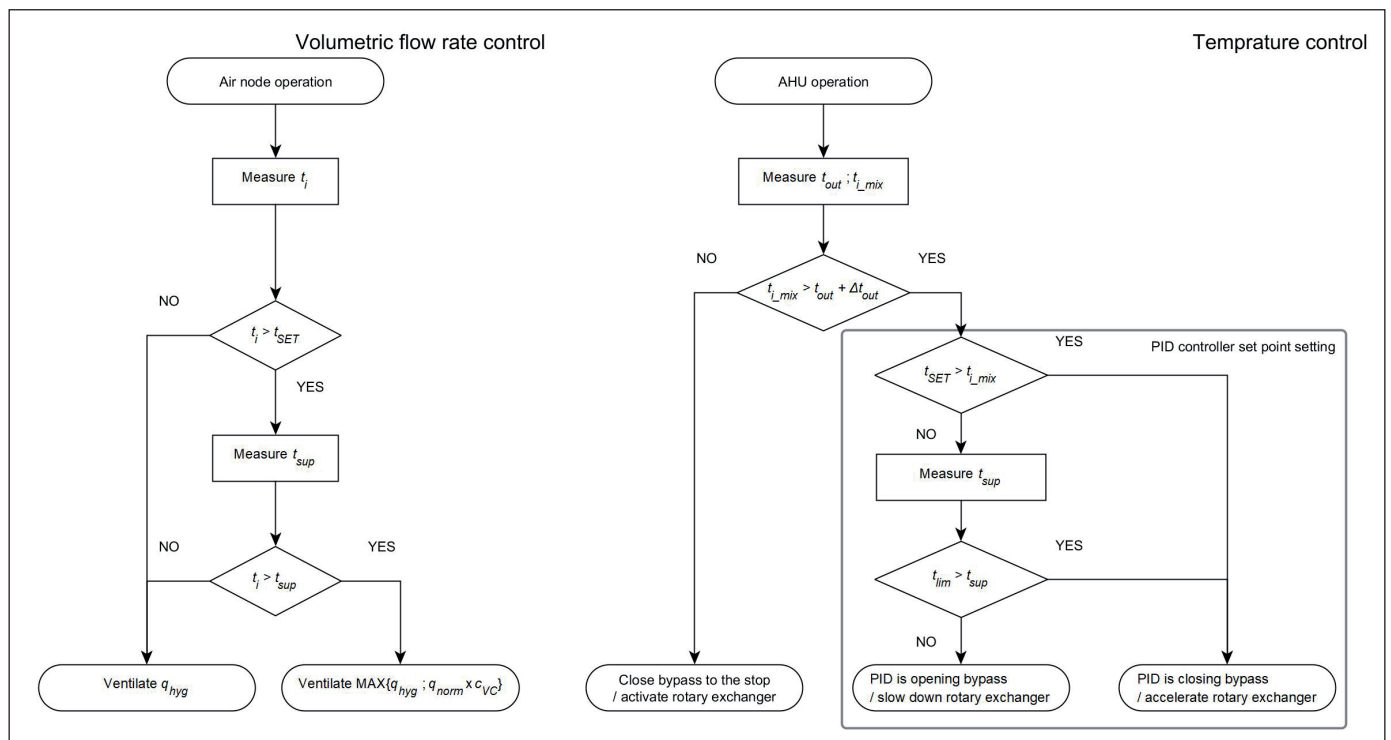


Fig. 1 Ventilative cooling operation flowchart

**Operation of the Ventilative cooling control**

The operation strategy is based on the concept that the temperatures and volumetric flow rates of the fresh air will be controlled by several criteria. The first of these is hygienic ventilation. Our study does not deal with the methods for setting the ideal hygienic flow rates of the fresh air supply for the occupants. This field is deeply discussed in [21, 29, 36-39].

The second criterion is the temperature in the ventilated spaces, which is connected with the information whether cooling is required.

The control mechanism is then divided in such a way that the VAV box uses a single air-node determining the volume of the ventilated air, and a single AHU part is used to regulate the temperature of the air intake, as shown in Figure 1. For most of the year in the Netherlands, it is possible to get fresh air at a lower temperature than the indoor temperatures without mechanical cooling.

**Operation – AHU part**

The AHU must supply fresh air to the air-ducts in order to satisfy the requirements of the VAV boxes. The AHU can regulate the temperature of the air by setting the position of the bypass valve around the heat-recovery exchanger, as shown in Figure 1, on the right side. The proportional-integral-derivative (PID) regulation must be implemented where the regulated quantity is the air temperature in the AHU's inlet duct from the ventilated spaces, where the mean temperature of all the ventilated spaces is measured. Similarly, the temperature of the ventilated zones obtained by a weighted average from local temperature sensors can be used. The set-point for this temperature is usually  $t_{com}$ , previously calculated as the set-point for the BMS. A rise in temperature in the air-duct above this set-point shows that the interior is becoming overheated, so the AHU must open the bypass to decrease the temperature at the fresh air inlet.

For the part of the year when the outdoor temperature is lower than the indoor temperature, this rule is appropriate. It can be suspended in the case where:

- the outdoor temperature  $t_{out}$  rises above the temperature measured in the AHU's inlet from the ventilated spaces, or
- the temperature at the fresh air inlet decreases to the comfort limit  $t_{lim}$ .

The temperature of the air supply to the ventilated spaces is then controlled in concert for all those spaces on the same AHU.

**Operation – VAV box part**

Simultaneously, each VAV box is also controlled to satisfy the individual requirements of a given space. The primary purpose of a VAV box is ventilation, so fresh air for hygienic ventilation must always be supplied. But when the temperature of the ventilated space rises above  $t_{com}$ , it is advantageous to supply a higher volume of cold air so as to extract the

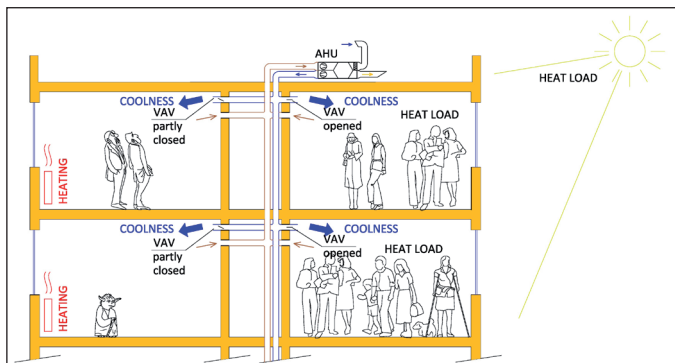


Fig. 2 Cross section of a group of rooms cooled by the ventilation [40].

heat load. The ideal flow-rate for the ventilative cooling is usually not the maximal flow-rate to a given space each and every time. This is due to the fan energy consumption and the pressure drop in the air-ducts. So, when the room is occupied, the fresh air requirement may be higher than the cooling requirement. However, during a lunch break or just after working hours, the fresh air requirement drops, while it still may be convenient to ventilate because of the accumulated heat dissipation.

Also, since the temperature is set for all the spaces collectively, and since no room can remain totally unventilated, overheated rooms may cause the slight ventilative overcooling in others, as is shown in Figure 2. This phenomenon can be mitigated by the design of the ventilation system – a small number of similar rooms connected to the same AHU behave better than a large number of variably sized spaces.

**Fan speed control**

The energy for the fans is almost the only energy required in ventilative cooling. The consumption of the controllers, motor dampers and sensors are negligible [41] (available in EN as [42]). Due to the low temperature differences between the fresh air and ventilated space, and also due to the low thermal capacity of the air, a high flow rate is required to ensure sufficient cooling power. But the transport of the air is highly energy intensive, and it is necessary to focus on the fans in ventilative cooling applications. Fan energy consumption is given as a multiplication of the volumetric flow rate and the pressure drop. For economical operation, both the pressure drop and the volumetric flow rate must be decreased in order to reduce the fan energy consumption under partial load to a minimum.

Ventilative cooling uses the Static Pressure Reset (SPR) principle based on [43], as is described below. Each VAV box must be connected to the BMS and must measure the air flow through itself (e.g., by the pressure drop on the distribution element), adjusting the damper position to reach the required flow rate, as is shown in Figure 3. Each air-node indicates its state by two logical outputs:

- OK, to indicate that the required flow rate has been reached
- FULLY to indicate that the damper has been totally opened

These signals are collected by the controller of the AHU, which adjusts the fan speed by means of the inverter. When a damper is fully open, but does not signal OK, it means that the static pressure is not high

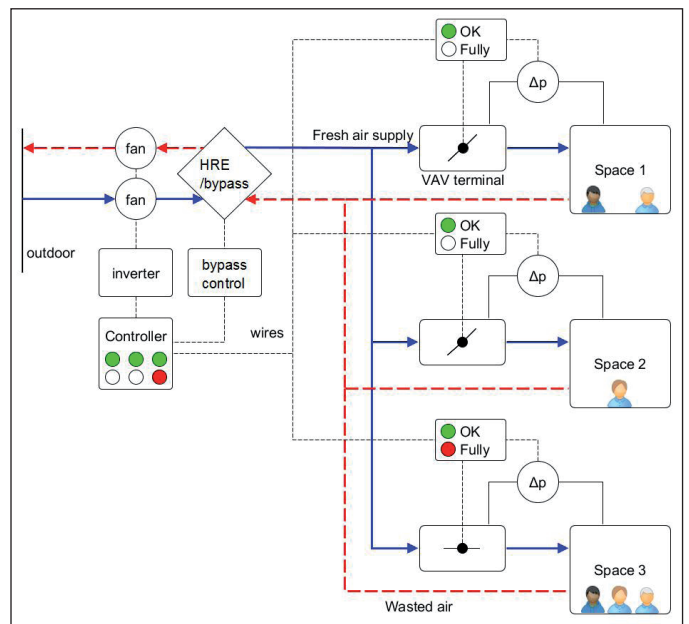


Fig. 3 SPR control, every time, at least one damper is fully opened.

enough to ventilate the requested air flow rate and, therefore, the static pressure set-point will be increased by a certain value, e.g., 5 Pa. When none of the terminals are fully opened, the static pressure set-point will be decreased by the same value, pushing the VAV terminals to open their valves.

This ensures that, at all times, at least one damper is fully opened, so that the dampers on the actual critical route will be opened. The number of opened dampers or dissatisfied terminals must be set higher than 1, for the sake of faults or improper settings in the VAV terminals [44]. Such faults or improper settings appear quite often, and a site survey indicated that 20.1% of the VAV terminals were found to be ineffective [45]. It is highly recommended that the entire system's operation should be assessed continuously, e.g., by AHU's performance assessment rules (APAR) [46].

From the perspective of practice, it is recommended to design the SFP in accordance with the recommendation of P.G. Schild and M. Mysen [47] (available in EN as [42]) or even lower.

**Coefficients and thresholds**

To set up all the control mechanisms, several constants must be set.

Ventilative cooling is practical only if the outdoor temperature is lower than the indoor temperature. However, the temperature of the air rises slightly when it passes through the fan. A threshold is necessary to switch the ventilative cooling on while condition (1) is met:

$$t_{i\_mix} - t_{out} > \Delta t_{out} \tag{1}$$

The difference  $\Delta t_{out}$  must be set between 0K and 3K, with respect to the efficiency of the ventilation system. A crucial aspect for ventilative cooling is the volumetric flow rate, which is represented by the coefficient  $c_{vc}$ . At the VAV terminal, if there is a cooling request, set the higher of the two volumes:

$$q_v = MAX \left\{ \begin{matrix} q_{hyg} \\ q_{norm} \cdot c_{vc} \end{matrix} \right\} \tag{2}$$

It was found to be ineffective to provide ventilative cooling at the maximal design speed ( $c_{vc} = 1$ ), because of the rise in the air temperature at the fan and the higher energy consumption, which decrease the overall system efficiency. Reducing the volume of the ventilated air increases the system efficiency while, at the same time, it decreases the total cooling power. Ventilative cooling can then be very useful after the working day, for example, to pre-cool the offices for the next day. The best value for  $c_{vc}$  depends on the nominal SFP, the control mechanism, the nominal ACH of the space, as well as on the EER of the additional cooling or thermal capacity of the building. To find the best value, a set of annual building energy simulations can be undertaken, analysing function (3) to seek its global minimum.

$$f(c_{vc}) = Q_{C\_an} + FEC_{an} \cdot EER \tag{3}$$

In addition, the set-point temperature  $t_{set}$  for the operation must be specified. The comfort temperature must be determined as in (4) [48]:

$$t_{com} = 0.09 \cdot t_{rm} + 22.6 \tag{4}$$

where  $t_{rm}$ , depending on the outdoor temperature history, is expressed iteratively as in (5) [48]:

$$t_{rm} = 0.2 \cdot t_{out\_yesterday} + 0.8 \cdot t_{rm\_yesterday} \tag{5}$$

Consider that the occupants can adapt to higher temperatures if the weather remains hot for a longer period [35, 48]. The range  $t_{com} \pm 2K$  is considered the comfort range, and the interior temperature should be kept within this range. It is recommended that the ventilation set-point be specified as  $t_{com}$  (6) for the majority of the time. Then the cooling set-point can be  $t_{com} + 2K$  (6), while the difference of 2K is the area where ventilative cooling can be used.

Unfortunately, two Kelvins is a very small difference, which does not allow higher pre-cooling of the interior. But the comfort range is also specified under the comfort temperature, down to  $t_{com} - 2K$ . During the cooling season, when a temperature rise over a day is expected, the ventilation set-point can be modified to  $t_{com} - 2K$  at a time when the building is not used (6), so as to prepare it for the following day. The space will then begin in the morning with a boundary comfort temperature  $t_{com} - 2K$ , which will then rise continuously during the entire

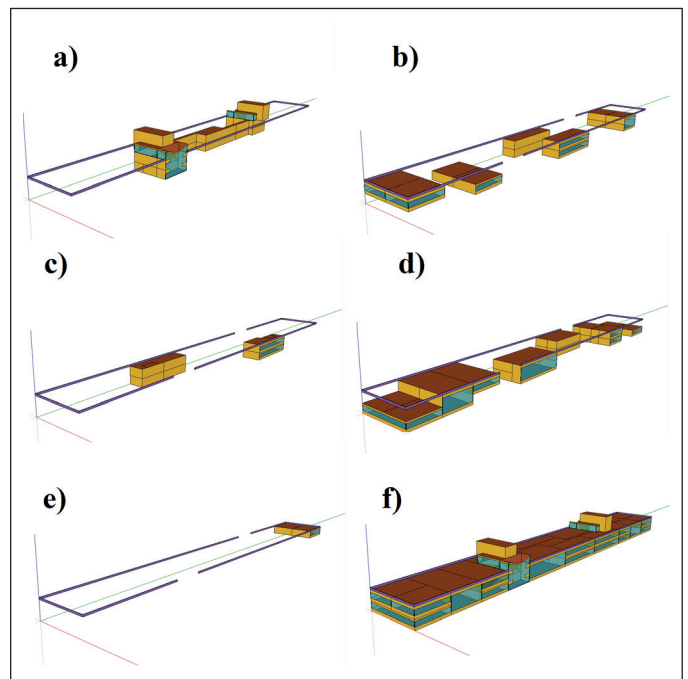


Fig. 4 Different types of air-nodes – a) corridors; b) classrooms; c) offices; d) open spaces; e) labs; f) whole model

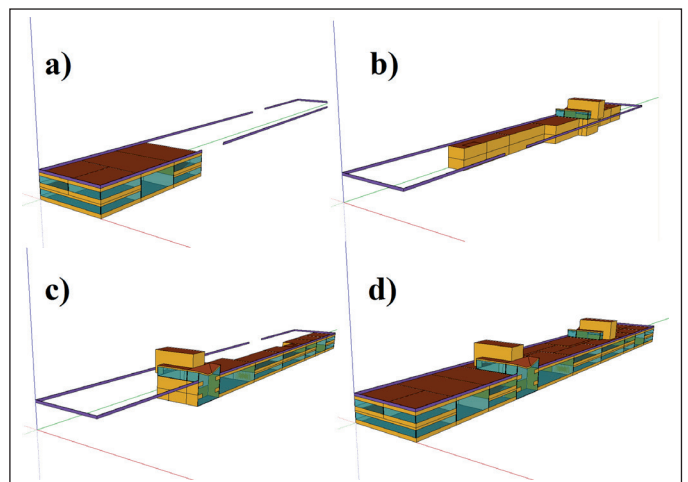


Fig. 5 Ventilated zones. a) South zone; b) West zone; c) East zone; d) whole model

day, up to the threshold for the mechanical cooling  $t_{com} + 2K$ , which ameliorates the rise in this temperature.

$$\begin{aligned} t_{set} &= t_{com} && \text{Normally, during winter and the workday} \\ t_{set} &= t_{com} - 2K && \text{In the cooling season, outside working hours} \\ t_{cool} &= t_{com} + 2K && \text{Mechanical cooling set-point, valid for the} \\ &&& \text{entire year.} \end{aligned} \quad (6)$$

To avoid discomfort for the occupants, a maximal allowed temperature difference between the air intake and room temperature should be defined. This is done by the variable  $t_{lim}$ , as a lower limit of the supply temperature  $t_{sup}$ . The recommended temperature difference between the room temperature and air supply temperature  $\Delta t_{l,s}$  is between 3K and 10K, depending on the method of air distribution. More mixed air distribution, such as swirl diffusers, allows a lower temperature at the air inlet. This limit is not justified after the working hours when the occupants are not present. The temperature limit of the supply air can be set as:

$$\begin{aligned} t_{lim} &= t_{l,mix} - \Delta t_{l,s} && \text{during the working hours} \\ t_{lim} &= 5^\circ C && \text{outside the working hours} \end{aligned} \quad (7)$$

The limit can be additionally corrected if there is the risk of condensation on the air-ducts.

### CASE STUDY

To verify the designed strategy and find the appropriate values for the coefficients and thresholds, a set of building simulations was performed. The ventilation strategy was implemented on a building, based on an existing school facility, as modelled in the TRNSYS simulation studio [49]. The building model was adopted from an evaporative cooling study made in 2014 [40].

#### Building model description

The building model represents the last two floors of the main building of the TU/e Eindhoven and is situated in the moderate maritime climate of the Netherlands. It contains 35 air-nodes on two floors, with different purposes and use profiles (see Figure 4), different volumes and heights, and different orientations. The air-nodes are grouped into three AHU's, which ventilate the group of neighbouring air-nodes, as is shown in Figure 5.

The building is considered modern, after refurbishment to Dutch standard qualities. This means that the lightweight building envelope has a  $U$ -value of 0.22 W/m<sup>2</sup>K of opaque walls, and 0.75 W/m<sup>2</sup>K of triple glazed windows with a  $g$ -value of 0.613. The roof has a  $U$ -value 0.106 W/m<sup>2</sup>K. The building is constructed from a concrete skeleton, where the concrete slab is on every second floor, while the remainder of the construction is lightweight, which easily allows the creation of spaces with a height of two floors. Therefore, the thermal accumulation ability of the building is limited.

Air handling units were simulated in detail. The SFP in the design speed is calculated according to [47] as 1 kW/(m<sup>3</sup>/s), which fulfils the requirements of [50] for 2018 and later. The fan motor works in the ventilated air flow, and all energy inputs are considered to transfer into the air, thereby increasing its temperature.

The design volumetric flow rate for each air-node is specified by the ACH setting, to avoid misguided values related to the occupancy or heat gains. The number of maximal air changes per hour is set as 0.5 h<sup>-1</sup> for the stairs and corridors, 1.5 h<sup>-1</sup> for the offices and labs, and 2.5 h<sup>-1</sup> for the classrooms. When a room is not occupied, the air change decreases to 0.1 h<sup>-1</sup>, but never entirely stops.

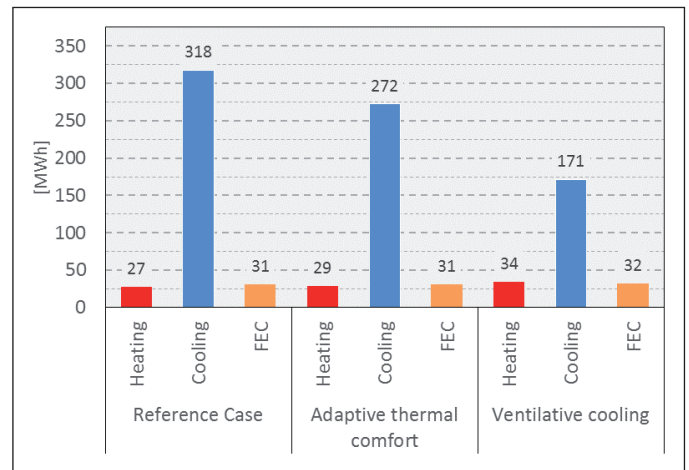


Fig. 6 Annual energy demand for three cases

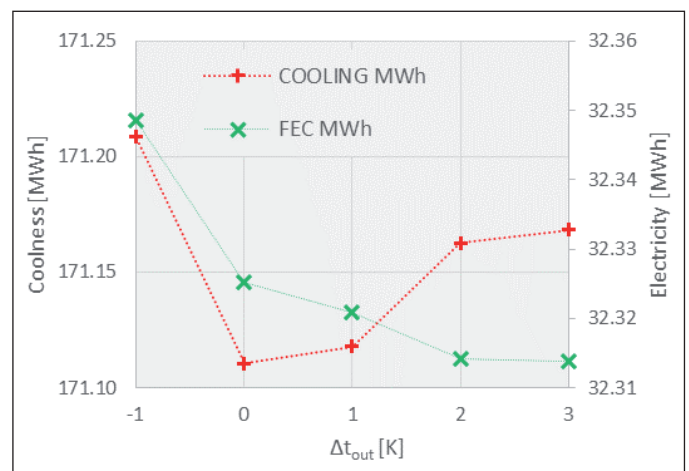


Fig. 7 Influence of  $\Delta t_{out}$  on the fan energy consumption and cooling demand

The heat recovery exchanger changes its efficiency in relation to the various temperature differences and volumetric flow rates of the air. The Number of Transfer Units (NTU) method is used for the heat recovery calculation [51]. For the bypass damper position regulation, a PID Type-23 is used. Comparative decisions are made by a Type-2, where hysteresis or thresholds are also implemented.

All simulations were on an annual basis and made with a 5-minute time-step, so as to capture the influence of the controllers, which switches the fans or dampers at the moment when the set-point or threshold on continuously changing (interpolated) temperatures was reached.

#### The ventilation control cases followed

As a **reference case**, no special approach was used. The ventilation serves as the fresh air supply only, with heat recovery during the winter and through the bypass during the cooling season. The heating set-point is 20 °C and the cooling set-point is 24 °C – which is normal in Dutch office buildings. All cooling loads are discharged by additional cooling equipment.

An **adaptive thermal comfort case** was considered so as to separate the influence of the adaptive model of the thermal comfort from the influence of ventilative cooling. In this case, if other conditions for this model are met (see [41]), the cooling set-point may be a floating variable that is dependent on the outdoor temperature (4). This can lead to cooling energy savings by itself, simply because of the lower temperature differences between the indoors and outdoors.

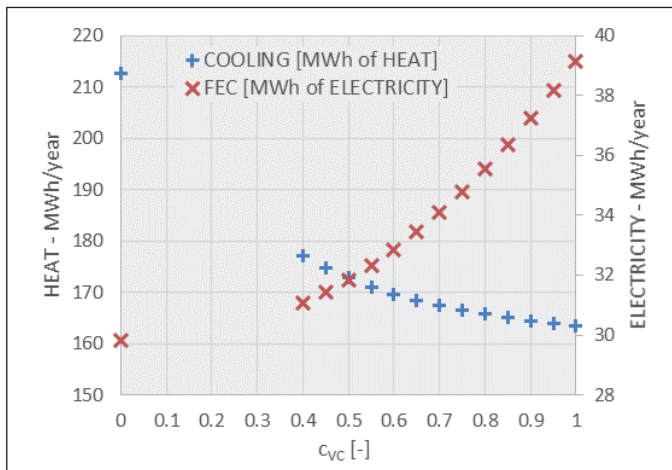


Fig. 8 Influence of the  $c_{VC}$  to the fan energy consumption and cooling demand

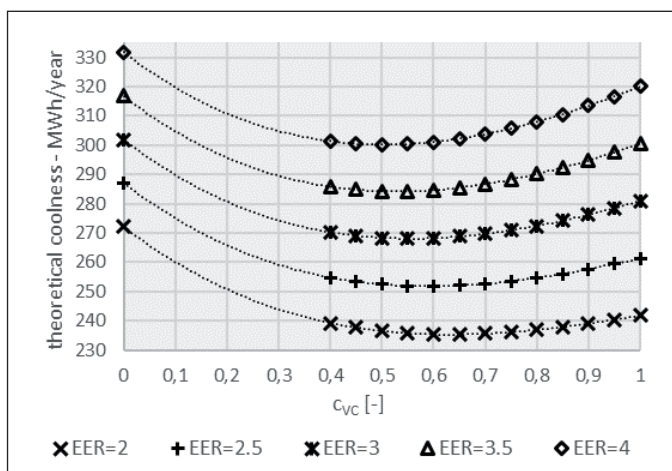


Fig. 9 The theoretical coolness, calculated accordingly (3).

**The ventilative cooling case** is the last one, and here all the findings and principles mentioned in the „Building Model Description” section above are included.

## RESULTS

The results of the annual simulation, after the coefficients and thresholds have been found, are given in Figure 6. In the reference case, the simulation shows a significant imbalance between the heating and cooling, which was expected. The annual cooling demand is 10 times higher than the annual heating demand. Using the adaptive model of thermal comfort, 14% of the cooling demand can be saved. Ventilative cooling can save another 32% of the initial cooling demand, so the overall savings are 46% of the coolness, which means 147 MWh in the case study.

The use of ventilative cooling also brings a slight increase in the heating demand, because of the unavoidable overcooling in some spaces, as is shown in Figure 6. This additional heating demand is 25% in total, while the initial heating demand in absolute numbers was very low: the rise accounts for 7 MWh of heat. The building is heated mostly by the fans, the equipment, the occupants and the sun. Of this 7 MWh additional heating demand, 2 MWh is caused by an increase in the indoor temperature by the adaptive model of the thermal comfort and the remaining 5 MWh by compensation of the overcooling related to the cooling via the ventilation. This fraction can be reduced if the building was divided into more independently ventilated zones.

Another set of simulations has been provided to prove the sensitivity of the results to a change in the coefficients  $\Delta t_{out}$  and  $c_{VC}$ . This is shown in Figure 7. The fan energy consumption increases with a lower  $\Delta t_{out}$  due to the additional operating hours. Simultaneously, the cooling demand decreases until  $\Delta t_{out}$  reaches zero. When  $\Delta t_{out}$  drops under zero, the ventilation brings an extra thermal load, and the cooling demand increases. In any event, the influence of the total amount of energy or coolness required is very small and only causes the fans to switch on or off a few minutes earlier or later. The sensitivity results of  $\Delta t_{out}$  was found to be negligible.

A marked effect with the same parameters was found in the  $c_{VC}$  coefficient, which has a major influence on the fan speed, as shown in the graph in Figure 8. With an increasing  $c_{VC}$ , the cooling demand decreases, while the fan energy consumption increases. When coefficient  $c_{VC}$  is set to zero, no additional air is ventilated other than that from the fresh air for the occupants. The cooling demand in this case is only 212 MWh whereas, without the ventilative cooling in the Adaptive Thermal Comfort case, it was calculated to be 272 MWh.

The difference relates to the bypass damper operation in the AHU. Increasing the  $c_{VC}$  leads to even more positive results. The energy demands in Figure 8 cannot be compared, because of the incomparability of the electricity and coolness. To find the optimum coefficient of the ventilative cooling, energies must be converted to a common base. This can be expressed as a theoretical coolness, expressed above as  $f(c_{VC})$  (3) as the sum of the coolness actually consumed and the coolness theoretically generated by the extra electricity used for the fans under the actual conditions.

In Figure 9, the theoretical coolness is shown in relation to the  $EER$  of the additional cooling. The higher the  $EER$ , the lower the appropriate  $c_{VC}$ . If a low-efficiency cooler is used, with an  $EER = 2$ , then it is appropriate to ventilate more air and set the  $c_{VC}$  to a higher value of around 0.7, as the function of theoretical coolness has a global minimum there. If a high-efficiency cooler is used, with an  $EER = 4$ , the ideal  $c_{VC}$  is around 0.5, ventilating less air. For all the usual ranges for machinery cooling, the preferred values of the  $c_{VC}$  are between 0.5 and 0.7.

It is important to note that this dependency is affected by the design  $SFP$  (equal to 1 kW/(m<sup>3</sup>/s) in our case) and the design air change rates in each space. The lower the design  $SFP$ , the higher the optimal  $c_{VC}$ .

## DISCUSSION

Cooling by outdoor air has great potential for energy savings, especially for highly insulated buildings in cold or mild climates. The simulations indicate that the energy savings potential, measured by the saved coolness, extra heat and extra electricity for fans, is still around 40% of the cooling energy demand when the presented operation strategy is used. No special equipment is necessary to provide ventilative cooling, other than an ordinary ventilation system with VAV, which is generally used to ensure hygienic air change.

Its entire potential is hidden in the control, and in the regulation of the bypass dampers around the heat recovery exchanger. Even better results might well be obtained using a PID-MPC, but these Model Predictive Controllers are far harder to implement [52]. Setting  $t_{set}$  within a range of  $t_{com} \pm 2K$  is a future task of weather-predictive regulation which has, in the past, proven to be a powerful tool for energy savings [10-12].

The air change rate has a major effect on the performance of the entire system. The coefficient of ventilative cooling, which determines the power of the ventilative cooling, deserves special attention. Due to the fan

energy consumption, it is not appropriate to ventilate with the maximum fan speed. Decreasing the volume of the ventilated air to 50% – 70% of the nominal leads to a significant increase in the overall system efficiency.

This phenomenon should be investigated more closely in the future, so that the relationship between the building mass, the specific fan power, the *EER* of the auxiliary cooling and the coefficient of ventilative cooling can be determined.

On the other hand, the results are not fully susceptible to the threshold of the temperature difference between the outdoor and indoor temperatures. Outdoor temperatures change continuously, and the threshold setting determines whether the fan switches on a few minutes earlier or later. But the overall effect of this on the entire question is negligible.

### CONCLUSION

We found that ventilative cooling is an excellent way to reduce the cooling loads and energy consumption related to the cooling of buildings equipped with VAV ventilation systems. Compared to a building cooled only by a mechanical chiller, savings of around 40% of cooling energy consumption can be reached.

Current trends leading to increased indoor climate requirements in a growing number of buildings result in an overall increase of building energy consumption. Ventilative cooling, using the presented operation strategy, can mitigate the impact of higher environmental requirements, and therefore save energy. At the same time, fan-driven controlled ventilative cooling has no adverse effects on the quality of the indoor environment, as is often seen in night-cooling via natural ventilation.

The strategy presented appears to be a strong tool that can be helpful in achieving the goal of nearly zero-energy buildings.

Contact: [ondrej.nehasil@fsv.cvut.cz](mailto:ondrej.nehasil@fsv.cvut.cz)

**ACKNOWLEDGEMENT.** This work has been supported by the Ministry of Education, Youth and Sports within National Sustainability Programme I (NPU I), project No. LO1605 - University Centre for Energy Efficient Buildings – Sustainability Phase.

### Literature

- [1] LESTER, P. History of Air Conditioning. 2015 [online]. Accessible from: <https://energy.gov/articles/history-air-conditioning>
- [2] SANTAMOURIS, M. Cooling the buildings – past, present and future. *Energy and Buildings*. 2016, vol. 128, pp. 617–638.
- [3] DIRKS, J. A., et al. Impacts of climate change on energy consumption and peak demand in buildings: A detailed regional approach. *Energy*. 2015, vol. 79, (C), pp. 20–32.
- [4] SANTAMOURIS, M., ASIMAKOPOULOS, D. Passive Cooling of Buildings. (1st pub. ed.) London: James & James, 1996.
- [5] FOLDJERG, P., THORBJØRN, A., HOLZER, P. Ventilative Cooling of Residential Buildings – Strategies, Measurement Results and Lessons Learned from Three Active Houses in Austria, Germany and Denmark. *International Journal of Ventilation*. 2014. Vol. 13 No. 2.
- [6] ARTMANN, N., MANZ, H., HEISELBERG, P. Climatic potential for passive cooling of buildings by night-time ventilation in Europe. *Appl. Energy*. 2007. Vol. 84, no. 2, pp. 187–201.
- [7] CHIESA, G., GROSSO, M. Geo-climatic applicability of natural ventilative cooling in the Mediterranean area. *Energy Build.* 2015. Vol. 107, pp. 376–391.
- [8] X. ZHU, Y. LIU and J. LIU. Night ventilation research of office buildings: Part 2 Cooling potential of continental climate zone in China. In: 2011, DOI: 10.4028/www.scientific.net/AMR.250-253.1066.
- [9] K. T. HUANG, R. L. HWANG. Parametric study on energy and thermal performance of school buildings with natural ventilation, hybrid ventilation and air conditioning. *Indoor and built environment*. 2016. Vol. 25 (7) , pp. 1148–1162.
- [10] MEDVED, S., BABNIK, M., VIDRIH, B., ARKAR, C. Parametric study on the advantages of weather-predicted control algorithm of free cooling ventilation system. *Energy*. 2014, Vol. 73, pp. 80–87.
- [11] ŠIROKÝ, J., OLDEWURTEL, F., CIGLER, J., PRÍVARA, S. Experimental analysis of model predictive control for an energy efficient building heating system. *Appl. Energy*. 2011, Vol. 88, no. 9, pp. 3079–3087.
- [12] HUANG, G. Model predictive control of VAV zone thermal systems concerning bi-linearity and gain nonlinearity. *Control Engineering Practice*. 2011, Vol. 19, (7), pp. 700–710.
- [13] CAMPANICO, H., HOLLMULLER, P., SOARES, P. M. Assessing energy savings in cooling demand of buildings using passive cooling systems based on ventilation. *Appl. Energy*. 2014, Vol. 134, pp. 426–438.
- [14] ALIZADEH, M., SADRAMELI, S. M. Development of free cooling based ventilation technology for buildings: Thermal energy storage (TES) unit, performance enhancement techniques and design considerations – A review. *Renew. Sustain. Energy Rev.* 2016, Vol. 58, pp. 619–645.
- [15] ENGELMANN, P., KALZ, D., SALVALAI, G. Cooling concepts for non-residential buildings: A comparison of cooling concepts in different climate zones. *Energy Build.* 2014, Vol. 82, pp. 447–456.
- [16] THAM, K. Indoor air quality and its effects on humans-A review of challenges and developments in the last 30 years. *Energy and Buildings*. 2016, Vol. 130, pp. 637–650.
- [17] CAO, X., DAI, X., LIU, J. Building energy-consumption status worldwide and the state-of-the-art technologies for zero-energy buildings during the past decade. *Energy and Buildings*. 2016, Vol. 128, pp. 198–213.
- [18] ALONSO, M. J., MATHISEN, H. M., COLLINS, R. Ventilative cooling as a solution for highly insulated buildings in cold climate. *Energy Procedia*. 2015, Vol. 78, pp. 3013–3018.
- [19] OKOCHI G., YAO, Y. A review of recent developments and technological advancements of variable-air-volume (VAV) air-conditioning systems. *Renewable & Sustainable Energy Reviews*. 2016, Vol. 59, pp. 784–817.
- [20] ZHANG, B. et al. Demand control ventilation: Influence of terminal box minimum airflow setting on system energy use. *Energy and Buildings*. 2014, vol. 79, pp. 173–183.
- [21] LIN X., LAU, J. Demand controlled ventilation for multiple zone HVAC systems: CO<sub>2</sub>-based dynamic reset (RP 1547). *HVAC R Res*. 2014, Vol. 20, no. 8, pp. 875–888.
- [22] MORADI, H., SAFFAR-AVVAL, M., BAKHTIARI-NEJAD, F. Nonlinear multivariable control and performance analysis of an air-handling unit. *Energy Build.* 2011, Vol. 43, no. 4, pp. 805–813.
- [23] YANG, X. et al. Evaluation of four control strategies for building VAV air-conditioning systems. *Energy and Buildings*. 2011, Vol. 43, (2), pp. 414–422.
- [24] MOSOLLY, M., GHALI, K., GHADDAR, N. Optimal control strategy for a multi-zone air conditioning system using a genetic algorithm. *Energy*. 2009, Vol. 34, (1), pp. 58–66.
- [25] XU, X., WANG, S., SUN, Z., XIAO, F. A model-based optimal ventilation control strategy of multi-zone VAV air-conditioning systems. *Appl. Therm. Eng.* 2009, Vol. 29, no. 1, pp. 91–104.
- [26] YUAN, S., PEREZ, R. Multiple-zone ventilation and temperature control of a single-duct VAV system using model predictive strategy. *Energy Build.* 2006, Vol. 38, no. 10, pp. 1248–1261.
- [27] WANG, S., QIN, J. Sensor fault detection and validation of VAV terminals in air conditioning systems. *Energy Convers. Manag.* 2005, Vol. 46, no. 15–16, pp. 2482–2500.
- [28] WANG, S., XU, X. A robust control strategy for combining DCV control with economizer control. *Energy Convers. Manag.* 2002, Vol. 43, no. 18, pp. 2569–2588.
- [29] WANG, S., JIN., X. CO<sub>2</sub>-Based Occupancy Detection for On-Line Outdoor Air Flow Control. *Indoor Built Environment*. 1998, Vol. 7, pp. 165–181.
- [30] KE, Y. P., MUMMA, S. A., Optimized supply-air temperature (SAT) in variable-air-volume (VAV) systems. *Energy*. 1997, Vol. 22, no. 6, pp. 601–614.
- [31] SCOFIELD, M., PERIANNAN, V. VAV System Heat Recovery Economizer to Furnish Free Humidification and Exceed Standard 62.1 Ventilation Requirements in Winter. ASHRAE Transactions, vol. 121, pp. 1111, 2015.

- [32] WANG, L., CURCIJA, D., BRESHEARS, J. The energy saving potentials of zone-level membrane-based enthalpy recovery ventilators for VAV systems in commercial buildings. *Energy Build.* 2015, Vol. 109, pp. 47–52.
- [33] ENGD AHL, F., JOHANSSON, D. Optimal supply air temperature with respect to energy use in a variable air volume system. *Energy Build.* 2004, Vol. 36, no. 3, pp. 205–218.
- [34] HUANG, G., JORDÁN, F. Model-based robust temperature control for VAV air-conditioning system. *HVAC R Res.* 2012, vol. 18, no. 3, pp. 432–445.
- [35] McCARTNEY, K. J., FERGUS, N. J. Developing an adaptive control algorithm for Europe. *Energy Build.* 2002, Vol. 34, pp. 623–635.
- [36] ZHUAN, R. N., LI, X., TU, J. An energy saving ventilation strategy for short-term occupied rooms based on the time-dependent concentration of CO<sub>2</sub>. *Int. Journal of Ventilation.* 2015, vol. 14, no. 1, pp. 39–52.
- [37] OLDEWURTEL, F., STURZENEGGER, D., MORARI, M. Importance of occupancy information for building climate control. *Appl. Energy.* 2013, Vol. 101, pp. 521–532.
- [38] WANG, Y., SHAO, Y., KARGEL, C. Demand controlled ventilation strategies for high indoor air quality and low heating energy demand. In: *2012 IEEE Int. Instrum. Meas. Technol. Conf., no. Dcv.* pp. 870–875, 2012.
- [39] FISK, W. J., De ALMEIDA, A. T. Sensor-based demand-controlled ventilation: a review. *Energy & Buildings.* 1998, Vol. 29, (1), pp. 35–45.
- [40] NEHASIL, O., ADAMOVS KÝ, D. Case study of indirect evaporative cooling in the main building of TU/e Eindhoven. In: *Simulace budov a techniky prostředí 2014.* Praha, 2014.
- [41] SCHILD, P.G., MYSEN, M. Recommendations on specific fan power and fan system efficiency – Part I [online]. 2014. Dostupné z: <http://vetrani.tzb-info.cz/uspory-energie-ventrání-klimatizace/11079-doporuceni-pro-merny-prikon-ventilatoru-sfp-a-ucinnost-vzduchotechnických-systemu-i>
- [42] SCHILD, P.G., MYSEN, M. *Recommendations on specific fan power and fan system efficiency.* AIVC Technical Note 65. 42 pp, 2009.
- [43] WARREN, M., NORFOLD, L.K. Integrating VAV zone requirements with supply fan operation. *ASHRAE Journal.* 1993, Vol. 35(4), pp. 43–46.
- [44] SHAN, K. et al. In-situ validation of a fault tolerant control strategy for VAV systems. *Applied Thermal Engineering.* 2015, Vol. 87, pp. 362–370.
- [45] QIN, J., WANG, S. A fault detection and diagnosis strategy of VAV air-conditioning systems for improved energy and control performances. *Energy Build.* Vol. 37, no. 10, pp. 1035–1048, 2005.
- [46] SCHEIN, J. et al, A rule-based fault detection method for air handling units. *Energy & Buildings.* 2006, Vol. 38, (12), pp. 1485–1492.
- [47] SCHILD, P.G., MYSEN, M. Recommendations on specific fan power and fan system efficiency – Part II [online]. 2014. Dostupné z: <http://vetrani.tzb-info.cz/vzduchotechnicka-zarizeni/11102-doporuceni-pro-merny-prikon-ventilatoru-sfp-a-ucinnost-vzduchotechnických-systemu-ii>
- [48] LAIN, M. *Nízkoenergetické Chlazení Budov.* Praha, 2007 Disertační Práce. České vysoké učení technické v Praze.
- [49] Thermal Energy System Specialists, LLC. TRNSYS Simulation Studio 17.01.0016 [software]. NOV 2009. Available: [www.trnsys.de](http://www.trnsys.de). System requirements: Windows 2000 / ME / Windows XP / Vista or later, 200 MB disc space, 128 MB RAM
- [50] The European Commission, Commission Regulation (EU) No. 1253/2014 of 7 July 2014.
- [51] KAYS, W. M., LONDON, A. L. *Compact Heat Exchangers.* (Repr. 1998 with corrections. ed.) Malabar: Krieger, 1998.
- [52] WANG, Y., KUCKELKORN, J., LIU, Y. A state of art review on methodologies for control strategies in low energy buildings in the period from 2006 to 2016. *Energy Build.* 2017, Vol. 147, pp. 27–40.

### Nomenclature:

$t_{com}$	comfort temperature [°C]
$t_{out}$	outdoor temperature [°C]
$t_{rm}$	outdoor running mean temperature [°C]
$t_i$	indoor temperature of an air-node (room) [°C]
$t_{mix}$	mean indoor temperature, measured in waste-air duct before the AHU (air handling unit) [°C]
$t_{sup}$	temperature of the supply air [°C]
$t_{lim}$	lower temperature limit of the supply air [°C]
$t_{set}$	set-point room temperature for the ventilation [°C]
$t_{cool}$	set-point room temperature for the mechanical cooling [°C]
$\Delta t_{out}$	threshold temperature difference between the outdoor and indoor temperatures [K]
$\Delta t_{i,s}$	temperature difference between the indoor and air supply temperature [K]
$c_{vc}$	coefficient of the ventilative cooling [-]
$q_v$	air-node volumetric flow rate [m <sup>3</sup> /h]
$q_{norm}$	air-node design volumetric flow rate [m <sup>3</sup> /h]
$q_{hyg}$	hygienic fresh air supply [m <sup>3</sup> /h]
$Q_{c,an}$	annual cooling demand of a selected building, non-ventilative [kWh]
$FEC_{an}$	annual energy consumption of the fans [kWh]
$SFP$	specific fan power [kW/(m <sup>3</sup> /s)]
$EER$	energy efficiency ratio of the cooling device [-]
$ACH$	air change per-hour ratio [-]

Arinda P. RACHMAN <sup>1)</sup>,  
Vojtěch ZAVŘEL <sup>1,2)</sup>,  
J. Ignacio TORRENS <sup>1,3)</sup>,  
Jan L.M. HENSEN <sup>1)</sup>

<sup>1)</sup> Building performance group,  
Dept. of Built Environment,  
Eindhoven University of  
Technology

<sup>2)</sup> CTU in Prague, Faculty of  
Mechanical Engineering, Dept. of  
Environmental Engineering

<sup>3)</sup> Building Technologies division,  
TECNALIA

Reviewer  
Ing. Pavel Herout

# A Simulation-Based Assessment of Humidity Treatment in Data Centre Cooling Systems with Air-Side Economisers

## Simulační posouzení úpravy vlhkosti v systémech chlazení data center s ekonomizérem na straně vzduchu

*The increasing digitalisation of data is resulting in the need for ever greater computational capacity, which in turn leads to the increasing energy consumption in data centres. A large percentage of this energy use arises from the need to mechanically remove an enormous amount of heat from the data centre environment. In fact, in current practice, the mechanical infrastructure (especially cooling systems) of the data centre accounts for up to half of the overall energy consumption. To reduce the energy consumption of the mechanical infrastructure, several economisation methods are commonly implemented in cooling systems, one of which is the application of a direct air-side economiser addressed in the current research. The use of an air-side economiser has been shown to lead to major savings of the cooling electricity demand, and, as such, it has been widely used as a necessary addition to conventional cooling systems. This study analyses the energy breakdown of data centre cooling systems that include an air-side economiser in order to determine which components within the system are responsible for the major energy consumption. This study investigates, via a computational simulation, the impact of the use of a conventional cooling system and a system with an air-side economiser on total energy demand in three locations representing different climate regions in Europe. The study is especially focused on the energy demand related to the humidity treatment in the data rooms, since the effect is rarely considered in the overall DC energy balance. The results demonstrate, as expected, that the air-side economiser can yield major savings of around 62.5% to 78.7%, depending on the given climate regions. However, the key result of this study is that the humidity treatment necessary for the direct air-side economiser system may consume up to 34.8% of the total energy demand of the cooling system with the air-side economiser.*

**Keywords:** data centre's cooling system, air-side economiser, humidity, energy analysis, energy simulation, simulation-based assessment

*Narůst digitalizace dat má za výsledek potřebu stále vyšší výpočetní kapacity, která má za důsledek významný růst globální energetické spotřeby data center. Značné procento z celkové energetické spotřeby data center je přičítáno chlazení, které mechanicky odebírá enormní množství tepla disipováno výpočetní technikou uskladenou v prostoru data centra. V současné době, mechanická infrastruktura data center (především systémy chlazení) spotřebovávají až polovinu celkové energie data center. Několik různých metod ekonomizace provozu chladicího systému je v současné praxi k dispozici, a jednou z nich je využití přímého volného chlazení na straně vzduchu, která je zkoumána v tomto článku. Využití volného chlazení již prokázalo, že vede ke značným úsporám a je často běžnou součástí systémů chlazení v data centrech. Tato studie analyzuje rozdělení energetické spotřeby chladicího systému datacenter, jehož součástí je také zařízení pro volné chlazení, tak aby bylo umožněno vyhodnotit spotřebu energie jednotlivých částí systémů a zkoumá za pomoci numerických simulací zmíněné rozložení energie pro systém s a bez ekonomizace pro tři lokality reprezentující různé klimatické zóny v Evropě. Tato studie se zvláště zaměřuje na energetickou spotřebu úpravy vlhkosti v data centrech, protože tento jev je jen zřídka brán v úvahu při celkové energetické bilanci data center. Výsledky demonstrují očekávanou energetickou úsporu při využití volného chlazení na straně vzduchu, a to v rozmezí 62.5 % až 78.7 % v závislosti na dané klimatické zóně. Avšak, hlavním výsledkem této studie je, že zařízení na úpravu vlhkosti, která je u přímého volného chlazení na straně vzduchu nezbytná, mohou spotřebovat až 34.8 % z celkové spotřeby systému chlazení s tímto ekonomizérem.*

**Klíčová slova:** chlazení data center, volné chlazení na straně vzduchu, vlhkost, energetická analýza, energetická simulace, posouzení na základě simulace

## INTRODUCTION

The energy consumption of data centres has increased in line with the recent demand for cloud computing. Overall, data centres consumed nearly 1.5% of the total world electricity consumption in 2005 [1]. According to the Natural Resources Defense Council (NRDC) findings, U.S. data centers consumed around 91 terawatt-hours (TWh) of electricity in 2013 and this figure is projected to increase to roughly 140 TWh annually by 2020 [2]. As such, there is significant potential and a great need

to reduce the energy consumption and the associated climate-changing pollution of data centres.

In general, power distribution consumed by systems in the data centre can be simply divided into two categories covering the IT equipment and data centre infrastructure, which includes the electrical, mechanical and auxiliary systems. Considering the overall power consumption of the conventional data centre infrastructure, up to half of its total energy is typically consumed by the mechanical systems [3], [4]. The cooling sys-

tems commonly consume around 40% of the total data room consumption [5], [6]. Therefore, reducing the power consumption of the cooling systems is considered a high priority in the operation of a data centre.

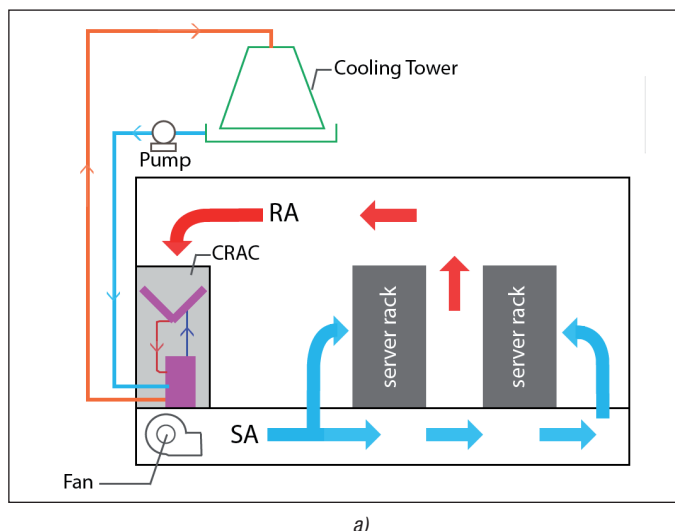
There are several energy efficiency measures and economisation methods to minimise the power consumption of the data centre's cooling system. Aside from increasing the setpoint of air supply temperature or improving the air distribution within the DC, utilising outside air for free cooling can lead to a major reduction in the total electricity demand [1], [2], [7]. One of the economisation methods is an air-side economiser, which can benefit greatly from the ambient temperatures below 18 to 21°C. Nowadays, economisers are integrated into the configuration of data centre cooling systems as an energy efficiency measure. These systems can be understood as the new benchmark, and their implementation is becoming widespread. In anticipation of this widespread implementation, this research represents an attempt to provide a detailed energy breakdown of such a cooling system as well as providing an initial screening for possible future in-depth research of the individual components.

The current research is aimed at the humidity treatment in the system with the direct air-side economiser. Considering these types of systems, when the outside air enters the critical environment of the data room, the tight humidity treatment is necessary to satisfy the strict requirements for the IT operational conditions given by the standards [8]. Indeed, the implementation of a direct air-side economiser results in the need of a tightly controlled indoor humidity level to prevent the data centre's space from negative effects such as condensation on the equipment when the outside air is too moist, or excess static electricity when it is too dry [4], [5].

The key focus area of this research is the energy demand related with the humidity treatment, which is often neglected during the calculation of the total energy demand. Indeed, in conventional configurations, where the indoor air is circulated and most of the cooling power demand is related to the energy-hungry refrigeration cycle, the energy demand related to the humidity treatment is relatively low. However, by introducing outside air to the data centre's environment in order to bypass the refrigeration throughout the year, the energy break-down will change, which means that it is unwise to continue to neglect the energy demand for the humidity treatment.

**RESEARCH QUESTION AND METHODOLOGY**

To reach the objective mentioned in the previous section, the following



research question was stated and will be answered: *What is the impact of the humidity treatment on the total energy consumption of the cooling system with the air-side economiser in data centres?*

The current research was conducted based on the methodological steps described below in order to quantify the impact of the humidity treatment on the total energy consumption.

- ❑ A literature study was performed on the related studies regarding data centres' cooling systems and economisers.
- ❑ A heuristic model of the data centre was developed in Matlab [11] to briefly understand the change in energy breakdown. Specifically, the model was built based on the reference mid-sized data centre [8]. The model consists of two cooling typologies; conventional cooling systems and a system with an air-side economiser.
- ❑ The simulation of the data centre model was executed for various climatic regions within Europe and for constant IT utilisation. The simulation focuses on the cooling energy demand broken down into the individual components. In order to assess the energy demand throughout the year. The simulation timestep of 1 hour was selected.
- ❑ The simulation results were evaluated for each climate by the selected key performance indicators. These are the annual energy use of the individual components and the power usage effectiveness (PUE) [12].

**DATA CENTRE AND SYSTEMS REPRESENTATION**

**Data centre model**

The data centre (DC) model used in this research represents a typical mid-sized DC and it is based on the description of a case study of an IBM test facility located in Poughkeepsie, New York [8]. This case study provides rich information with a sufficient level of detail, in a field (i.e., commercial DCs) with documentation scarcely available, generally due to confidentiality issues. The facility houses 135 servers, has a floor area of 693.68 m<sup>2</sup> and layout dimensions of 23.3×29.9 m. The servers were arranged based on a hot and cold aisle arrangement without separation. A U-value of 0.24 W/m<sup>2</sup>K was assumed for the building envelope.

The performance of the DC is represented by variables such as power consumption, airflow, and air temperature in the IT environment. According to the available specification of the case-study, the overall power consumption of the IT infrastructure is 1098.2 kW. This electrical power is assumed to be converted to heat, which is dissipated in the data room space. This enormous heat gain must be mechanically removed from the space to ensure the required operational conditions of the IT equipment.

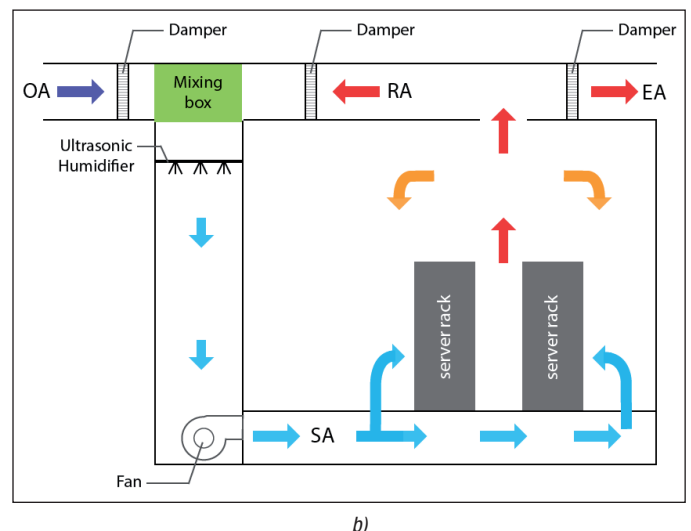


Fig. 1 schematic diagram of: (a) a conventional cooling system and (b) a cooling system with an air-side economiser

Therefore, two cooling systems are assumed in this study: (a) a cooling system with a computer room air conditioner (CRAC) unit using a refrigeration circuit, which represents the conventional approach, and (b) a cooling system with an air-side economiser, which represents the new generation of DC cooling systems. These two systems are schematically depicted in Fig. 1.

**Computer Room Air Conditioner (CRAC)**

Generally, a computer room air conditioner (CRAC) unit is used to reduce the return air temperature by removing the dissipated heat from the IT environment. The indoor environment of the modelled data centre was assumed to fall within the recommended temperature range. The recommended range according to data centre’s thermal guidelines of ASHRAE TC 9.9 [13] is highlighted in yellow in Fig. 2, which also includes the allowable ranges in which the inlet server temperature may fall for short periods of time [14].

Although it is allowed to set a higher server inlet temperature, the appropriate indoor environment should be carefully controlled for data centres without a hot and cold aisle separation, so-called containment. When the sum of the airflow throughout the servers is higher than supply airflow of the cooling system, unseparated aisles can potentially cause hot air recirculation into the cold aisle resulting in higher server inlet temperatures [15]. Since the hot and cold aisle in this data centre model was mixed, the modelled cooling systems were operated with a setpoint of the air supply with dry-bulb and dew-point temperatures of 21°C and 11°C, respectively.

The specification of the CRAC unit used in the model is given in Table 1. The amount of airflow  $\dot{m}_{air}$  needed to remove the heat from the IT room can be calculated using Equation (1).

$$\dot{m}_{air} = \frac{\dot{Q}_{overall}}{c_{p,air} \Delta T} \tag{1}$$

where  $\dot{Q}_{overall}$  is the total heat to be removed from the data room space,  $\Delta T$  is the temperature difference between the inlet and outlet air from CRAC unit,  $c_{p,air}$  is the specific heat capacity of the dry air.

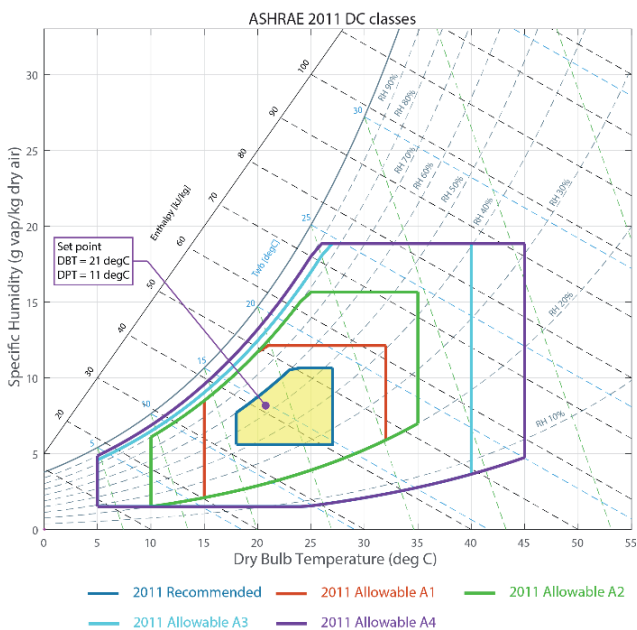


Fig. 2 ASHRAE proposed thermal condition for data centres

Tab. 1 CRAC unit model specification

<b>Configuration: Down-flow Down</b>	
Refrigerant	R410A
Net sensible cooling capacity	46.1 kW
Fan power input	2.1 kW
Unit power input	12.79 kW
COP	3.1
Air pressure loss (underfloor air distribution)	20 Pa
Maximum air flow	14500 m³/h
<b>Condenser Section</b>	
Water inlet temperature	30 °C
Condensing temperature	45 °C
Maximum water flow	1.31 L/s

**Air-side economiser**

The air-side economiser is used to reduce the cooling system related energy consumption and cost by utilising the outside air to reject the heat from the IT environment [16]. The outside air (OA) is brought into the building and distributed via a series of dampers and fans. The servers ingest the cool air, transfer the heat, and expel the hot air from the room. Rather than being recirculated and cooled, the exhaust air (EA) is simply directed outside. If the outside air is particularly cold, the economiser may mix the outside air (OA) and the return air (RA), ensuring that the air supply (SA) temperature falls within the desired range for the equipment. The ratio of the outside and the return air used in the mixing process was estimated using Equations (2) and (3).

$$m_{RA} = \frac{m_{SA} (t_{SA} - t_{OA})}{t_{RA} - t_{OA}} \tag{2}$$

$$m_{OA} = m_{SA} - m_{RA} \tag{3}$$

The air-side economiser model that was used in this study is schematically illustrated in Figure 1b. In this model, the economiser is equipped with an ultrasonic humidifier. The humidifier was used to maintain the recommended air supply moisture level when the outside air moisture level was low. In addition, dampers were used to control the amount of the outside air and the return air that was mixed in the mixing box.

**Humidifier**

The humidifier is used to maintain the humidity level of supply air as recommended in the ASHRAE TC 9.9 standard. In this study, an ultrasonic humidifier was chosen as the humidifier model, alternatively a high pressure fog system can be an option. The device was activated when the supply air humidity was lower than the ASHRAE recommended range for the data centre. The power consumption of the humidifier was estimated using Equations (4) and (5).

$$P_{uh} = e_{ult} \dot{m}_{w,uh} \tag{4}$$

$$\dot{m}_{w,uh} = \frac{\dot{m}_{w,hum}}{\eta_{de-ionised}} \tag{5}$$

It was assumed that the de-ionising effectiveness ( $\eta_{de-ionised}$ ) was 0.75, while the electricity consumption per unit mass of water ( $e_{ult}$ ) was defined as 0.053 kW/kg [17].

### Cooling tower

In this study, cooling towers were used to reject the heat from the IT room to the outside environment by spraying warm condenser (cooling) water onto the filler at the top of the towers. The water spreads out, and some of it evaporates away as it drips through the sponge-like material [18]. The evaporation reduces the temperature of the remaining water, which is collected at the bottom of the towers. The cooling water is pumped back via pipes to the CRAC units' condenser.

The heat removed by the cooling tower was calculated using Equations (6) and (7). Furthermore, Eq. (8) was used to determine the total absorbed heat from the CRAC units' condenser.

$$Q_{CT} = \eta m_a \rho_a (h_{swi} - h_{ai}) \quad (6)$$

$$\eta = \frac{T_{wi} - T_{wo}}{T_{wi} - T_{wb,ai}} \quad (7)$$

$$Q_{condenser} = m_w \rho_w c_{p,w} (T_{wi} - T_{wo}) \quad (8)$$

Since air is needed to reduce the water temperature through an evaporation process, the cooling tower is equipped with fans to supply the air. The power input of the fan is dependent on the amount of airflow, as described in Equation (12). In order to calculate the power input of the fan, the airflow needs to be calculated using Equation (9). In this study, the amount of released heat by the cooling tower was assumed to be 20% higher than the absorbed heat from the condenser.

$$m_a = \frac{1.2 \cdot Q_{condenser}}{\eta \rho_a (h_{swi} - h_{ai})} \quad (9)$$

### Pump and fan

A pump was used to deliver the cooling water from the cooling towers to the CRAC units, and the volume of the water was assumed to be constant. Equations (10) and (11) were used to calculate the power consumption of the pump model [3], [10], [11]. In this study, the pump efficiency ( $\eta_{pump}$ ) was assumed to be 60%.

$$P_{pump} = \frac{\dot{m}_{w,pump} \Delta p_{pump}}{\rho_w \eta_{pump}} \quad (10)$$

where,

$$\dot{m}_{w,pump} = \frac{\dot{Q}_{overall} \Delta T_{w,pump}}{c_{p,w}} \quad (11)$$

The fans are modelled with the assumption of a constant airflow rate. This control simplification is made because the total dissipated heat from the IT equipment was also assumed to be constant. The fan power consumption can be calculated using Equation (12) where the fan efficiency ( $\eta_{fan}$ ) was assumed to be 60% [3], [10], [12].

$$P_{fan} = \frac{\dot{V}_{RA} \sum \Delta p}{\eta_{fan}} \quad (12)$$

## ENERGY SIMULATION DEFINITION

### Geographical location and climate properties

This study estimated the impact of the humidity conditions on the overall and individual energy consumption of the air-side economiser. To ana-

lyse this impact, several locations from the north to the south of Europe with different climate conditions were used in the simulations. The tested locations are described in Table 2.

Tab. 2 Climate information of the tested locations

City	Location		Design temperature [°C]		Climate type	Köppen classification
	Latitude	Longitude	Dry bulb	Wet bulb		
Helsinki, FI	60.17° N	24.94° E	22.8	18.0	Humid Continental Climate	Dfb
Groningen, NL	53.22° N	6.56° E	24.2	19.8	Temperate Oceanic Climate	Cfb
Rome, ITA	41.90° N	12.49° E	27.9	25.4	Mediterranean Climate	Csa

### Case 1: Conventional cooling system

The conventional cooling system, shown in Figure 1, cooled the return air and supplied the cooled air to the servers. In this case, the refrigeration unit was used continuously to maintain the air condition inside the IT environment. In this study, it was assumed that the return air was 33 °C and that the CRAC units would cool the return air to 21°C before supplying it to the server racks.

In this model, the amount of make-up water that was used to replace the evaporated water was not taken into consideration. As such, the energy input for the make-up water pump was not included in the simulation. The efficiency of the cooling tower was determined based on the design temperature of each location, as given in Table 2.

### Case 2: Direct air-side economiser system

In this case, the air-side economiser system with an ultrasonic humidifier was used for the data centre cooling system. In order to meet the range as recommended by ASHRAE TC 9.9, the dry bulb temperature (DBT) of the supply air was set to 21°C with the dew point temperature was set at 11.1°C. The operation of this system was divided into four modes, depending on the outdoor air condition. As illustrated in Figure 3, the mode of the conventional refrigeration of the circulated indoor air was utilised when the outdoor air dry-bulb and dew point temperatures were higher than the recommended temperature range. Otherwise, the air economiser is utilised in the following modes: the direct use of the outside air, the mixing mode with the return air to heat up the supply air, and the mixing mode with the return air plus additional humidification.

According to the data centre model, the dissipated heat of servers and lighting was 1098.2 kW. Therefore, in order to remove the heat to the outside environment, 24 CRAC units were required with a total cooling capacity of 1106.4 kW. Since the amount of heat losses through the building envelope is negligible (less than 1%) in context of the enormous amount of dissipated heat from the IT equipment, the total mass flow of the air required to cool down the IT environment can be calculated using Equation (1) described in the previous section. Assuming the temperature difference between the return and air supply ( $\Delta T$ ) was 12 °C, the required airflow to remove the dissipated heat and lighting was  $273 \times 10^3$  m<sup>3</sup>/h. The economiser was active when the outside air dry-bulb temperature was equal to or lower than the setpoint temperature. The outside air was directly introduced to the IT environment when its dry bulb temperature was equal to the set point, and its dew point temperature was within the recommended range given by the ASHRAE standard for data centres.

Otherwise, when the outdoor air dry-bulb temperature was lower than the set point (21 °C), the outside air was mixed with the return air until the set point condition was reached. However, when the dew point temperature of the mixed air was within the allowable range, the mixed air was supplied to the IT environment without being humidified. In contrast, when the dew point temperature of the mixed air was lower than the setpoint ( $T_{dp} < 11.1^{\circ}\text{C}$ ), the humidifier operated to maintain the humidity of the air. The air was supplied when the set point was reached.

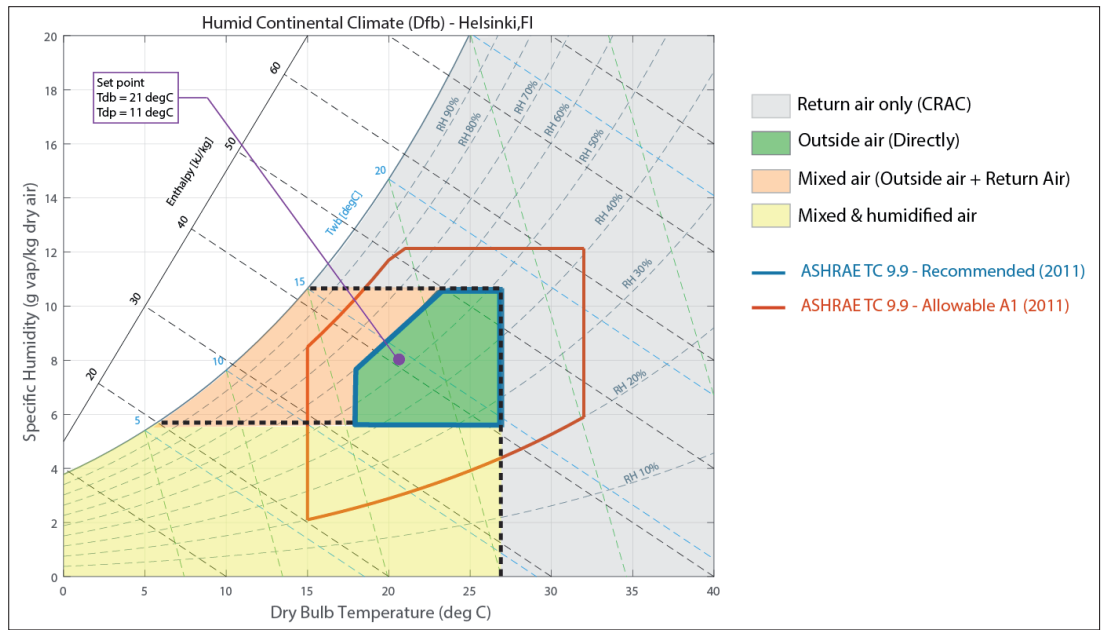


Fig. 3 Air-side economiser operation scheme

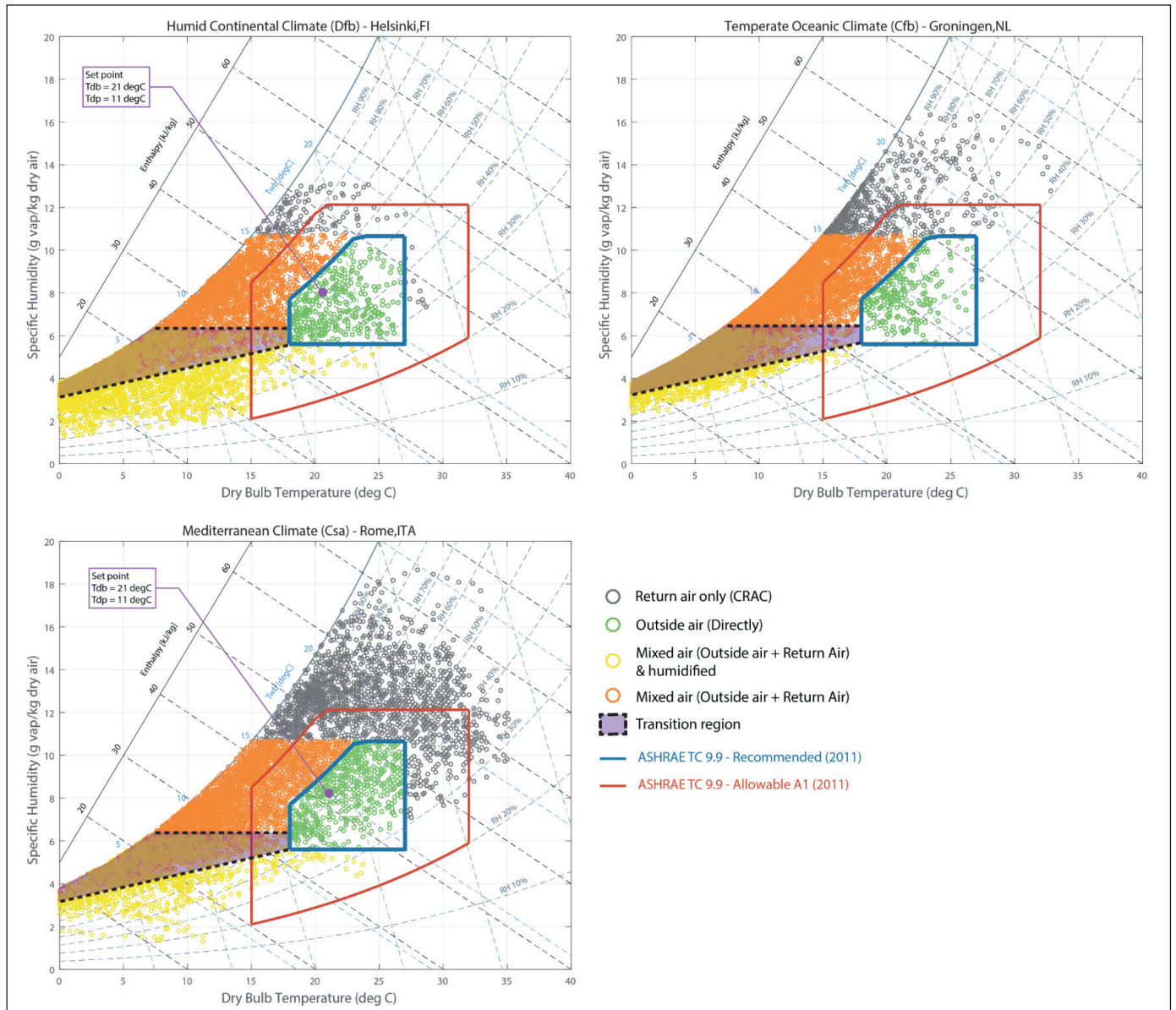


Fig. 4 Comparison of the weather conditions for each tested location

**RESULTS AND DISCUSSION**

The total annual energy saving potential of the tested cooling systems was calculated for three different locations to address various climatic zones within Europe. Fig. 4 shows the psychrometric charts for the outside air for each tested geographical location in this study. This figure is used to analyse the potential of the air-side economiser in each operational mode described above. The theoretical straight boundary shown in Fig. 3 between mixing modes with and without additional humidification was not observed in dynamic simulations. Instead, a transient region was found between these two modes. In this area, which is highlighted in purple, the outside air can be conditioned in two different ways, depending on the return air conditions. A high moisture content of the return air contributes to a higher moisture content of the mixed air. Thus, humidification was not necessary for these scenarios. On the other hand, when the moisture content of the return air was not rich enough, a humidification process was needed to maintain the humidity level of the mixed air before it was supplied to the IT environment.

Based on the information in Fig. 5, the location with a Humid Continental Climate profile (Dfb) represented by Helsinki has the highest potential to utilise the air-side economiser compared to the other tested locations. However, the graph shows that the humidity conditions of the outside air in this location were predominantly lower compared to the other locations. Consequently, the operational time of the mixing mode with humidification was higher for this location. On the contrary, the other tested climatic zones, which are represented by Groningen and Rome,

have a higher number of operational hours of the air-side economiser in modes of direct use and mixing without the need of additional humidification. Therefore, the results lead to the lower energy consumption of the humidifier in these locations.

In order to analyse the energy consumption, Fig. 6 demonstrates the energy consumption of each cooling system, which was obtained from the simulations and their PUE values. Meanwhile, Fig. 7 shows the proportion of the energy consumed by each component in the system. The simulation results of scenario 1 (baseline) only show the energy consumption of the conventional cooling system with refrigeration. In our study, this cooling system performed similarly regardless of the geographical location. As shown in Tab. 3, The simulated results were in the range of 3.24 to 3.26 GWh, resulting in a PUE of 1.34 for all locations. Such a small range for each location is the result of selecting a simplified heuristic modelling method focused mainly on modelling the air-side economiser. A slightly higher variance could be reached by implementing a dynamic coefficient of performance of the refrigeration cycle. However, the simplified model gives sufficient information to generate a common baseline for the study of the air-side economiser.

As depicted in Fig. 7, generally, 96% of the total energy of the conventional cooling system was used by the refrigeration units. The cooling tower took 3% of the total energy used by the conventional cooling systems, while the rest was used for pumping the cooling water and for the fans.

Tab. 3 PUE and Annual total electricity use for given locations

	scenario 1 Baseline	scenario 2 Helsinki	scenario 3 Groningen	scenario 4 Rome
PUE	1.34	1.07	1.07	1.12
Total electricity use (GWh)	12.88	10.29	10.31	10.80
Total electricity use by mechanical systems (GWh)	3.26	0.67	0.69	1.18

The second design (Case 2), where the air-side economizer is implemented, led to reduction of the total energy consumption by 73.2% on average in comparison with the baseline. The reduction of the total energy consumption resulted in the improvement of the PUE of each location to 1.07, 1.07, and 1.12 for the Humid Continental Climate (Dfb), the Temperate Oceanic Climate (Cfb) and the Mediterranean Climate (Csa), respectively. The most significant saving, which was 78.7%, was reached when the economiser was utilised in a location with a Humid Continental Climate (Dfb), represented by Helsinki. It is

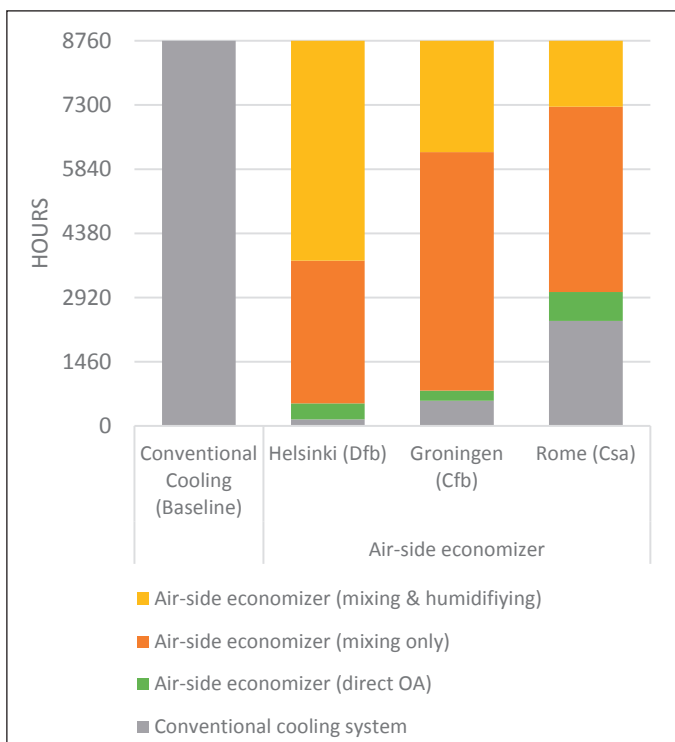


Fig. 5 Annual operating hours of the cooling system models

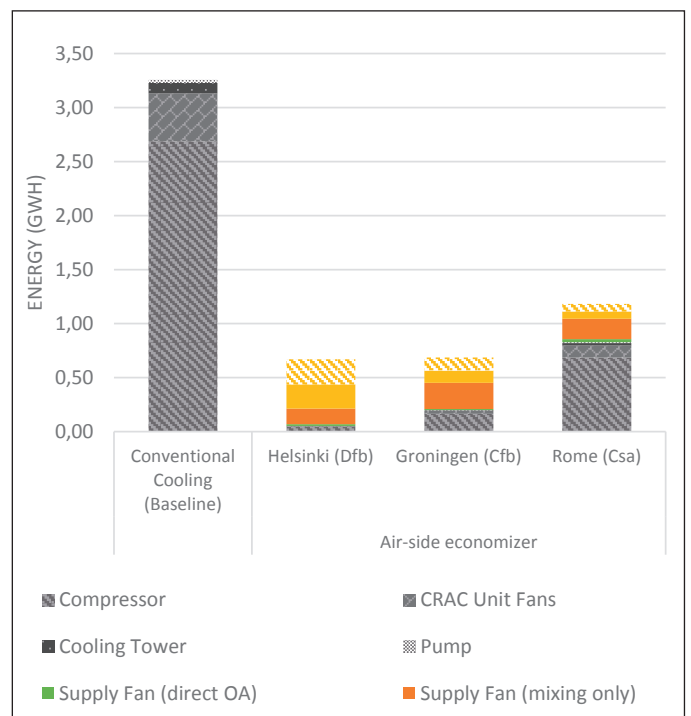


Fig. 6 Annual individual equipment energy consumption of the cooling systems in given locations

worth noting that the energy demand of the humidity treatment in this scenario reached 34.8% of the total energy use of the cooling system. Therefore, the Temperate Oceanic Climate (Cfb), represented by Groningen, with a lower proportion of humidification hours offers almost the equivalent economisation potential, even though the utilisation of the refrigeration unit is higher. The relative energy savings for the Temperate Oceanic Climate was 78.4%. The proportion of humidifier energy use of the total energy use was 16%. The simulation results demonstrate that the air-side economiser is able to significantly reduce the annual energy consumption of the cooling system by 73.2% on average. The savings vary from 62.5% to 78.7%, depending on the given climatic region. The resulting major savings were expected and similar figures are provided by the cooling unit manufacturer, e.g., [22], which states a range of 70% to 95% for similar conditions. However, this study was specifically focused on the impact of the humidity treatment within the air-side economiser on the total energy demand, which is likely neglected in other studies.

Considering the effects of the location and climate condition, the utilisation time of the air-side economiser, as depicted in Fig. 5, decreases as the latitude decreases. The temperature of the out-

side air and its specific humidity increase as the location nears the equator. Due to this reason, the number of hours when the outside air condition lies below the set point temperature was decreased, which resulted in the higher utilisation time for the conventional cooling system. Among the tested locations, the largest annual energy consumption of the conventional cooling system was found in a location with a Mediterranean Climate (Csa), which was represented by Rome. In this location, the conventional cooling system consumed 70% of the total annual energy consumption. To summarise, although the air-side economiser was able to significantly reduce the energy consumption in comparison to the conventional cooling system, introducing the outside air to the IT environment resulted in a higher proportion of energy consumption of the humidifier and fans (the consumption of the fan is divided into categories according to the operational regime: direct outside air, mixing and humidifying & mixing). The energy consumption of the humidifier varies between 6% to 34.8% depending on the given climatic regions. Compared to other locations, the utilisation of the air-side economiser in the climate represented by Helsinki resulted in the most significant energy consumption by the humidifier; the humidifier consumed 233.6 MWh, which represents 34.8% of the annual energy consumption.

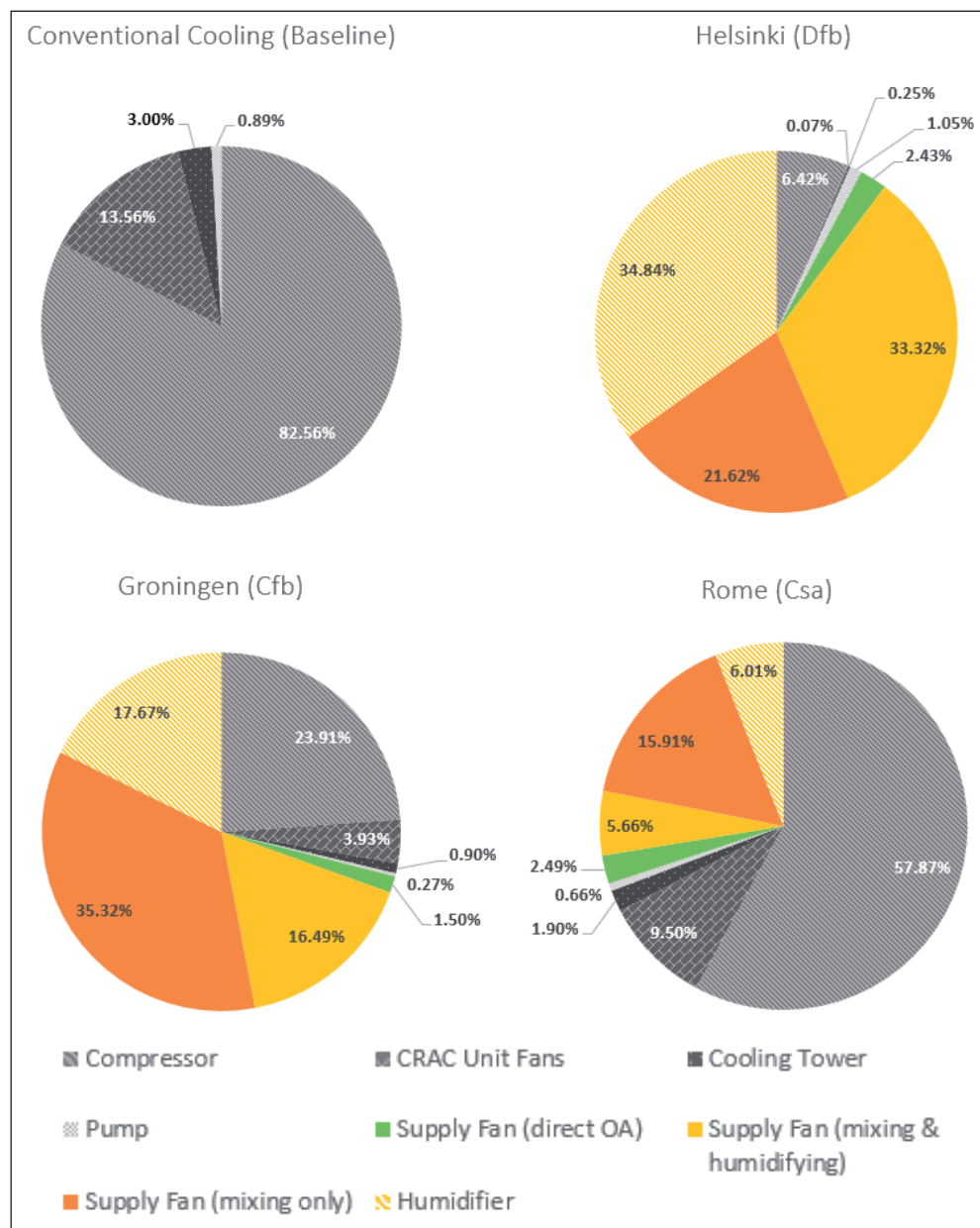


Fig. 7 The energy consumption breakdown by the individual equipment in percentage

## CONCLUSION

The results presented provide an indication of the impact of the humidity treatment within the direct air-side economiser system. As expected, the air-side economiser offers a significant savings opportunity of energy use in comparison to the conventional cooling system. Since the economiser systems have become the new standard in data centre cooling, addressing the savings was not the main goal of this study. The key finding of this study was the energy breakdown of the cooling system using the direct air-side economiser, which includes the energy use of the humidifier. Even though, the air-side economiser was found to be a very promising way to improve the energy efficiency of the DC cooling, this research demonstrated that additional energy is needed to maintain the humidity level of the air supply to reach the recommended conditions suggested by ASHRAE TC 9.9. The results of this study indicated that the annual energy consumption of the humidifier in the system with direct air-side economiser varies between 6%, 18% and 34.8% for climates represented by Rome, Groningen and Helsinki respectively, which cannot be neglected.

In conclusion, this research has shown that the design of new-generation cooling systems with air-side economisers requires consideration with the humidity treatment and its energy efficiency. The impact of the humidity

treatment can be relatively high, especially for the direct air-side economiser. The other economiser systems (e.g., an indirect air-side economiser) are generally less sensitive to the ambient environment, thus, the energy impact of the humidity treatment will be lower. Also, the energy demand of the humidity treatment can be also reduced using another humidifier device (e.g., a high-pressure fog system). Based on the study addressing the extreme situation, the highest possible impact of the humidity treatment was estimated to be up to 34.8% of the total DC energy demand.

Contact: [Vojtech.Zavrel@fs.cvut.cz](mailto:Vojtech.Zavrel@fs.cvut.cz)

## References

- [1] J. G. KOOMEY. Worldwide electricity used in data centers. *Environ. Res. Lett.* 2008, vol. 3, no. 3, p. 034008.
- [2] P. DELFORGE and J. WHITNEY. Data Center Efficiency Assessment. *Nat. Resour. Def. Counc.* August, 2014.
- [3] M. IYENGAR, R. SCHMIDT, J. CARICARI. Reducing energy usage in data centers through control of Room Air Conditioning units. *12th IEEE Intersoc. Conf. Therm. Thermomechanical Phenom. Electron. Syst.* 2010, pp. 1–11.
- [4] M. DAYARATHNA, Y. WEN, R. FAN. Data Center Energy Consumption Modeling: A Survey. *IEEE Commun. Surv. Tutorials.* 2015, vol. 18, no. September, pp. 1–1.
- [5] A. HABIBI KHALAJ, T. SCHERER, S. K. HALGAMUGE. Energy, environmental and economical saving potential of data centers with various economizers across Australia. *Appl. Energy.* 2016, vol. 183, pp. 1528–1549.
- [6] W. TSCHUDI, P. SHREEDHARAN, T. XU, D. COUP, P. ROGGENSACK. Data Centers and Energy Use: Let's Look at the Data. In: *ACEEE Summer Studies on Energy Efficiency in Industry.* 2003, pp. 113–123.
- [7] J. YOGENDRA, K. PRAMOD. *Energy Efficient Thermal Management of Data Centres.* London: Springer, 2012.
- [8] ASHRAE Datacom Series. *High Density Data Centers Case Studies and Best Practices.* 7th ed. Atlanta: ASHRAE, 2008.
- [9] J. CLARK. Humidity in the data center do we still need to sweat it? *The Data Center Journal.* 2012.
- [10] APC Schneider Electric. Humidity Issued in IT Data Centers.
- [11] The MathWorks. MATLAB 2014b. Natick, 2014.
- [12] C. BELADY (Microsoft), A. RAWSON (AMD), J. PFLEUGER (Dell), T. CADER (Spraycool). Green Grid Data Center Power Efficiency Metrics : PUE and DCIE Editors. *Green Grid.* 2008, pp. 1–9.
- [13] The American Society of Heating Refrigerating and Air-Conditioning Engineers (ASHRAE). *Thermal Guidelines for Data Processing Environments.* 3<sup>rd</sup> ed. Atlanta: W. Stephen Comstock, 2012.
- [14] The Green Grid. Updated Air-Side Free Cooling Maps: The Impact of ASHRAE 2011 Allowable Ranges. 2012.
- [15] V. K. ARGHODE, Y. JOSHI *Air Flow Management in Raised Floor Data Centers.* Springer, 2016.
- [16] K. MACKAY. Energy Efficient Cooling Solutions for Data Centres. *Syst. Res.* 2007, pp. 1–128.
- [17] B. A. HELLMER. Consumption analysis of telco and data center cooling and humidification options. *ASHRAE Trans.* 2010. vol. 116, no. 1, pp. 118–133.
- [18] T. EVANS. The different types of air conditioning equipment for IT environments. *APC White Pap.* 2004, p. 24.
- [19] S.-W. HAM, M.-H. KIM, B.-N. CHOI, J.-W. JEONG. Energy saving potential of various air-side economizers in a modular data center. *Appl. Energy.* 2015, vol. 138, pp. 258–275.
- [20] T. J. BREEN, E. J. WALSH, J. PUNCH, A. J. SHAH, C. E. BASH. From chip to cooling tower data center modeling: Part I Influence of server inlet temperature and temperature rise across cabinet. In: *Thermal and Thermomechanical Phenomena in Electronic Systems (ITherm), 2010 12th IEEE Intersociety Conference on.* 2010, pp. 1–10.
- [21] S.-W. HAM, J.-S. PARK, J.-W. JEONG. Optimum supply air temperature ranges of various air-side economizers in a modular data center. *Appl. Therm. Eng.* 2015, vol. 77, pp. 163–179.
- [22] DANTHERM. Dantherm official. 2017.

Nikolaos SKANDALOS <sup>1)</sup>,  
Jan TYWONIAK <sup>1,2)</sup>,  
Kamil STANEK <sup>1,2)</sup>,  
Lenka MAIEROVA <sup>1,2)</sup>

<sup>1)</sup> CTU in Prague, University  
Centre for Energy Efficient  
Buildings

<sup>2)</sup> CTU in Prague, Faculty of Civil  
Engineering

Reviewer  
Vasilis C. KAPSALIS, Ph.D.

# The PV Potential in the City of Prague: Methodology and Assessment for Residential Buildings

## Fotovoltaický potenciál v Praze – Metodika a hodnocení pro obytné budovy

*This work highlights the Building-Integrated Photovoltaics (BIPV) potential in two urban areas with different characteristics in the city of Prague. The representative building blocks were selected and the CitySim software tool was used for the assessment of the hourly irradiation profiles on each surface over a one-year period. Considering appropriate irradiation thresholds, suitable surfaces were then quantified. Integration criteria are discussed and suitable BIPV applications are proposed considering, not only energy performance, but also their impact on the quality of the built environment. The Photovoltaic (PV) potential is compared with the estimated local electricity demand derived from the population distribution within the building block. Analysis indicated that only 5.5% of the total area can be used in Vinohrady and 13.7% in Jizni Mesto contributing by 32% and 31% on average on the hourly electricity demand, respectively. The PV generation exceeds the local non-baseload demand during the summer period, but is less significant during winter. A preliminary financial analysis reveals a payback time of 17.5 and 20 years for Vinohrady and Jizni Mesto areas, respectively. It is evident that, even in the areas with a sensitive built environment, adoption of solar energy is still possible for balancing local electricity needs.*

**Keywords:** Building-integrated photovoltaics, solar PV potential, architecture, load matching

*Príspevek sa zaoberá potenciálom využitia stavebně integrované fotovoltaiiky v odlišné zástavbě Prahy. Pro dva reprezentativní obytné bloky byly pomocí software CitySim stanoveny hodinové profily ozáření všech povrchů v průběhu roku. Z toho pak byly určeny vhodné plochy pro fotovoltaiické instalace. Uvažovány byly nejen energetické vlastnosti ale i vliv na kvalitu zastavěného prostoru. Potenciál fotovoltaiické produkce je porovnávan s místní potřebou elektrické energie pro obyvatele. Analýzy ukazují, že celkově jen 5,5% ploch může být využito na obytném bloku na Vinohradech a až 13,7% ploch na obytném bloku na Jižním Městě, což přispívá k pokrytí potřeby elektrické energie domácností v průměru z 32% a ve druhém případě z 31%. Fotovoltaiická produkce v takovém případě v letním období přesahuje místní spotřebu. Předběžná finanční analýza ukazuje návratnost 17,5 roku pro Vinohrady a 20 let pro Jižní Město. Potvrzuje se, že i v architektonicky náročném prostředí je využití solární energie pro významné pokrytí místní spotřeby možné.*

**Keywords:** stavebně-integrovaná fotovoltaiika, fotovoltaiický potenciál, architektura, soulad produkce a spotřeby

## INTRODUCTION

The building sector is classified among the major energy consumers, contributing by 40% of the primary energy consumption in Europe [1]. Currently, there is a major transformation taking place through national building codes, roadmaps and building rating systems. In addition, emphasis has been put on the adoption of renewable energy systems on the building envelope [2]. Among other options, solar photovoltaics are expected to be the main technology to generate on-site electricity to match the building's consumption [3]. This is enhanced by the fact that the location of the energy source is commonly the same as the location of the energy use. Consequently, the generated electricity cannot be used instantly to cover the building needs only (e.g., lighting, appliances, heating, etc.), but also exchanged between the buildings and the electrical grid.

Building-Integrated Photovoltaics (BIPV) – defined as photovoltaic cells integrated into the building envelope as part of the building structure – have great potential to be used in a city context. It can replace conventional building materials, and also be used as external separation elements, like balconies, shading devices and other applications [4]. Rooftop PVs are, so far, considered to be the most common application since it provides the best annual energy harvesting. However, due to the significant decrease in prices and increase in technological improve-

ments in the PV industry, building facades now represent a good potential, especially for high-rise buildings. Even if they receive less irradiation compared to rooftops, they could make a major contribution because of the larger surface areas involved. In addition, vertical-integrated PV modules will produce relatively more power in winter, as well as in the early and late hours of the day.

Consequently, it is important to adjust the slope and azimuth of the PV installations, in order to spread the electricity generation over a larger period of time increasing the PV self-consumption of residential buildings [5]. However, the successful integration of PVs in a city context requires not only technical optimisation to maximize production, but also to preserve the quality of the urban, landscape and cultural environments. A match between the building's energy needs, the solar energy potential and the site's identity has to be targeted [6].

Several case studies have already been performed for incident solar radiation on individual buildings, small neighbourhoods or on a city scale, indicating the nice PV potential in existing locations. Depending on the availability of the data, regional characteristics, as well as scale of study, several methodologies have been suggested to determine the PV potential. Brito et al. [5] investigated the PV potential for two areas in the city of Lisbon using LIDAR data. It was found that the roof and facade PV potential can contribute to 50–75% of the total electricity demand.

Assouline et al. [7] using a combination of support vector machines (SVMs) and geographic information systems (GIS) found that the potential PV production for the urban areas in Switzerland corresponded to 28% of Switzerland's electricity consumption in 2015.



Fig. 1 Aerial view of the selected locations in a) Vinohrady and b) Jizni Mesto.

There are also studies on the effects of the urban form on the solar PV potential. According to Compagnon [8], a building's layout for constant density can lead to variations of the solar potential. Besides, increasing the building aspect ratio or site coverage has a positive effect on the PV potential, although the effect of mutual shading becomes more significant according to Li *et al.* [9]. In this context, a new algorithm for the spatio-temporal calculation of a shadow in the urban environment was proposed by Vulkan *et al.* [10]. The methodology implemented for a neighbourhood in Rishon LeZion, Israel, with diverse building typologies indicated that some facades can make a substantial contribution to the overall solar potential of urban buildings.

Solar energy harvesting for individual buildings in the city of Prague has been studied in the past, but the PV potential in urban areas has not yet been investigated. This study aims to fill this gap indicating how the detailed mapping of the existing architecture can quantify the PV potential of urban residential buildings in the historical and modern city areas. Using data from IPR Praha (the Institute of Planning and Development of the city of Prague), we describe the topography, for two case study areas. Considering the solar availability and shadings for the surrounding buildings, the available area for installation is determined and suitable PV applications are proposed based on the characteristics and cultural aspects of the location. Then, the hourly PV generation of the roofs and facades is compared with the estimated local electricity demand on an hourly basis discussing strategies for better load matching.

## METHODOLOGY

### Location characteristics

Prague is the capital and largest city in Czech Republic located in the north-west (at 50°05'N and 14°25'E) of the country. The climate is considered to be semi-continental, characterised by large seasonal temperature differences, with cold winters and warm (and often humid) summers. In order to investigate the PV potential, solar radiation and other meteorological data (temperature, wind speed, etc.) were provided from a local weather station. An annual global horizontal radiation is approaching 1065 kWh/m<sup>2</sup> with a peak value of 161 kWh/m<sup>2</sup> in June, while lower values of solar irradiation are observed during winter months (a min value in December).

In this work, two urban areas in the city of Prague with different characteristics were selected as the application sites for the assessment of the PV potential. A representative building block, constituted of residential buildings, was identified for each location as presented in Fig. 1. Case one, Vinohrady, is within a highly dense area of the city centre with considerable architectural and cultural value. Houses built around 1900 are characterised by sloped roofs in different shapes and heights. Case two, Jizni Mesto, is a suburban area built in the 1970s. Prefabricated high

rise buildings are characterised by their simple shape, flat roofs and big vertical facades with balconies with a South and West orientation. They are lighter, with a higher fenestration ratio and better thermal insulation compared to the ones in Vinohrady.

### Solar PV potential

Appropriate 3D models for each building block were prepared based on the geometry of the buildings, including the dimensions and shape of the roof superstructures (dormer, chimney, etc.). The building surfaces were divided according to the floor level, excluding areas that for some reason cannot be considered for PV integration (e.g., north facade). Radiation on the building surfaces is commonly influenced by the nearby environment and, thus, the heights of the surrounding buildings, trees and elements in each direction were considered in the model for evaluating the shading. Afterwards, the 3D model was imported to CitySim Pro [11], an urban energy modelling tool developed at LESO-PB/EPFL, for further analysis. The incoming solar radiation was calculated in hourly values, according to the type of the building surface and the climate data collected by a nearby weather-station. Each building surface was defined by its area, orientation and tilt angle. Finally, the percentage of solar obstruction was calculated as the ratio of the solar radiation within the surrounding context to the one without the surrounding obstacles. The hourly values were solar weighted, the annual shading index (*SI*) was derived according to Eq. 1.

$$SI = \frac{\sum_{i=1}^{N=8760} F_{sh,i} G_i}{G_t} \quad (1)$$

where

$F_{sh,i}$  is the hourly shading factor of each building surface,  
 $G_i$  is the hourly solar radiation [W/m<sup>2</sup>]  
 $G_t$  is the annual solar radiation [W/m<sup>2</sup>]

Once the radiation values on each surface are available, they can be analysed to assess the PV potential. For this purpose, an irradiation threshold was used, indicating the minimum amount of annual radiation required for the PV system to be beneficial. Such thresholds are somewhat arbitrary; a conservative value of 800 kWh/m<sup>2</sup> annually is proposed by many authors [9], while others define it as a percentage of the horizontal insolation [10]. Considering the technological progress and enormous decline in PV costs over the last decade, approximately a 58 %, according to [12], lower value such as 650 kWh/m<sup>2</sup> [13] is still reasonable. To this end, the PV potential calculated as the relative fraction (percentage) of the roofs and facades of the buildings that can be used for PV integration. Based on the area of the suitable surfaces, a simple model was applied to quantify the annual energy output ( $E_{pv}$ ) of each building block according to Eq. 2:

$$E_{PV} = \eta \cdot PR \cdot \sum_{i=1}^{n_{threshold}} (I_i A_i) \quad (2)$$

where

- $\eta$  is the PV conversion efficiency,
- $PR$  is the performance ratio
- $n_{threshold}$  is the number of surfaces exceeding irradiation threshold,
- $I_i$  is the cumulative insolation (kWh/m<sup>2</sup>.year) and
- $A_i$  is the relative area (m<sup>2</sup>) of surface  $i$ .

### Electricity demand and system performance

Afterwards, the following procedure was used to derive the annual electricity load curves of the representative buildings on an hourly basis. Only the non-thermal use of electricity is considered in this study, i.e., the derived load curves include all means of the households' electricity consumption except the use for space heating and hot water preparation.

In the first step, a normalised hourly electricity consumption profile of a typical Czech household was constructed based on data published by the Czech electricity and gas market operator (OTE a. s.) for consumer class 4 – households with non-thermal use of electricity (TDD4) [14]. This normalised hourly consumption profile consists of 8760 values between 0 and 1, with a typical differentiation between working days and weekends, and with higher consumption in winter compared to summer. In the second step, the number and area of the households, and the number of the occupants in the representative buildings were estimated. These basic statistics describing the representative buildings were then matched to the data on the annual non-thermal electricity consumption in Czech households, reported by the Czech Statistical Office (ČSÚ) [15] and the REMODECE Project [16], to estimate the total annual electricity consumption (MWh/year) in the representative buildings. Finally, in the third step, the normalised hourly consumption profile and the total annual electricity consumption were combined into the hourly load curves of the representative buildings, in kW (see Figure 2). A more detailed description of the whole procedure can be found in [17].

Based on the peak loads and the selection criteria that apply in each location, the PV systems were sized properly, in order to enhance the PV self-consumption and reduce excess power during the summer period. In addition, a comparison between the electrical loads and the PV generation for the selected locations was made through the calculation of the load match index as described in [18]. According to eq. 3, it was calculated for hourly time intervals indicating the average hourly contribution of the PV systems on the building loads.

$$f_{load,i} = \frac{1}{n} \sum_{i=1}^n \min \left[ 1, \frac{g_i}{l_i} \right] \cdot 100 \quad [\%] \quad (3)$$

where

- $i$  is the time interval (hour, day, month)
- $g_i$  is the instantaneous on-site electricity generation
- $l_i$  is the instantaneous electricity demand
- $n$  is the sum of time steps over a year period

### Financial analysis

Finally, a financial analysis was undertaken to investigate the profitability of the proposed systems. In this context, the Net Present Value (NPV) – defined as the sum of present incoming (benefits) and outgoing cash flows over the lifetime of the project – was calculated according to eq. 4 [19].

$$NPV = -C + \sum_{t=1}^N \frac{F(t)}{(1+i)^t} \quad (4)$$

where

- $C$  is the initial investment costs (€)
- $F(t)$  is the annual income generated by the PVs (€/year)
- $N$  is the lifetime of the investment (years)
- $i$  is the real rate of interest (%)

The initial investment includes the cost of the PV modules, electrical components (inverters, cables, etc.) and claddings (frames, aluminium sub-structures, etc.). It is worth mentioning that the size of the PV plant has an effect on the cost of the installation. Considering the actual size of the installation, in this work, typical values of 1350 €/kWp, and 1290 €/kWp were used for crystalline silicon and thin-film PV technologies, respectively [20]. In the case of Vinohrady, more advanced PV products are used and, therefore, the cost of the BIPV increases. The end user prices are converted to €/m<sup>2</sup>, with an average value of 300 €/m<sup>2</sup> [21]. Finally, a fixed maintenance cost of 0.5 % per the initial cost was assumed in both cases.

For the calculation of the annual income, the following inputs were used: annual energy output (kWh), coefficient of performance considering representative degradation rates (%/year) for each PV technology, energy price (€/kWh) and possible Feed-in-tariff or fiscal incentives. Then, the cash flow over the life time of the PV system (25 years-expected) was prepared and the payback time (PBT) [19] was estimated as an indicator for the number of years needed to compensate for the initial investment.

### BIPV integration criteria

It is evident that excessive use of PV systems can often have an adverse effect on the built environment and, thus, the criteria and recommendations about dimensioning and positioning are needed. In order to select an appropriate BIPV application, both technical, architectural and economic aspects should be included. In the case of Jizni Mesto, there are no limitations arising from the near environment and, thus, several scenarios and PV technologies can be considered (Fig. 3). High performance modules can be installed horizontally on the flat roof of the buildings to camouflage the installation or tilted to optimise the performance. On the vertical facades, the PV modules should be grouped together in an ordered way creating unique textures (e.g., horizontal stripes). In this context, ceramic panels or solar glazing in various colours [22] could be a solution, providing good durability and an aesthetic quality. Finally, complementary building elements such as windows and existing balconies are well suited to support the PV integration representing a good compromise in terms of the energy performance and aesthetics. In addition, optimised semi-transparent PV elements could be used as shading devices to increase the indoor thermal comfort by mitigating overheating during the summer, but to still provide daylight and to make use of passive heating during winter [23].

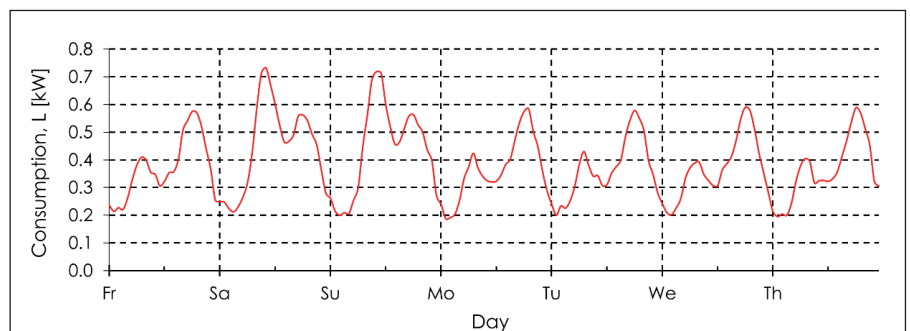


Fig. 2. A typical load profile for the electricity consumption of a household in Prague [17].



Fig. 3. Examples of architecturally integrated PV systems in the two building blocks: (1) PV balconies. Source: Etsprojects; (2) Coloured PV- facade. Source: Swissinso; (3) Roof-added PVs. Source: Cromwellsolar; (4) PV tiles. Source: Tradeford; (5) PV shutter and PV blinds. Source: COLT international, Solargaps; (6) PV terrace [26].

On the other hand, the BIPV integration in a sensitive built environment, such as the Vinohrady district, is a more challenging task. The applicability of conventional PV modules in buildings with strong architectural or cultural value is limited. Since the full integration and imperceptibility of the technical elements from the public domain is the most important criteria for the acceptance of the BIPV within a historical context [24], small scale highly innovative PV products are needed. Suitable surfaces are limited to the sloped roof, flat terraces and vertical facades facing the courtyard. Based on the geometry of each surface, BIPV applications such as solar glazing or PV tiles, balustrades and PV shutters (Fig. 3) constitute effective practices of integration in the building envelope providing a balanced solution between the technical and architectural standards as defined in [25].

## RESULTS & DISCUSSION

### Solar PV potential

The results from the solar analysis in both locations are presented in the form of annual irradiation colour maps. As expected in Vinohrady, the best solar resources were observed for the sloped roofs (35° slope) facing south, exceeding 1200 kWh/m<sup>2</sup> annually (Fig.4). However, the different roof typologies were recognised and, thus, the solar potential varies according to its slope and orientation. The facades were found to receive a significantly lower level of irradiation, which is explained from the mutual shading effects (high density), especially for the lower part of the buildings. The calculated annual shading indexes can reach up to 57 %. Only 19.7 % of the total surface area exceeds the irradiation

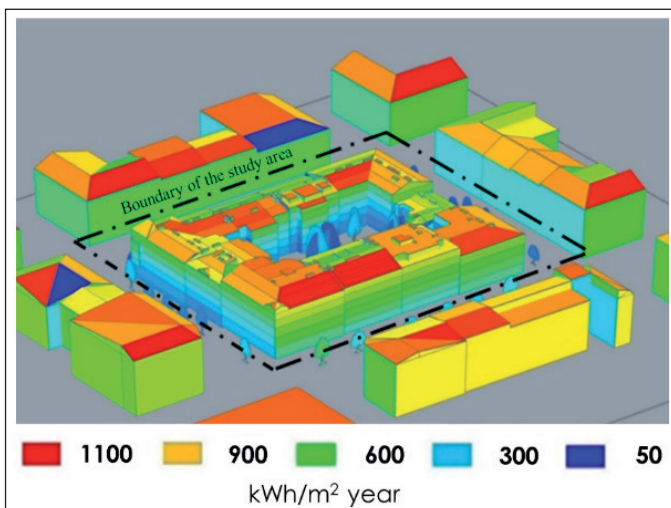
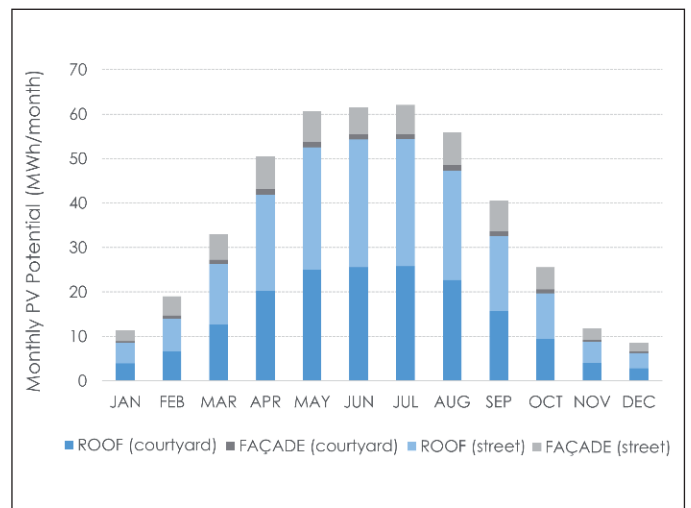


Fig. 4. The annual solar irradiation map and relative PV potential of the building block based on the selected irradiation thresholds in the Vinohrady area.



threshold of 650 kWh/m<sup>2</sup> and is mainly related to the roof areas. With respect to the hourly irradiation profiles, the maximum PV potential in the area was calculated and presented in Fig. 4. The PV modules were assumed to be installed on the same plane with the building surface considering the typical values for the conversion efficiency ( $\eta$ ) according to the BIPV application ( $\eta = 15\%$  for the roofs and  $\eta = 8\%$  for the facades/balconies/glazing). Additionally, an appropriate performance ratio (PR) was used to take all system losses (inverter, mismatch, etc.) into account. For Vinohrady, the annual PV generation is estimated to be 440 MWh approximately, with a peak value in July (62 MWh) and the least generation in December (8.5 MWh). It is worth mentioning that only 42% of this generation corresponds to the building surfaces facing the courtyard and, thus, could be considered according to the criteria discussed in the previous section.

The relative results for the building block in Jizni Mesto are presented in Fig. 5. The max potential was slightly reduced (around 10%) compared to Vinohrady, but still exceeds 1000 kWh/m<sup>2</sup> annually. This corresponds to flat roof on top of the buildings, followed by the south-facing facades. Furthermore, solar obstruction was found to be significantly lower due to the less dense urban environment of the location. The highest shading indexes calculated in the range of 23%, indicating acceptable resources even for the East/West facades (to some extent). According to the selected irradiation threshold (650 kWh/m<sup>2</sup>), 35% of the total building area can be considered as suitable for the PV integration. Based on the irradiation profiles, the simulated PV potential is equal to 1195 MWh/annually, 2.7 times higher when compared to the Vinohrady case. The highest contribution refers to the roof area, followed by the vertical facades and balconies with the relative percentages of 49%, 45% and 6%, respectively (Fig. 5). Extensive PV integration on the vertical facades in Jizni Mesto has an impact on the monthly values (compared to the Vinohrady case) shifting the peak generation to June (Fig. 5).

### Electricity demand

The statistical data regarding the population distribution and annual consumption per household [16] were used to determine the electricity demand in both areas. For the given number of apartments, the estimated number of occupants was then multiplied by the per capita electricity demand. The limited available data, regarding the consumption of the selected building blocks, was also used for the validation. For the building block in Vinohrady, the overall electricity demand was estimated at 478 MWh/year. As for building block in Jizni Mesto, the increased number of residents due to the high-rise buildings, results in a higher annual electricity demand of 1214 MWh/year. The analytical results for the annual demand and production per building are presented in Table 1. One

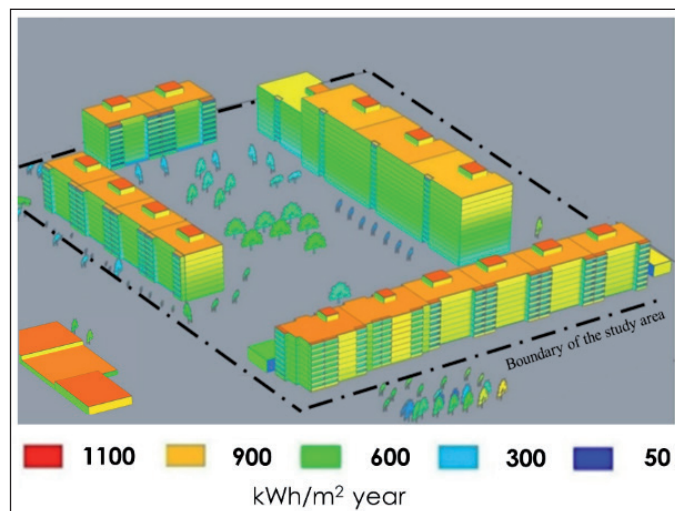


Fig. 5. The annual solar irradiation map and relative PV potential of the building block based on the selected irradiation thresholds in the Jizni Mesto area.

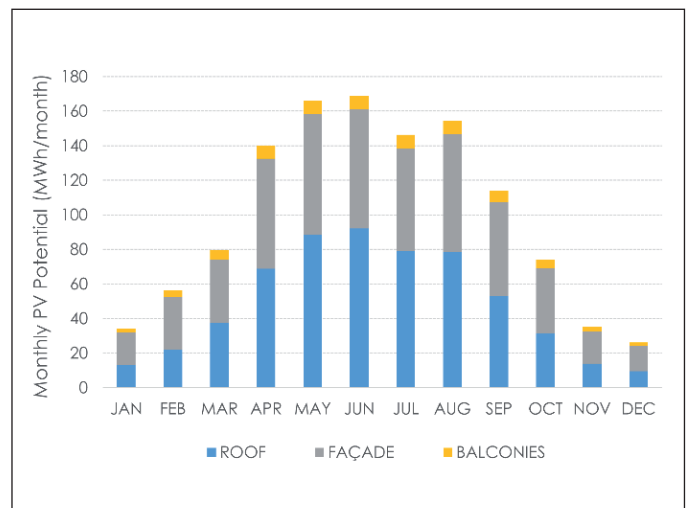
can observe that the PV production is significantly reduced compared to the PV potential of the area in Vinohrady. The available space is limited to only 5.5% of the total building area due to the integration criteria applied (discussed in previous sections).

### System evaluation

Having a look at the comparison between the demand and the production in monthly intervals, it is clear that the generated electricity is not enough to cover the loads of the building block in Vinohrady. On the contrary, there are no such barriers limiting the PV integration in Jizni Mesto and, thus, even for higher irradiation thresholds, the PV generation is enough to compensate the electricity demand during the summer period. From that point of view, it is important to investigate the load match over a shorter time step to ensure a minimum excess of PV energy. For that purpose, typical load profiles (Fig. 2) for residential buildings were used to analyse the electricity demand in hourly time-steps.

During this process, the hourly peak loads were calculated and used as an indicator, to properly size the PV systems in each building. In the case of Vinohrady, the maximum loads observed for building 6 is equal to 17.2 kW, while ranging between 27–120 kW for the whole block. An excess of energy was observed for small periods during the summer only, but still the PV self-consumption accounts for 92%. Almost all the generated PV energy can be used locally within the building block and it is enough to compensate by 32% (the max value of 49% for the building case) the hourly electricity demand on average.

In the case of Jizni Mesto, the PV generation is enough to cover the electricity demand during the summer period, but also leads to an excess of energy for 35% of the PV operation time (hourly). Therefore, better interaction between the generated and consumed electricity is needed to increase the self-consumption of the buildings providing more efficient performance. If the maximum load matching is taken into account, integration will be limited to only 13.7% of the total building area leading to lower PV generation. Fig. 6 depicts the interaction between the electricity demand and the production for the new system over a typical winter and summer day. A wider peak power production and, thus, a better match to the load diagram is observed. A small excess of energy is observed at noon and can be used for cooling purposes to eliminate overheating risks. Alternatively, this can be delivered to the surrounding buildings and facilities across the street. Finally, the average and max values for the load match index (hourly intervals) among the buildings in Jizni Mesto were found to be 31% and 43%, respectively. The larger PV system size hardly improves the load match index if no measures for electricity storage are taken.



Tab. 1 The annual electricity demand and production per building in Vinohrady and Jizni Mesto area.

Building No.	Electricity demand (MWh/year)		PV production (MWh/year)	
	Vinohrady	Jizni Mesto	Vinohrady	Jizni Mesto
1	40.8	112.2	13	54.1
2	62.7	576.6	20	300.7
3	56.1	196.8	10.4	121.3
4	63.6	328.5	17.4	266
5	39.2	-	14.3	-
6	68.4	-	19.9	-
7	35.9	-	15.2	-
8	31.3	-	15	-
9	63.6	-	17.9	-
10	16.9	-	6.7	-

It can be observed that even with a higher percentage of surface area used in Jizni Mesto, the average hourly load match is similar to the case of Vinohrady. The higher population density of the high-rise buildings leads to different consumption patterns compared to the family households in Vinohrady. This is also explained from the PV production per unit area in Vinohrady (163 kWh/m<sup>2</sup>), which was found to be up to 32 % higher compared than the one in Jizni Mesto (111 kWh/

m<sup>2</sup>). This is a direct consequence of the limited vertical integration on the facades (lower solar resources), when the contribution approaches 50 % of the area used for Jizni Mesto.

Fig. 7 depicts the accumulated PV generation for the proposed systems in both locations. Apart from the total electricity demand discussed earlier, the PV generation is also compared to the non-baseload load demand - determined by subtracting the minimum load of the previous 24 h from the hourly demand load [5]. Assuming that the baseload demand can be covered from alternative sources, the results clearly indicate that the PV generation exceeds the non-baseload demand in both areas during the summer period. More specifically, the demand is satisfied for five consecutive months from April to August. Surprisingly, even for a lower extent of PV integration, the Vinohrady area achieves better results. In contrast, during the winter months, the PV generation decreases drastically and is not enough to meet (the increased) the total nor the non-baseload demand.

**Financial analysis**

Based on the methodology presented in Section II, a preliminary financial analysis was performed for a period of 25 years (expected lifetime of the investment). The NPV was calculated by subtracting the initial cost from the discounted annual income from the PV generation. For the calculations, a real rate of interest of  $i = 2.26\%$  and an initial energy price of 0.142 €/kWh with a growth rate of 1.8 % (according to Eurostat) were assumed, based on the current situation in the Czech Republic.

The annual electricity generation for the next 25 years was estimated, considering the degradation rates from a recent study with similar conditions [27]. The results, already discussed, indicated 92 % self-consumption in Vinohrady and 10% lower in Jizni Mesto. This means that

most of the PV electricity is consumed directly from the buildings in both areas. In 2013, the Czech Parliament amended Act No. 165/2012, which *de facto* abolished the feed-in tariff scheme for PVs by the end of 2013. Since there is no financial support right now, the excess part of the PV generation, exported to the grid, was not taken into account in the results presented in Fig. 8.

In the graph, the value of year 0 is associated with the initial investment cost of the system. Based on the PV costs discussed in Section II, this is equal to 360000 € for Vinohrady and 873000 € for Jizni Mesto. The payback time, i.e., the number of years needed to make the NPV positive, was found to be 17.5 and 20 years for Vinohrady and Jizni Mesto, respectively. The payback time can be reduced further considering the sav-

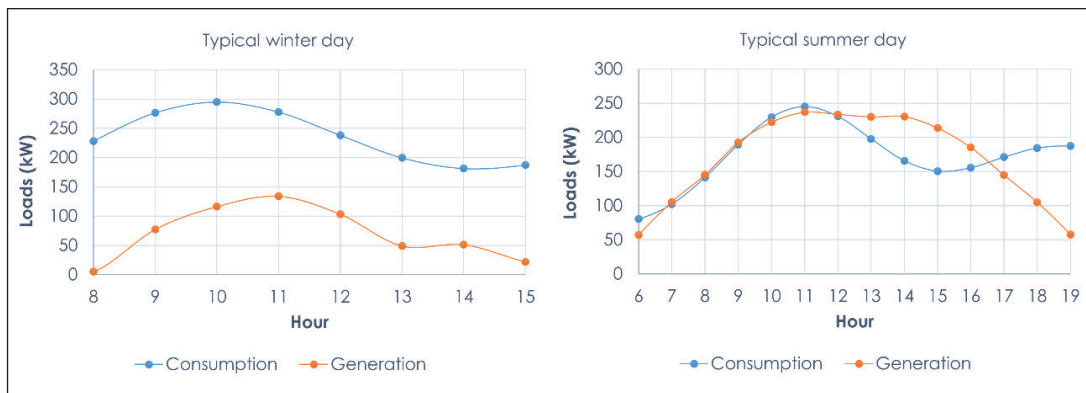


Fig. 6. The hourly electricity demand (blue line) and generation (red line) over a typical a) winter and b) summer day for the building block in Jizni Mesto.

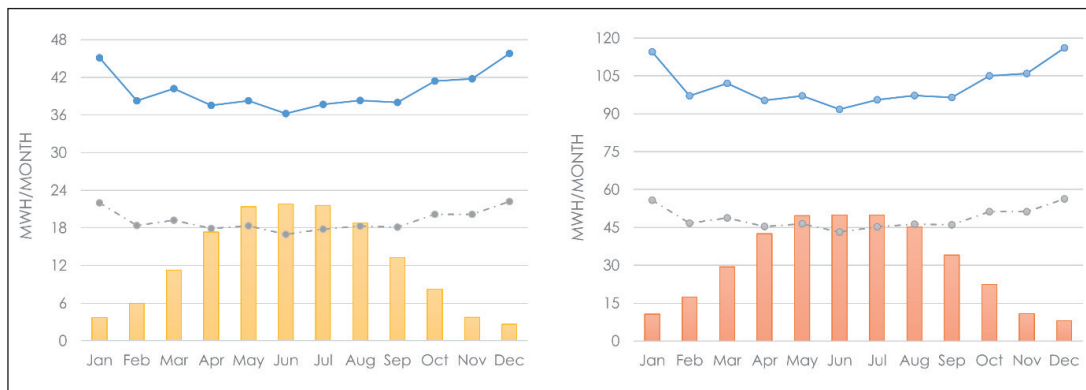


Fig. 7. The monthly PV generation and electricity demand (blue line: total electricity demand; grey line: non-baseload demand) of the proposed system for a) the Vinohrady (left) and b) Jizni Mesto (right) areas.

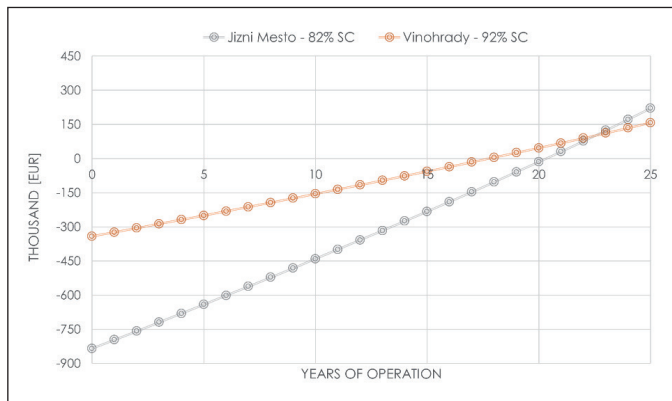


Fig. 8. The Net Present Value (NPV) associated with the investment of the PV installation in the Vinohrady (92% self-consumption) and Jizni Mesto (82% self-consumption) areas.

ings from the conventional building materials, and the energy saving provided by the applied solutions and more efficient strategies to increase self-consumption. Given that facilities like schools, supermarkets, etc. exist across the street (at the boundaries of the study area), the excess PV energy can be delivered and decrease the payback time in Vinohrady by 1.5 years and up to 4 years in Jizni Mesto. Consequently, a more detailed study should be considered to thoroughly investigate these scenarios.

## CONCLUSIONS

Two representative building blocks, with different characteristics and levels of preservation, were selected and analysed to quantify the PV potential of urban residential buildings in historical and modern city areas. According to the selected irradiation thresholds, the analysis revealed almost a 3 times higher potential in Jizni Mesto compared to the Vinohrady area. As expected, most of the potential is intrinsically related to the roofs, while the facades suffer more of a shadowing effect caused by the surroundings. The phenomenon is more intense in the Vinohrady area, where only 13 % of the PV potential is related to the facades, when the additional contribution in Jizni Mesto is approaching 50 %.

The integration criteria was discussed and suitable PV applications are proposed, considering not only energy performance, but also their impact on the quality of built environment. Afterwards, a methodology was used to estimate and compare, in an hourly time-step, the electricity generation and demand. It was found that only small part of the building area can be used accounting for 5.5 % in Vinohrady and 13.7 % in Jizni Mesto. Interaction between the electricity demand and consumption revealed that the proposed PV systems could compensate, on average, 32 % of the hourly energy demand in Vinohrady and 31% in Jizni Mesto. Considering the actual self-consumption rate and actual market conditions (BIPV prices, installation costs and electricity tariffs), the economic assessment indicated that the payback time of the investment is equal to 17.5 years for Vinohrady and 20 years for the Jizni Mesto area. A summary of the results obtained for the two case studies is presented in Table 2.

It is evident that even in areas with a sensitive built environment, adoption of solar energy is still possible for balancing the local electricity needs. Further work is needed to assess the indirect effect of the BIPV systems on the built environment by means of thermal and daylighting performance. This paper can be used as reference for future case studies in the process of building a sustainable city.

Tab. 2 An overview of the PV potential for the two case studies.

Case study area	Vinohrady	Jizni Mesto
Total Area (m <sup>2</sup> )	21775	34200
Percentage of Area ( $\geq 650$ kWh/m <sup>2</sup> .y)	19.7	36.5
PV potential (MWh/year)	440	1195
Percentage area used for PVs (%)	5.5	13.7
Electricity demand (MWh/year)	478	1214
PV generation (MWh/year)	150	370
Avg. Load match index (%)	32	31
PV self-consumption	92	82
Payback Time (years)	17.5	20

Contact: Nikolaos.Skandalos@cvut.cz

**ACKNOWLEDGEMENT.** This work has been supported by the Ministry of Education, Youth and Sports within National Sustainability Programme I (NPU I), project No. LO1605 – University Centre for Energy Efficient Buildings – Sustainability Phase and by the Operational Programme Research, Development and Education of the European Structural and Investment Funds, project CZ.02.1.01/0.0/0.0/15\_003/0000464 Centre for Advanced Photovoltaics.

The authors would also like to acknowledge Solar Energy and Building Physics Laboratory (LESO-PB) of EPFL in providing the CitySim software.

## REFERENCES

- [1] UNEP. Building Design and Construction: Forging Resource Efficiency and Sustainable Development. 2012.
- [2] IEA-PVPS. Trends 2015 in photovoltaic applications: Survey report of Selected IEA countries between 1992 and 2014. Paris, FR. 2015.
- [3] TRIPATHY, M., SADHU, P. K. and PANDA, S. K. A critical review on building integrated photovoltaic products and their applications. *Renewable and Sustainable Energy Reviews*. 2016, 61, 451-65.
- [4] SHUKLA, A. K., SUDHAKAR, K., BARENDAR, P. Recent advancement in BIPV product technologies: A review. *Energy and Buildings*. 2017, 140, 188-95.
- [5] BRITO, M. C., FREITAS, S., GUIMARÃES, S., CATITA, C., REDWEIK, P. The importance of facades for the solar PV potential of a Mediterranean city using LiDAR data. *Renewable Energy*. 2017, 111, 85-94.
- [6] FLORIO, P., PROBST, M. C. M., SCHÜLER, A., SCARTEZZINI, J-L. Visual prominence vs architectural sensitivity of solar applications in existing urban areas: an experience with web-shared photos. *Energy Procedia*. 2017, 122, 955-60.
- [7] ASSOULINE, D., MOHAJERI, N., SCARTEZZINI, J-L. Quantifying rooftop photovoltaic solar energy potential: A machine learning approach. *Solar Energy*. 2017, 141, 278-96.
- [8] COMPAGNON, R. Solar and daylight availability in the urban fabric. *Energy and Buildings*. 2004, 36, 321-8.
- [9] LI, D., LIU, G., LIAO, S. Solar potential in urban residential buildings. *Solar Energy*. 2015, 111, 225-35.
- [10] VULKAN, A., KLOOG, I., DORMAN, M., ERELL, E. Modeling the potential for PV installation in residential buildings in dense urban areas. *Energy and Buildings*. 2018, 169, 97-109.
- [11] ROBINSON, D., HALDI, F., KÄMPF, J., LEROUX, P., PEREZ, D., RASHEED, A., WILKE, U. CitySim: Comprehensive micro-simulation of resource flows for sustainable urban planning. In: *Eleventh International IBPSA Conference: Building Simulation*. Glasgow, UK. 2009.
- [12] MATURI, L., ADAMI, J., LOVATI, M., TILLI, F., MOSER, D. BIPV Affordability. In: *33rd European Photovoltaic Solar Energy Conference and Exhibition*. Amsterdam, the Netherlands, pp. 2621 - 5. 2017.

- [13] KANTERS, J., WALL, M., DUBOIS, M-C. Typical Values for Active Solar Energy in Urban Planning. *Energy Procedia*. 2014, 48, 1607-16.
- [14] Czech electricity and gas market operator (OTE a. s.) [online]. 2011. Available from: <http://www.ote-cr.cz/>
- [15] Czech Statistical Office (ČSÚ). Energy consumption in households in the Czech Republic in 2003. (Energó 2004), Report 8109-05. Prague, 2005.
- [16] REMODECE. Residential Monitoring to Decrease Energy Use and Carbon Emissions in Europe. In: *Annual electricity use in the Czech Republic* [online]. 2008. Available at: <http://remodece.isr.uc.pt>
- [17] STANĚK, K. *Photovoltaics for buildings*: Grada for the Department of Building Structures at the Faculty of Civil Engineering of the Czech Technical University in Prague. 2012.
- [18] VOSS, K., MUSALL, E., LICHTMESS, M. From Low-Energy to Net Zero-Energy Buildings: Status and Perspectives. *Journal of Green Building*. 2011, 6, 46-57.
- [19] EVOLA, G., MARGANI, G. Renovation of apartment blocks with BIPV: Energy and economic evaluation in temperate climate. *Energy and Buildings*. 2016, 130, 794-810.
- [20] HONRUBIA-ESCRIBANO, A., RAMIREZ, F. J., GÓMEZ-LÁZARO, E., GARCIA-VILLAVERDE, P. M., RUIZ-ORTEGA, M. J., PARRA-REQUENA, G. Influence of solar technology in the economic performance of PV power plants in Europe. A comprehensive analysis. *Renewable and Sustainable Energy Reviews*. 2018, 82, 488-501.
- [21] VERBERNE, G., BONOMO, P., FRONTINI, F., VAN DEN DONKER, M. N., CHATZIPANAGI, A., SINAPIS, K., FOLKERTS, W. BIPV Products for Façades and Roofs: a Market Analysis. In: *29th European Photovoltaic Solar Energy Conference and Exhibition*. (Amsterdam, the Netherlands, pp. 3630 - 6. 2014.
- [22] JOLISSAINT, N., HANBALI, R., HADORN, J-C., SCHÜLER, A. Colored solar façades for buildings. *Energy Procedia*. 2017, 122, 175-80.
- [23] SKANDALOS, N., KARAMANIS, D., PENG, J., YANG, H. Overall energy assessment and integration optimization process of semitransparent PV glazing technologies. *Progress in Photovoltaics: Research and Applications*. 2018, 26, 473-90.
- [24] MUNARI PROBST, M. C., ROECKER, C. Solar Energy Promotion & Urban Context Protection: Leso-qsv (quality- Site-visibility) Method. In: *31th PLEA Conference*. Bologna, Italy. 2015.
- [25] FRONTINI, F., MANFREN, M., TAGLIABUE, L. C. A Case Study of Solar Technologies Adoption: Criteria for BIPV Integration in Sensitive Built Environment. *Energy Procedia*. 2012, 30, 1006-15.
- [26] LÓPEZ, C. S. P., FRONTINI, F. Energy Efficiency and Renewable Solar Energy Integration in Heritage Historic Buildings. *Energy Procedia*. 2014, 48, 1493-502.
- [27] KICHOU, S., WOLF, P., SILVESTRE, S., CHOUDER, A. Analysis of the behaviour of cadmium telluride and crystalline silicon photovoltaic modules deployed outdoor under humid continental climate conditions. *Solar Energy*. 2018, 171, 681-91.